

**Exploring the intimate relationship between the host and its microbes:
Implications for hypertensive-end organ damage**

Inaugural-Dissertation
to obtain the academic degree
Doctor rerum naturalium (Dr. rer. nat.)

submitted to the Department of Biology, Chemistry, Pharmacy
of Freie Universität Berlin

by

Ellen Germaine Avery
from
Winnipeg, Manitoba, Canada

2021

prepared in the group of Prof. Dr. Dominik N. Müller at the Experimental and Clinical Research Center, a joint cooperation of Max Delbrück Center for Molecular Medicine and Charité - Universitätsmedizin Berlin from October 2017 until September 2021

1st Reviewer: Prof. Dr. Dominik N. Müller

2nd Reviewer: Prof. Dr. Oliver Daumke

Date of defense: December 6th 2021

Acknowledgements

I would like to take this opportunity to express my gratitude for all the people who have contributed to the success of my doctoral thesis. When I came to Berlin in 2017, I was excited to embark on an adventure, but I could've never imagined what was to come over the next four years. I had only ever been to Germany to interview for the position, so it is safe to say I had no idea what I was getting into. I was fortunate enough to stumble into an amazing lab, and to make many lifelong friends through this process. To my mentors, colleagues, friends, and family, thank you for supporting me in both my personal and professional endeavors during this period.

I would like to first thank my supervisor Dominik. I was admittedly terrified when I first arrived and realized that you and I would share an office space, but it has turned out to be such a blessing. It is very difficult to sum up the past four years working together, as it has been a long and winding path for a multitude of reasons. I am glad that you took a chance on me and offered me the opportunity to join your group. I am incredibly grateful to have had you as a mentor. Thank you for consistently prioritizing my career success, advocating for my safety in the face of truly unforeseen circumstances, and for being a constant source of creativity to propel my projects forward. I am deeply appreciative of your consistency, patience, and kindness; and I look forward to seeing what the lab will accomplish in the future.

I would also like to thank several individuals who have gone above and beyond to contribute to the success of my thesis. To my thesis committee members Nicola, Sofia, Holger and Oliver, thank you for your support and for offering valuable feedback throughout the completion of my thesis. A special thank you to Oliver for helping me plan the thesis writing period effectively and agreeing to review this thesis in its entirety. To Helge, I have enjoyed greatly what time we've spent together over the last few years, your mentorship has been such an asset and has contributed greatly to my success. Even when I've finished my thesis, I hope to still receive updates about your amazing travels. To Sofia, I am so grateful to have met you, your confidence in my abilities has pushed me to work harder and achieve more than I thought that I could. To Andras, I have learned so much from you scientifically and personally, I am grateful for your thoughtful input, your cheerful outlook, and your friendship throughout the last four years. To Nicola, your drive and commitment to your work is admirable, I value all the time we've spent together over the years, and I wish you nothing but success in your future endeavours.

To Gabi, you are truly an amazing colleague and such a wonderful person. Thank you for your work, the delicious cakes, your translation services, and most of all for your tenacity. To Marie, thank you for answering my endless questions about proteomics; your work has contributed to the success of my thesis, and you've been an excellent teacher in the process. To Hendrik, the first aim of my thesis would not have been achievable without your support, I'm proud of what we were able to accomplish as a team, and I wish you all the best in the bright future that lies ahead of you. To Sabrina, from sharing an office to becoming collaborators; you are a skilled scientist, and I'm grateful for your hard work as well as your friendship. To Theda, I would like to thank you for being a great friend and colleague over the past few years, and I can't wait to see what you accomplish in the future; I'm sure it will be remarkable. To Lajos, Sarah, Ariana, and Alex, thank you all for your camaraderie and contributions inside and outside of the lab. To all the other lab members and collaborators that I haven't mentioned individually, I am thankful for the time we've spent together, and I hope you will forgive that my memory failed me when writing these acknowledgements. In my eyes, science is a team sport, and this body of work would never have been possible without all of you.

I would additionally like to thank my partner Alexander and my family. To Alexander, I am so lucky that you agreed to pack up your whole life and move to Berlin with me, I don't think I would have been brave enough to take such a leap if you were not by my side. Thank you doesn't even begin to cover it; your generosity and companionship has been vital to me throughout this process. To my parents and my sisters, I have missed you all so much over the last four years and I am incredibly excited to be closer to home once my thesis has been completed. Thank you for the endless hours of Facetime calls, I can't wait to finally see your faces in person. I absolutely could not have done this without you. Thank you for believing in me and cheering me on, your confidence in me has made all the difference.

Publications

Parts of this thesis have contributed to the following publications:

1. **Avery EG**, Bartolomaeus H, Maifeld A, Markó L, Wiig H, Wilck N, Rosshart SP, Forslund SK, and Müller DN. *The Gut Microbiome in Hypertension: Recent Advances and Future Perspectives*. *Circulation Research* (<https://doi.org/10.1161/CIRCRESAHA.121.318065>). 2021; 128:934-950.
2. **Avery EG***, Bartolomaeus H*, Rauch A, Chen CY, N'diaye G, Löber U, Bartolomaeus TUP, Fritsche-Guenther R, Tsvetkov D, Park JK, Markó L, Maifeld A, Kempa S, Kirwan JA, Forslund SK, Müller DN, and Wilck N. *Quantifying the Impact of the Gut Microbiota on Inflammation and Hypertensive Organ Damage*. *Biorxiv* (<https://doi.org/10.1101/2021.09.17.460671>). 2021.
3. **Avery EG**, Kirchner M, Geisberger SY, Yarritu A, Kedziora SM, Maifeld A, Bruening U, Karlsen TV, Bartolomaeus H, Bartolomaeus TUP, Wimmer MI, Klopffleisch R, Kirwan JA, Kempa S, Mertins P, Wiig H, and Mueller DN. *Interstitial Fluid Isolation from the Gut Mucosa as a Novel Technique to Study Host-Microbiome Interactions* (In preparation). 2021.

Peer-reviewed publications during the reporting period not included in this thesis:

1. Maifeld A, Bartolomaeus H, Löber U, **Avery EG**, Steckhan N, Markó L, Wilck N, Hamad I, Susnjar U, Mahler A, Hohmann C, Chen CY, Cramer H, Dobos G, Lesker TR, Strowig T, Dechend R, Bzdok D, Kleinewietfeld M, Michalsen A, Müller DN, and Forslund SK. *Fasting Alters the Gut Microbiome Reducing Blood Pressure and Body Weight in Metabolic Syndrome Patients*. Nature Communications. 2021; 12:1970.
2. Bartolomaeus TUP, Birkner T, Bartolomaeus H, Löber U, **Avery EG**, Mahler A, Weber D, Kochlik B, Balogh A, Wilck N, Boschmann M, Müller DN, Markó L, and Forslund SK. *Quantifying Technical Confounders in Microbiome Studies*. Cardiovascular Research. 2021; 117:863-875.
3. Kviatkovsky I, Chrzanowski HM, **Avery EG**, Bartolomaeus H, and Ramelow S. *Microscopy with Undetected Photons in the Mid-Infrared*. Science Advances. 2020; 6.
4. Bartolomaeus H, **Avery EG**, Bartolomaeus TUP, Kozhakhmetov S, Zhumadilov Z, Müller DN, Wilck N, Kushugulova A, and Forslund SK. *Blood Pressure Changes Correlate with Short-Chain Fatty Acid Production Potential Shifts Under a Synbiotic Intervention*. Cardiovascular Research. 2020; 116:1252-1253.
5. Bartolomaeus H, Balogh A, Yakoub M, Homann S, Markó L, Hoges S, Tsvetkov D, Krannich A, Wundersitz S, **Avery EG**, Haase N, Kraker K, Hering L, Maase M, Kusche-Vihrog K, Grandoch M, Fielitz J, Kempa S, Gollasch M, Zhumadilov Z, Kozhakhmetov S, Kushugulova A, Eckardt KU, Dechend R, Rump LC, Forslund SK, Müller DN, Stegbauer J, and Wilck N. *Short-Chain Fatty Acid Propionate Protects from Hypertensive Cardiovascular Damage*. Circulation. 2019; 139:1407-1421.

Table of contents

Acknowledgements	3
Publications.....	5
Table of contents.....	7
List of tables	10
List of figures.....	11
List of abbreviations	13
Summary.....	15
Zusammenfassung	17
1. Introduction	19
1.1 The global burden of hypertensive disease.....	19
1.1.1 Hypertension and human health	19
1.1.2 Understanding the consequences of BP dysregulation.....	21
1.2 The gut microbiome in health and disease	22
1.2.1 Introduction to microbial symbionts.....	22
1.2.2 GI tract physiology.....	23
1.2.3 Inflammation and the gut microbiome	25
1.3 The microbiome in hypertension.....	27
1.3.1 Associations between the microbiome and BP.....	27
1.3.2 Immune mechanisms in hypertension: is the microbiome the missing link?.....	28
1.3.3 Metabolites as mediators of the host-microbiome interaction in hypertension	29
1.4 Interstitial fluid as a window into the microenvironment in the GI tract	31
1.4.1 Regional specificity of the host-microbiome axis.....	31
1.4.2 Interstitial fluid biology principles and relevance within the GI tract	34
2. Study aims	37
2.1 Define the contribution of the gut microbiome in hypertension	37
2.2 Develop novel methods for the isolation of interstitial fluid from the GI tract	37
3. Materials and methods.....	38
3.1 Germ-free hypertensive mice.....	38

3.1.1	Animal Protocol.....	38
3.1.2	Echocardiography.....	39
3.1.3	Splenic immunophenotyping.....	39
3.1.4	Urine analysis.....	40
3.1.5	Bacterial growth in thioglycolate medium.....	40
3.1.6	Histological analysis of renal and cardiac tissue.....	40
3.1.7	Quantitative real-time RT-PCR of renal and cardiac tissue.....	42
3.1.8	<i>In vivo</i> BP measurement and Ang II pressor response.....	44
3.1.9	Serum metabolomic measurements using MxP Quant 500.....	44
3.1.10	Serum metabolomic analysis.....	46
3.1.11	DNA isolation and extraction for microbiome analysis.....	46
3.1.12	Microbiome sequencing data processing and analysis.....	47
3.1.13	Fecal qPCR.....	48
3.1.14	Comparative analysis with Pluznick study data.....	48
3.1.15	<i>In vitro</i> Th17 polarization.....	49
3.2	Interstitial fluid isolation and analytics.....	50
3.2.1	Animal protocols.....	50
3.2.2	Centrifugation method.....	51
3.2.3	Elution method.....	52
3.2.4	Ion chromatography.....	53
3.2.5	⁵¹ Cr-EDTA extracellular tracer – centrifugation method.....	53
3.2.6	⁵¹ Cr-EDTA extracellular tracer – elution method.....	54
3.2.7	Total tissue water determination.....	54
3.2.8	Proteomics analysis.....	55
3.3	Shared methods.....	57
3.3.1	Metabolomics analysis of short chain fatty acids.....	57
3.3.2	Statistical analysis.....	58
4.	Results.....	59
4.1	The contribution of the gut microbiome to hypertensive end-organ damage.....	59
4.1.1	Verification of experimental integrity.....	59

4.1.2	Hypertensive kidney damage is exacerbated under GF conditions	60
4.1.3	Hypertensive heart damage is impacted by microbiome status	63
4.1.4	The kidney is more sensitive to microbial status in hypertension than the heart	66
4.1.5	The impact of the microbiome on vascular reactivity and BP	70
4.1.6	Inflammation in hypertension is impacted by the microbiome.....	71
4.1.7	Serum metabolome is impacted by microbiome status.....	75
4.1.8	Not all microbiomes in C57BL/6J mice are created equal	77
4.2	Interstitial fluid isolation from the GI tract	79
4.2.1	Properties of the interstitial fluid reservoir within the GI tract	79
4.2.2	Development of the Elution method.....	80
4.2.3	Elution method captures unique IF signature compared to serum	85
4.2.4	The impact of time and segmentation on the proteomic elution IF signature.....	89
4.2.5	Elution IF contains metabolites known to be locally produced in the GI tract.....	92
4.2.6	Centrifugation as an alternative method to capture the IF space	94
4.2.7	Comparability of the proteomic signature from elution and centrifugation IF	97
4.2.8	SCFA from Centrifugation and Elution IF are similarly identifiable in the colon and cecum in healthy rats	105
5.	Discussion.....	108
5.1	Conclusions.....	119
	References	120
	Declaration of Independence.....	136
	Curriculum vitae – Ellen Germaine Avery.....	137

List of tables

Table 1. qPCR primer and probe information.....	42
Table 2. Antibodies used for GF immunophenotyping.....	50
Table 3. Immune cell subsets measured in GF and COL mice.....	71
Table 4. Proteins separating duodenum 1 samples at 8 compared to 2-hour timepoint are mostly intracellularly related	92
Table 5. Differential GOCC enrichment between the elution and centrifugation methods.....	99

List of figures

Figure 1. Regional specialization along the GI tract	24
Figure 2. The host-microbiome interaction in hypertension	31
Figure 3. Schematic of the GI microenvironment	33
Figure 4. Schematic of GF project experimental design	39
Figure 5. Microbiome status verification from GF experiments	59
Figure 6. Microbiome status verified by qPCR and shotgun sequencing	60
Figure 7. Hypertensive kidney dysfunction is exacerbated in GF mice	61
Figure 8. Hypertensive renal inflammation is worsened under GF conditions.....	62
Figure 9. Hypertensive kidney fibrosis is increased in GF mice relative to COL.....	63
Figure 10. Cardiac dysfunction is moderately increased in GF mice	64
Figure 11. Cardiac fibrosis is regulated in GF and COL mice	65
Figure 12. Hypertensive cardiac inflammation is regulated in both GF and COL mice	66
Figure 13. Comprehensive univariate evaluation of the kidney and cardiac phenotype	68
Figure 14. Comprehensive multivariate evaluation of the kidney and cardiac phenotype.....	70
Figure 15. <i>In vivo</i> vascular reactivity of COL and GF mice	71
Figure 16. Inflammation is influenced by microbial status.....	73
Figure 17. Th17 and MDSC cells are differentially regulated in GF and COL mice	74
Figure 18. <i>In vitro</i> Th17 polarization of naïve T cells from GF and COL mice in the presence of Ang II	75
Figure 19. Serum metabolome is impacted by hypertension in GF and COL	76
Figure 20. Microbially-produced metabolites TMAO, 3-IPA, and IS are only present in COL mice	77
Figure 21. Fecal SCFA in GF and CONV mice	77
Figure 22. Hypertension in mice with a microbiome elicits divergent metabolome effects.....	78
Figure 23. Extracellular fluid volume within the GI tract of C57BL6/J mice	80
Figure 24. Schematic for the collection of IF using an elution-based method	81
Figure 25. Timepoint but not buffer plays a role in eluted ion composition.....	82
Figure 26. Shorter timepoints result in significantly less K ⁺ in elution IF	83
Figure 27. ⁵¹ Cr-EDTA elution indicates the rapid equilibration of this extracellular tracer with the surrounding elution buffer	84
Figure 28. The serum and elution IF proteomes are unique in C57BL/6J mice	86
Figure 29. Known proteins of importance within the GI tract were detectable in elution IF.....	87
Figure 30. Robustly identified serum proteins and their relationship with elution IF	88

Figure 31. High abundance of intracellular proteins can be found in Elution IF.....	89
Figure 32. Elution IF samples from the same GI region have a similar proteomic profile	90
Figure 33. Elution time minimally influences the protein profile within a given segment.....	91
Figure 34. SFCA within IF reflects the enrichment in localized fecal content in the GI tract.....	94
Figure 35. Schematic for centrifugation-based method for IF isolation.....	95
Figure 36. Centrifugation IF isolation efficiency from the gut is not significantly different from skin IF ...	96
Figure 37. Centrifugation IF volume in mice and rats	97
Figure 38. Overall proteomic signature is distinct between the two methods	98
Figure 39. Proteins of interest in rats show a similar enrichment pattern in the GI tract for both methods	101
Figure 40. REG3G is selectively enhanced in the ileum in both centrifugation and elution IF	102
Figure 41. Independent z-scoring by method results in high congruence of the overall proteomic signature from GI segments	103
Figure 42. Inflammation-related and proteins expected in IF are similarly enriched in various GI segments in both the elution and centrifugation methods	104
Figure 43. SCFA in IF is similar enrichment along the GI tract in both methods.....	106
Figure 44. Fecal SCFA enrichment is specific to the colon and cecum in SD rats	107

List of abbreviations

CVD	Cardiovascular disease
GF	Germ-free
GI	Gastrointestinal
IF	Interstitial fluid
BP	Blood pressure
Th17	T helper 17 cells
Th1	Type 1 helper cells
Treg	T regulatory cells
MDSC	Myeloid-derived suppressor cells
SI	Small intestine
LI	Large intestine
FMT	Fecal microbiota transplantation
NGS	Next-generation sequencing
PBMC	Peripheral blood mononuclear cell
SHR	Spontaneously hypertensive rat
GC-MS	Gas chromatography–mass spectrometry
LC-MS	Liquid chromatography–mass spectrometry
WKY	Wistar-Kyoto rats
LPS	Lipopolysaccharide
IL	Interleukin
HTN	Hypertension
GO	Gene ontology
GOCC	Gene ontology cellular component
C2	Acetate
C3	Propionate
C4	Butyrate
isoC4	Isobutyrate
IS	Indoxyl sulfate
COL	Colonized
CONV	Conventionally raised

TMAO	Trimethylamine N-oxide
3-IPA	3-indolepropionic acid
PCA	Principal component analysis
PCOA	Principle coordinate analysis
CTRB1	Chymotrypsinogen B
LGALS1	Galectin-1
LGALS3	Galectin-3
REG3G	Regenerating islet-derived protein 3 gamma
ECV	Extracellular fluid volume
ICV	Intracellular fluid volume
MAIT	Mucosal associated invariant T
LFQ	Label-free quantification
EVs	Extracellular vesicles
BEVs	Bacterial extracellular vesicles

Summary

The microbiome plays a key role in the maintenance of health, as well as in the pathogenesis of various diseases including hypertension and cardiovascular disease. The global aim of my thesis was to understand the role of bacteria in hypertensive organ damage, and to develop a new method for the precise phenotyping of proteins and microbiota-derived metabolites within the GI tract.

To address the former, I used germ-free mice (GF), which are devoid of bacteria, to investigate if bacterial colonization modulates the response to a hypertensive stimulus. Compared with fully colonized (COL) mice, hypertensive GF mice showed significantly more severe renal damage, which was associated with increased systemic and local inflammatory responses. The hypertension-induced differences in the heart were less pronounced than in the kidney. Furthermore, metabolites within the serum from these mice showed broadscale differences elicited by hypertension in GF and COL mice. These results highlight that the presence of intestinal bacteria and bacterially produced metabolites, in particular short-chain fatty acids, inhibits inflammatory responses and hypertension-induced organ damage. These findings emphasize the importance of the homeostasis between the host and its colonizing microbes in hypertensive disease.

Next-generation sequencing (NGS) and metabolomics analyses from fecal samples are typically used to characterize the dysbiotic state, providing an inventory of the microbes or microbial products. Both serum and fecal measurements present challenges because they are indirect measurements of the compartment of interest, the microenvironment of the gastrointestinal (GI) tract in the host. The prevailing hypothesis within the field is that metabolites and small molecules in the GI tract, which can be either host- or microbially-derived, impact the polarization and function of immune cells, thereby impacting inflammation in the gut and in distal organ systems (e.g., the heart and the kidney). Currently, no direct methods are available to evaluate the microenvironmental signature which is presumed to exist within the interstitial fluid (IF) of the GI tract. I applied two known methods to isolate the IF from the GI tract, to directly assess the local microenvironment at the site-of-action. Here I have shown that the isolation of GI IF reflects a unique compartment which had previously been largely uncharacterized. The IF from both rats and mice was found to contain elevated levels of SCFA within the lower intestinal segments, whereas the levels in the upper GI tract were not different from serum. I was also able to identify proteins which were specific to a given GI region (e.g., REG3G, LGALS1) within the IF using two independent methods.

In conclusion, with these newly established methods for obtaining IF from different segments in the intestine, it is now possible to characterize the intestinal micromilieu in detail. In the future, IF isolation may facilitate a better understanding of the host's interactions with the microbiome in health and disease.

Zusammenfassung

Das Mikrobiom spielt eine wichtige Rolle beim Erhalt der Gesundheit, wie auch bei der Pathogenese verschiedener Erkrankungen u.a. bei der Entstehung von Bluthochdruck und kardiovaskulären Erkrankungen. Hauptziel meiner Doktorarbeit war zum einen die Untersuchung des Einflusses von Bakterien bei hypertoniebedingten Organschäden und zum anderen die Entwicklung einer neuen Methode zur Charakterisierung von mikrobiotaproduzierter Proteine und Metabolite im Interstitium des Darmtraktes.

Zur Untersuchung der Rolle von Bakterien bei hypertoniebedingten Organschäden wurden keimfreie Mäuse, welche keinerlei Bakterien besitzen, verwendet und überprüft inwieweit sich das Fehlen von Bakterien bzw. eine Rekolonisierung der Bakterien (Wiederherstellung eines Vollflorazustandes) bei hypertoniebedingten Organschäden auswirkt. Verglichen zum Vollflorazustandes zeigten hypertone keimfreie Mäuse einen signifikant stärker ausgeprägten Nierenschaden, der mit einer verstärkten systemischen und lokalen Entzündungsreaktion einher ging. Die Schädigung des Herzens aufgrund des Hypertonus war weniger ausgeprägt als der Nierenschädigung. Die Serummetabolitensignaturen waren in beiden hypertensiven Versuchsgruppen signifikant verändert. Diese Ergebnisse verdeutlichen, dass das Vorhandensein von Darmbakterien, insbesondere die bakterienvermittelte Bildung von kurzkettigen Fettsäuren, und deren Homeostase mit dem Wirt die Entzündungsreaktionen und die hypertoniebedingte Organschädigung hemmt, was deren Bedeutung für hypertensive Organschädigung verdeutlicht.

Um die Bakterienzusammensetzung bzw. das Muster der bakteriengebildeten Metabolite (Metabolom) zu charakterisieren, setzt man aktuell „Next-generation Sequenziertechniken“ (NGS) bzw. Massenspektrometrie bei Stuhlproben ein. Diese Ansätze eignen sich, um Rückschlüsse auf einen dysbiotischen (nicht gesunden) Zustand zu erhalten. Untersuchungen von Blut- und Stuhlproben sind aus unterschiedlichen Gründen nicht unproblematisch, da sie beide nur indirekt auf das lokale Geschehen im Darmmikromilieu abzielen. Die vorherrschende Hypothese im Forschungsgebiet postuliert, dass lokal produzierte Proteine, Metabolite und kleine Moleküle, welche sowohl durch Bakterien als auch den Wirt gebildet sein können, einen direkten lokalen Einfluss auf Immunzellfunktion im Darm und nachgeschaltet auf das Entzündungsgeschehen in entfernten Organen (wie z.B. Herz und Niere) haben. Aktuell stehen keine Methoden zur Analyse des Mikromillieus des Interstitiums des Darms zur Verfügung. Um die Lücke zu schließen, wurden zwei Methoden verwendet, welche bereits zur Gewinnung von interstitieller Flüssigkeit anderer Organe/Gewebe eingesetzt werden. Diese wurden mit dem Ziel der Anwendbarkeit

bei Darmgewebe weiterentwickelt. In der eingereichten Arbeit konnte gezeigt werden, dass eine Isolation von interstitieller Flüssigkeit verschiedener Abschnitte des Dün- und Dickdarms möglich ist und es segmentspezifische Unterschiede gibt, die bisher nicht direkt messbar waren. Die interstitielle Flüssigkeit des Dickdarms von Mäusen und Ratten enthielt unter anderem signifikant höhere kurzkettigen Fettsäure-Spiegel als die des Dünndarms oder des Bluts. Mittels Proteomanalysen konnte mit beiden neu entwickelten Methoden gezeigt werden, dass Markerproteine wie REG3G und LGALS1 segmentspezifisch vorhanden sind. Darüber hinaus zeigten die Etablierungsversuche, dass die Methodik die Integrität des biopsierten Darmgewebes nur unwesentlich beeinflusst.

Zusammenfassend kann festgestellt werden, dass mit den neu etablierten Methoden zur Gewinnung von interstitiellen Flüssigkeiten aus verschiedenen Segmenten des Darms, es nun möglich ist, das Darmmikromillieu detailliert zu charakterisieren. Des Weiteren können dadurch neue Erkenntnisse des Kompartiments bei der Pathogenese von Erkrankungen, aber auch beim Erhalt der Gesundheit gewonnen werden.

1. Introduction

1.1 The global burden of hypertensive disease

1.1.1 Hypertension and human health

Hypertension is the most prevalent risk factor for cardiovascular disease and all-cause mortality globally.¹ Worldwide the prevalence of hypertension is 31.1%¹, although in industrialized countries rates can be over 50%², depending on sex, age group and country of origin. The human cost and the financial burden of hypertension are nontrivial. In 2001, the cost of high blood pressure (BP) was estimated to be around 10% of the total healthcare cost globally¹. Hypertension is classically defined as an increase in BP which is consistently elevated above a threshold level of 140/90 mm Hg³, though some believe that the threshold should be even lower to reduce the risk of complications.⁴ Essential (primary) hypertension, or hypertension without a discernable cause, is the most common form of the disease, accounting for more than 90% of cases.⁵ Secondary hypertension is, as implied, secondary to an identifiable source or trigger, such as an endocrine disorder, or use of certain types of medications (e.g. oral contraception).⁵ Hypertension is often called the “silent killer” because most patients are asymptomatic, although the long-term consequences of untreated hypertension are anything but silent and include the development of various kidney, heart, and vascular maladies.^{5, 6} It has been suggested that hypertension could be managed well in 90% of patients with combination therapy using first-line drugs like thiazide diuretics, calcium antagonists, angiotensin converting enzyme (ACE) inhibitors, or angiotensin receptor blockers (ARBs).⁴ Patients whose blood pressure can not be brought under control using traditional drug therapy have treatment resistant hypertension. Although it is difficult to estimate the true number of treatment resistant patients, some have suggested that this affects between 12 to 30 % of patients^{7, 8}, suggesting that a wide treatment gap exists despite all that is known about the disease. Indeed, the National Health and Nutrition Examination Survey found that the percentage of treated hypertensive patients that had their blood pressure under control was only 53% (<140/90 mm Hg).^{8, 9} Barriers to treatment are still significant worldwide and in industrialized countries.¹⁰ Because cost and treatment availability are major barriers to treatment in the developed world¹, continued discovery of novel and cost-effective treatment strategies is required.

Hypertension is known as a multifactorial disease state, where several mechanisms typically co-occur to lead to a persistent increase in BP. The Mosaic Theory, proposed by Dr. Irvine Page in 1949, originally included the participation of four key features in the pathogenesis of hypertension; the heart, kidney,

nervous and endocrine systems.¹¹ The theory has been adapted over the years to include a diverse range of disease mechanisms including environmental determinants, genetic causes, and hemodynamic factors.⁶ The renin-angiotensin-aldosterone system (RAAS) has long been known to influence the pathogenesis of hypertension. While the intricacies of the RAAS system are outside of the scope of this thesis, importantly, Angiotensin II (Ang II) is one of the active molecules produced during RAAS activation.¹² Two of the four first-line drugs (ACE inhibitors and ARBs) which are effective in reducing BP are meant to directly block RAAS activation.¹³ Ang II has high utility for experimentalists, because infusion with Ang II is a potent inducer of experimental hypertension in animal models.¹⁴ More recently immune mechanisms of hypertensive disease have garnered significant attention. Immune cells such as T helper cell subtypes T_H17 (producing interleukin (IL)-17) and T_H1 (producing IFN γ), regulatory T cells (Treg), macrophages, and myeloid-derived suppressor cells (MDSCs) have all been implicated as either positive or negative regulators of hypertensive disease pathogenesis.^{15, 16} As our understanding of the microbiome and its intimate relationship with immune cells in the gut has expanded, the microbiome has also emerged as a promising target for the development of novel hypertension treatment strategies.¹⁵ The microbiome and immunity in the context of hypertension will be elaborated on in section 1.3.

Lifestyle factors have long been known to play a role in the development of hypertension.¹⁵ Lifestyle factors like dietary salt intake, diets low in fruit and vegetables, and physical inactivity are all known to worsen the severity of disease.¹⁰ A recent review identified at least 27 different dietary factors which have been associated with hypertension.¹⁷ Dietary salt reduction, weight loss (per 10 kg) and switching to a healthy diet (Dietary Approaches to Stop Hypertension otherwise known as the DASH diet) are known to improve the BP by 2-8, 5-20 and 8-14 mm Hg, respectively.¹⁰ Even a modest reduction of 2 mm Hg in BP is known to decrease overall CVD mortality by 7%.^{15, 18} As mentioned above, there exists a treatment gap in hypertension which many have suggested should be targeted using lifestyle interventions, especially in low-resource settings.¹⁰ Unfortunately, compliance to lifestyle modification programs is often a challenge.¹⁹ Nevertheless, understanding the mechanisms which lead to the success of a lifestyle intervention would allow us to potentially exploit these mechanisms more effectively by either using more targeted interventions or developing new drug targets that capitalize on existing pathways to improve patient outcomes. One of the expected modes-of-action of a successful lifestyle intervention is via modulation of the gut microbiome.^{6, 15} As the gut microbiome is integrally linked to the consumption habits of the host²⁰, it stands to reason that the GI microenvironment may be the right place to look when investigating how lifestyle interventions reduce hypertensive disease. Indeed, our group and others have

shown that dietary salt²¹ and fiber intake²²⁻²⁴ impact the production of microbial metabolites (tryptophan metabolites, short-chain fatty acids²⁵) and can reduce hypertensive disease severity. These findings are reviewed in more detail in section 1.3. A deeper understanding of the existing connections between the host and its microbes will allow the discovery and exploitation of endogenous mechanisms which already contribute to BP control.

1.1.2 Understanding the consequences of BP dysregulation

Hypertension that goes un- or under-treated can lead to a wide variety of adverse events. Hypertensive damage to the heart, kidney and vasculature are some of the most well-recognized and dangerous consequences, although damage to other organ systems has also been documented (e.g. brain and eyes).^{5, 6, 14, 26} In patients, Ang II levels have also been found to correlate with left-ventricular hypertrophic remodeling,²⁷ indicating that RAAS activation does play a role in the development of end-organ damage. Fortunately for experimentalists, the Ang II infusion model for hypertension also induces the development of damage to the heart, kidneys, and vasculature, similar to what is seen in humans with essential hypertension.¹⁴ End-organ damage in the form of hypertensive heart disease often involves inflammation in the tissue, hypertrophic remodeling (particularly in the left ventricle) and fibrosis.^{12, 13} In humans, electrocardiography or magnetic resonance imaging are the standard-of-care for hypertensive heart disease diagnostics.^{12, 13} If left untreated hypertensive heart disease can lead to myocardial infarction, heart failure, and sudden cardiac death.¹² Endothelial dysfunction and vascular remodeling are common vasculopathy findings in hypertension, and can lead to plaque formation, stenosis and aneurysms.¹² Over time, hypertensive damage to the kidneys leads to increased albuminuria, decreased glomerular filtration rate, and increased serum creatinine; each of which can be measured for diagnostic purposes.¹³ Kidney dysfunction often involves tissue-specific inflammation, structural damage, and fibrosis, and is particularly troubling because of its high-mortality rate.^{12, 28} Furthermore, kidney dysfunction further contributes to CVD risk above and beyond what is explicable by traditional cardiovascular risk factors.²⁹ Although animal models are not a perfect recapitulation of the human situation, they have a high utility to link associative findings with mechanistic insights.^{14, 15} Of course, animal models are highly important in translational research because they allow the use of invasive techniques, and can be used to assess the safety and efficacy of novel targets for pharmacological and non-pharmacological treatments.¹⁴

1.2 The gut microbiome in health and disease

1.2.1 Introduction to microbial symbionts

Microbes are everywhere in the natural world and can thrive in several niches on the surface of or within their human hosts. The complexity of the microbial world can not be underestimated, as these microorganisms are known for their high capability to inhabit the uninhabitable and rapidly adapt to their surroundings.³⁰ Within the human body more than 50% of cells are microbial, outnumbering the cells of the host.³¹ While microbes can find a home for themselves in a variety of body sites, the GI tract is one of the most popular locales.³¹ The bacterial content within the colon outnumbers all other sites by at least two orders of magnitude.³¹ One of the most unique and interesting features of human microbiomes is the striking heterogeneity found in fecal matter.^{31, 32} Over half of the microbial genes found in human samples are unique to the individual.³¹ Microbial symbiosis shapes the lived experience of the host. Although animals and humans can survive without gut microbes, life is certainly better with these symbiotic organisms.³³ In fact, one of the most valuable models we have to study the host-microbiome interaction are GF mice, which are devoid of all bacteria.^{33, 34} NGS technologies have greatly improved our ability to study the gut microbiome.³⁰ Previous research was limited by which microbes could survive in a culture setting, whereas the falling cost of sequencing has facilitated the discovery and study of a plethora of microbes which were previously unknown.³⁰ Although much is now known about the composition of the human gut microbiome, there are many unanswered questions with respect to the host-microbiome interaction.

Each individual's respective 'healthy' gut microbiome was found to be relatively stable over time and coexists in equilibrium with the surrounding environment.³⁵ It appears that the microbiome's resilience and capacity to help fight off infection is a much more important determinant of host health than the presence of a particular set of microbes.³⁶ The ecosystem within the GI tract is known to be susceptible to transient or persistent changes resulting from antibiotic use, intestinal infection, and profound dietary or lifestyle modifications.^{35, 37} Although the universality of a "healthy" microbiome composition has been elusive, there are commonalities that have been demonstrated in perturbations from a healthful state (i.e. *dysbiosis* as opposed to *eubiosis*).^{32, 38} Changes to the microbiome have been demonstrated in a variety of diseases, including but not limited to inflammatory conditions (e.g. colitis, Crohn's disease), cardiovascular, and metabolic disorders.³⁹⁻⁴³ As the compositional features of each individual's microbiome are highly variable³¹, research is increasingly shifting from a taxonomic to functional focus.^{38, 44} Researchers have increasingly found that metabolites produced by the microbiome are potent mediators

of host function, particularly via their interactions with the immune system.^{44,45} The gut microbiota is now considered an endocrine organ for its capacity to generate metabolites that can act as effectors in the host, locally or in distal target organs.⁴⁶ The interrelation between lifestyle, diet, pharmacotherapy, and the gut microbiome is still the subject of ongoing research.

1.2.2 GI tract physiology

The intestines act as an interface between the external environment and the host, and their role in host health goes far beyond nutrient absorption. The lumen of the GI tract is home to a wide variety of microbial inhabitants, while the tissue epithelium acts as the largest compartment of host immune cells in the body (Figure 1).⁴⁷ Anatomically, the intestines consist of different segments with distinctive properties, thereby fostering a unique microenvironment from both the perspective of the host and the colonizing microbes.^{47, 48} The longest stretch of the GI tract is the small intestine (SI), made up of the duodenum, jejunum, and ileum. The SI then empties into a blind-ended sac called the cecum, which connects the SI to the large intestine (LI); comprised of the colon and rectum. The SI, cecum and LI have distinct physiological functions. While the duodenum and jejunum are involved in the process of digestion, absorption of nutrients, and motility, the LI has 3 primary functions: absorption of water and electrolytes, production and absorption of vitamins, and formation and transport of feces for elimination.⁴⁹ Rodents have a large cecum, which acts as a reservoir for fiber-fermenting commensal microbes.⁴⁷ In humans, the cecum itself and the volume of microbes within it is much smaller, but this space still contributes significantly to facultative anaerobic fermentation.⁵⁰ The transit time within the SI is around 3-5 hours compared to around 30 hours in the colon, which allows the colon to foster more microbial diversity, richness and abundance than the upper tract.⁴⁸ The abundance of microbes in the adult SI (<10⁵ microorganisms per mL) is less than half of what is found in the LI (10¹²)⁴⁷, although interestingly disruptions to intestinal transit time can alter the volume of microbes within these regions.⁴⁸ Variation along the GI tract is not limited to its microbial inhabitants or nutrient uptake, indeed the oxygen content, pH level, and the production of metabolites (bile acids, SCFA, tryptophan) are also site-specific.⁴⁷

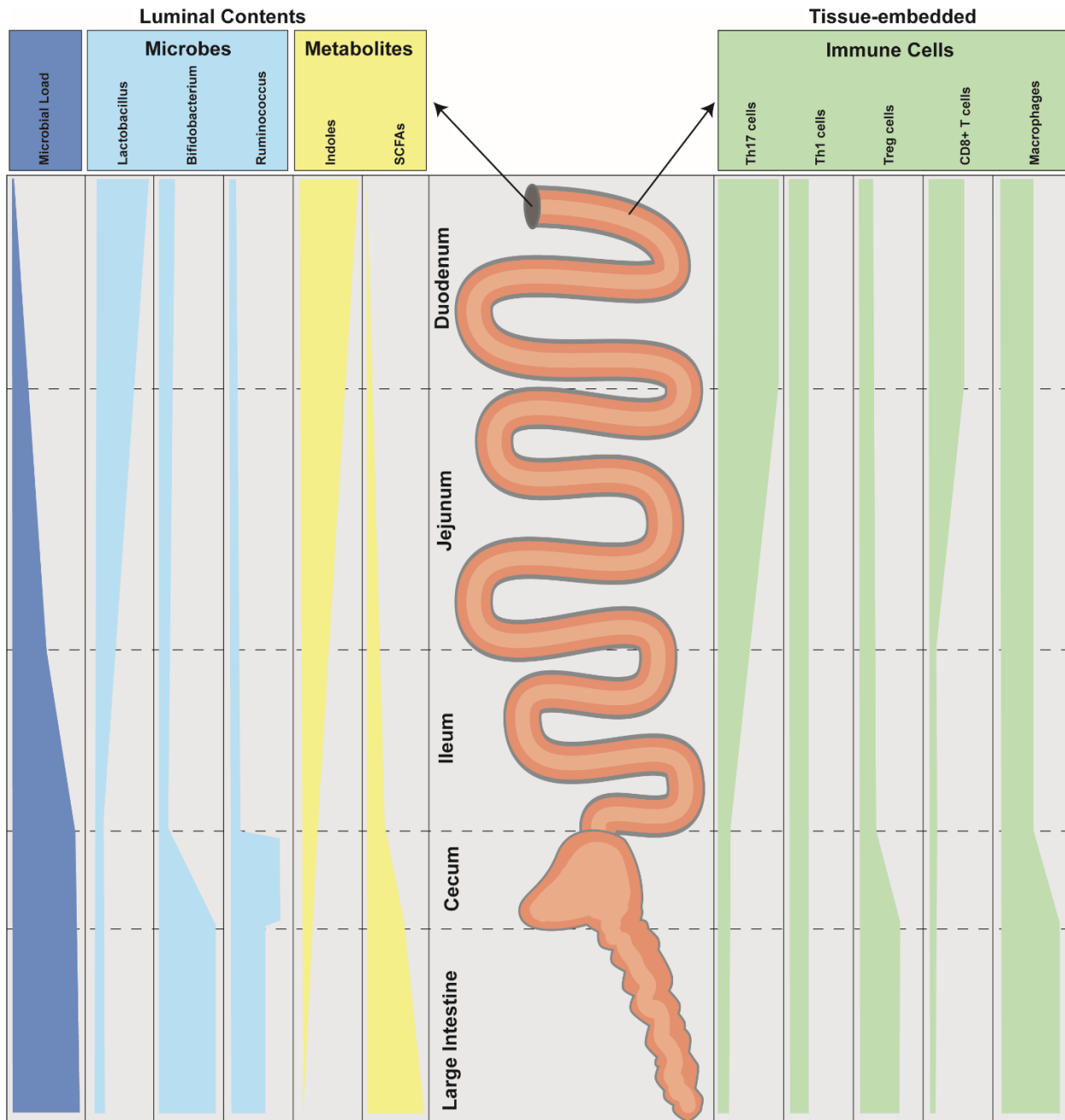


Figure 1. Regional specialization along the GI tract

Relative levels of luminal and tissue-embedded content are shown here reflecting host and microbiome dynamics within the GI tract. Microbial load, inhabitants, and the resultant microbially-produced metabolites can vary along the tract.^{47, 51} The graphic here illustrates one example of the luminal contents expected along the GI tract, although the regional dynamics are subject to interindividual or disease-specific modifications. Host immune regional specificity during homeostasis is also illustrated here, and corresponds to changes in the luminal contents.^{47, 52} Figure was inspired by Mowat & Agace⁴⁷, and was originally published in Avery et al.¹⁵ DOI: 10.1161/CIRCRESAHA.121.318065.

The GI tract tissue consists of several distinct layers: an epithelial layer which is closest to the luminal mucus, the lamina propria layer which sits beneath the epithelia and houses the largest compartment of intestinal immune cells, a thin muscular layer called the muscularis mucosa, followed by the submucosa which is muscular and rich with arteries, veins, lymphatics, and nerves, and lastly the serosa which separates the intestines from the peritoneum.⁴⁷ The lamina propria and the intestinal epithelium both house immune cells, though these spaces are immunologically distinct from one another.⁴⁷ While the epithelium mostly contains T cells, the lamina propria is rich in B cells, T cells, and a various innate immune subtypes like macrophages, dendritic cells and mast cells, to name a few.⁴⁷ Under healthy conditions, the tight epithelial layer prevents the invasion of pathogenic microbes while certain stimuli like inflammatory disease or a 'Western Diet' can lead to leaky gut syndrome.⁵³ Mucus lines the lumen of the GI tract, and the thickness of the mucus layer varies in different gut segments.⁴⁷ Mucus acts as a physical barrier against bacterial infections and can bind toxins.⁵⁴ Mucus can act as a nutrient source for specific mucus-degrading bacteria (e.g. *Akkermansia muciniphila*) and can be colonized by various microbes.^{55, 56} Loss of integrity of the colonic mucus layer increases host susceptibility to pathogens.^{56, 57} The symbiosis of humans and microbes is no doubt supportive for both parties under normal conditions, though the precarity of this interaction is palpable.

1.2.3 Inflammation and the gut microbiome

The intestines are continually exposed to immunomodulatory stimuli like food particles, food antigens, and a wide array of symbiotic and/or pathogenic organisms. Specialization of immune cells within the different gut compartments has led some to wonder whether GI segments should actually be considered independent organs.^{15, 58} A recent study demonstrated that regional distinctions within the microbiota from the human colon are associated with single-cell level alterations to immune cell composition and activity.⁵⁹ This small-scale regional specificity has been documented extensively in the literature. For example, Th17 and mast cells and Type 3 innate lymphoid cells are higher in the SI, whereas Tregs and macrophages cells are enriched in the LI.^{47, 58} While it can be difficult to determine whether this segment-specific immunity is a cause or a consequence of the GI microenvironment, it nevertheless has an impact on the presentation of various GI diseases. For example, ulcerative colitis and Crohn's disease typically impact the LI, and both have been associated with deficiencies in IL-10 production (a cytokine known to be produced by Treg cells).^{47, 58} Additionally, the metabolic status of the microenvironment can cause pathogenic bacteria to outcompete their commensal counterparts, for example, *Shigella flexneri* blooms in the LI under high oxygen conditions.^{58, 60} In the SI, the immature immune systems of children are also

believed to give rise to many more opportunistic infections, like SI bacterial overgrowth (SIBO), where a variety of normally commensal microbes build up and can cause inflammation, tissue damage, and even premature mortality.^{58, 61} Immunosuppression via antibiotic consumption is also a common cause of LI dysfunction by pathogens like *Clostridium difficile*.^{58, 62} Interestingly, restitution of healthy metabolic conditions within the GI tract was found to stimulate resistance to *Clostridium difficile* infection.⁶²

The high level of complexity and the wide range of microbial species within the GI tract makes it rather difficult to understand cause and effect. GF mice are an extreme but useful model system used to elucidate the impact of bacteria (either individually or as a community) on the host immune system and physiology. For example, colonization experiments with segmented filamentous bacterium in GF mice demonstrated the capacity of these bacteria to site-specifically induce Th17 cells.⁶³ Though there are drawbacks to using GF mice, in that they have increased gut permeability (which is reversible upon colonization)⁶⁴ and compromised immune cell function as well as irregular lymphoid organ development.⁶⁵ Furthermore, the feasibility of some interventions or surgical procedures can be limited when using GF mice, because maintaining sterile conditions is essential for proper use of the model.⁶⁶ Antibiotic-depleted mice have also been used to explore the impact of the microbiota on host physiology, although this model is less than ideal because of the unintended consequences of antibiotic treatment.⁶⁶ Antibiotic-depletion has been shown to induce fungal outgrowth and can stimulate the evolution and expansion of antibiotic-resistant bacterial strains.⁶⁶ Altogether, the GF model system is more easily controlled, and allows us to understand the effect of colonization with one or many species.

While several recent studies have shown that tissue-specific immunity is highly relevant to health and disease^{67, 68}, changes to the gut microbiome can have far reaching effects. For example, studies investigating a particular set of murine microbes which are derived from a “wild” environment rather than a lab setting was found to have a broad impact on immunity.^{69, 70} Wild and wildling mice (mice with microbes from the wild on a C57BL/6NTac background), compared with standard lab-raised mice, had much higher concordance of mouse data with the phenotypic results of clinical trials⁶⁹, and were more resistant to disease.⁷⁰ Importantly, the immune signature within the GI tract is not necessarily limited to this tissue space, and can interact with other organs which are distinct from the original site of inflammation per se. A recent paper used photolabeling to demonstrate that Th17 cells primed in the gut are able to traffic to the kidneys and impact inflammation distally.⁷¹ GI inflammation and microbial dysregulation is also thought to play a role in various autoimmune diseases like multiple sclerosis, arthritis,

and Type 1 diabetes, suggesting the broadscale inflammatory consequences of GI dysfunction.⁷² Furthermore, a recent study used high-resolution clinical metadata from hematopoietic cell transplantation (HCT) patients to show that day-to-day variation in the microbiome corresponds to immune cell changes in circulating peripheral blood mononuclear cells (PBMCs).⁷³ It is clear that while the microbiome is a potent regulator of local inflammation, other organ systems and tissues can also be impacted by shifts within the GI tract.

1.3 The microbiome in hypertension

1.3.1 Associations between the microbiome and BP

A growing body of clinical data has emerged showing an association between gut microbiome and hypertension and/or BP regulation.⁷⁴⁻⁸³ Data from the HELIUS cross-sectional study recently estimated that the microbiome explained 4.4% of systolic BP variance.⁷⁸ Of course BP regulation is complex and cross-sectional studies have a multitude of limitations, but this is a significant finding, considering that the many genetic associations with hypertensive disease altogether only explain 5.7% of BP variability.⁸⁴ Many human studies have identified that a reduction in alpha-diversity (a metric of microbial variance) associated with hypertension or increased BP.^{75-80, 83} Interestingly, fecal microbiota transplantation (FMT) in GF mice from a hypertensive human donor developed elevated systolic and diastolic BP after 8 weeks when compared to GF with a normotensive FMT donor.⁷⁶ The use of cross-species FMT is contentious because the protocols for these types of studies are not standardized.⁸⁵ Additionally, mice and humans only share about 15% of bacterial lineages⁸⁶, therefore it is possible that the reaction of GF mice to hypertensive FMT is not specific to the implanted microbes. Because microbes are so adept at niche-specific specialization⁸⁷, even implantation of defined species may not induce the desired effect and should be verified post-colonization.⁸⁸ Indeed, a recent study showed that the colonization of GF mice with human or rat microbes did not induce immune maturation, and only colonization with mouse-specific microbes was able to induce full immune competence.⁸⁹

An association between hypertension and the gut microbiome has been identified in several rodent models.^{21, 23, 24, 80, 90, 91} Dysbiosis has been identified in Ang II-infused mice²³, Dahl salt-sensitive rats⁹¹ as well as high salt-treated mice²¹ and deoxycorticosterone acetate-salt hypertensive mice.²⁴ A recent study found that the gut microbiota of stroke-prone spontaneously hypertensive rats (SHR) is dysbiotic and significantly different than normotensive Wistar-Kyoto rats (WKY); and FMT from stroke-prone SHR to

WKY controls increased the systolic BP of these otherwise normotensive rats.⁹⁰ In SHR rats, this microbial dysbiosis was additionally be linked to pathophysiological changes in the GI tract and compromised intestinal integrity.⁹² Nevertheless, only one study from Karbach et al. has attempted to estimate the overall contribution of the microbiome to hypertensive organ damage in an *in vivo* model; though this study utilized distinct C57BL/6J colonies of GF and conventionally raised (CONV) mice.⁹³ Isolation of lab-raised mouse communities for extended periods of time can cause divergence in the genetics, microbiome, and associated immune competency of sub-strains.⁹⁴⁻⁹⁶ Littermate controls are consequently a standardization technique for microbiome studies.^{97,98} The implications of not using littermates can be significant. For example, two recent studies suggested a role for Nlrp6- and ASC-mediated inflammasomes in shaping commensal gut microbiota composition^{99, 100}, although when the appropriate littermate controls were used these results were not reproducible.¹⁰¹ Therefore there is a unique opportunity to understand the microbiome in hypertension and hypertension-related organ damage with the use of appropriate littermate controls.

1.3.2 Immune mechanisms in hypertension: is the microbiome the missing link?

Immune mechanisms in hypertension have been recognized as a contributing factor to hypertensive disease since the late 1960's.¹⁰² Now experimental and clinical studies have demonstrated the important role that both innate and adaptive immune cells can play in BP regulation and the development of hypertensive end-organ damage.^{15, 16, 102-104} Although immune mechanisms in hypertension are still subject to ongoing research, immune cells have been shown to interact directly with the RAAS system.¹⁰² In fact, receptors for the active molecule Ang II are expressed by monocytes, macrophages, neutrophils, B cells and T cells.¹⁰² The accumulation of inflammatory T cells and macrophages has been shown to occur during the development of hypertensive organ dysfunction.¹⁰⁴ Pro-inflammatory effector memory T cells (T_{EM}), T_H17 and T_H1 promote hypertension and cardiovascular target organ damage, while Treg cells can ameliorate vascular, cardiac and renal damage.¹⁰⁵⁻¹¹⁰ Myeloid derived suppressor cells¹¹¹, dendritic cells (DCs)¹¹², gamma delta T cells ($\gamma\delta$)¹¹³, and macrophages¹¹⁴ have all been shown to influence hypertension as well. In addition to the physical deposition of immune cells in target organs, cytokine secretion from these and other immune cells (e.g. Th17 secretion of Il-17, Th1 secretion of IFN γ , macrophage or DC secretion of Il-6) have been shown to impact vascular and renal function.¹⁰⁴ For example, Il-17 has been shown to contribute to elevated BP and vascular dysfunction in the presence of Ang II, which was not observed in Il-17-deficient mice.¹⁰⁷ Additionally, circulating levels of Il-6 have been shown to correlate

positively with BP in patients.¹¹⁵ Il-6 is also known to contribute to the induction of CD4+ T cells towards an Il-17 producing phenotype.¹⁰⁴ The CANTOS trial also showed that anti-inflammatory treatment targeting Il-1 β was effective at reducing cardiovascular events in patients with a history of CVD.¹¹⁶

As detailed in section 1.2.3, the microbiome plays a significant role in the modulation of inflammation in multiple organ systems. Because of the documented importance of inflammation in hypertension, the microbiome garnered significant attention in recent years. Recent evidence has shown that bacteria can communicate with different immune cells involved in CVD. For example, dendritic cells were shown to increase in salt-responsive hypertension and were associated with underlying microbial dysbiosis in mice.¹¹⁷ Additionally, our group recently demonstrated a high-salt challenge in patients was able to reduce GI *Lactobacillus spp.*, which was associated with an increase in Th17 cells and an elevation of BP.¹¹⁸ An increase in the circulating lipopolysaccharide (LPS) has also been documented in patients with hypertension.⁸¹ LPS, an endotoxin derived from the outer membrane of gram-negative bacteria, should normally be retained within the intestinal lumen, but under pathological conditions with compromised intestinal integrity, LPS can enter the circulation, and is a potent inducer of inflammation.⁸¹

1.3.3 Metabolites as mediators of the host-microbiome interaction in hypertension

It has been suggested that the mechanism by which the microbiome can impact host immune function in hypertension is mediated by metabolites. This concept is not unique to hypertension; indeed, metabolites of microbial origin have been found to facilitate the communication between the host immune system and its microbial inhabitants in several other disease states. For example, indole metabolites produced by *Lactobacillus* metabolism of tryptophan have been found inhibit fungal infection and inflammation in colitis via increased Il-22 production.¹¹⁹ Additionally, bacterially-derived polyamine metabolites (spermidine, spermine, putrescine) have been shown to influence macrophage activity in the colon, and the metabolite putrescine was found to ameliorate DSS-induced colitis.¹²⁰ The interplay between host-produced and microbially-produced metabolites has been unexplored in the context of hypertension, though in other disease states, both have been documented as mediators of the host-microbiome interaction. A recent study found that host-produced serotonin was able to alter bacterial communities within the gut which in return led to changes in host metabolite production, indicating bi-directional communication between the host and microbiome.¹²¹ Furthermore, it was shown that in obesity, there is a shift from the metabolism of tryptophan by microbes into indoles towards the production of kynurenine

by the host enzyme Indoleamine 2, 3-dioxygenase.¹²² Knockout of this tryptophan metabolizing enzyme rescued the phenotype, suggesting that the interplay between host and microbial tryptophan metabolism has implications for the progression of disease.¹²² Furthermore, host conjugation of microbially-produced metabolites often occurs when they reach the liver through uptake via the portal vein. Conjugation of p-cresol and indole produces the end-products P-cresol sulfate or P-cresol glucuronide as well as indoxyl sulfate (IS), respectively.¹²³ Normally P-cresol metabolites and IS are easily cleared, but they are known to build up in chronic kidney disease as a result of kidney dysfunction. They have been suggested to participate in a wide range of pathogenic processes contributing to cardiovascular and overall mortality in patients.¹²³ These metabolites may play a role in hypertension as well, although it is unclear whether their activity is relevant at lower titers typical to those with intact kidney function.

Microbially-produced metabolites have been found to have pro- and anti-inflammatory activity in hypertension and CVD. The suspected interplay between microbes, metabolites, and hypertension is summarized in Figure 2. Short-chain fatty acids (SCFA) such as acetate (C2), propionate (C3), and butyrate (C4), are perhaps the most well-documented anti-inflammatory metabolites that have been shown to reduce BP in humans and animal models.^{23-25, 75, 78} The fermentation of dietary fiber by bacteria in the colon leads the production of SCFA.¹²⁴ C2 has been shown to ameliorate hypertensive cardiac and renal damage in mice.²⁴ Our group recently demonstrated that treatment with C3 is protective against Ang II-induced inflammation and cardiovascular damage, and this metabolite acts in a Treg-dependent manner.²⁵ Two clinical studies also found that decreased abundance of SCFA producing bacteria is associated with increased BP.^{78, 125} Another metabolite produced through bacterial metabolism called Indole-lactic acid (ILA) was shown to suppress Th17-driven inflammation in salt-sensitive hypertension.²¹ Metabolites of microbial origin can exacerbate disease in some contexts. For example, pro-inflammatory metabolites like trimethylamine N-oxide (TMAO) and 3-hydroxyanthranilic acid (a tryptophan metabolite) have been shown to aggravate atherosclerosis and CVD.^{126, 127}

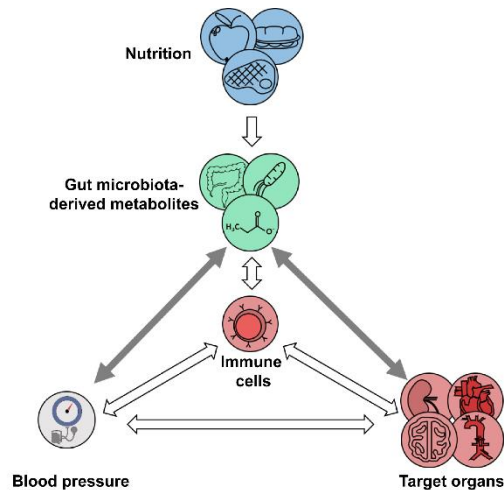


Figure 2. The host-microbiome interaction in hypertension

Food consumed by the host is metabolized by microbes along the GI tract into small metabolites. Inflammation and immune cell activity are regulated by microbially-derived metabolites, food antigens and microbes, among other things. The interaction between hypertension and the microbiome is thought to be primarily mediated by the immune system, and perturbations to the host-microbiome symbiosis can result in BP changes, as well as hypertensive heart, vascular, brain, or kidney damage. This figure was adapted from Avery et al.¹⁵ DOI: 10.1161/CIRCRESAHA.121.318065.

1.4 Interstitial fluid as a window into the microenvironment in the GI tract

1.4.1 Regional specificity of the host-microbiome axis

The dynamic uptake of metabolites into the circulation in hypertension is not well-understood. Whether metabolite levels in the feces, serum, or in some other compartment should be considered relevant for health and disease is still debated. While metabolites have been suggested to mediate the host-microbiome interaction via the immune system; whether metabolites can also reach the distal target organ to effect function is unknown. As the field of microbiome research in the context of hypertension is still young, there is a large opportunity to begin to understand how the host-microbiome interaction occurs during disease, and how this contributes to the mosaic of hypertension. Given the known interaction between metabolites of microbial origin and host immune function in health and disease (see section 1.2.3 and 1.3.2), naturally the mechanisms by which these compounds interact with immune cells is of interest. While *in vitro* experiments can demonstrate the effect of metabolites on primary cells, we are limited currently in our ability to capture the signature within the GI microenvironment. Contents of the luminal space or the serum are currently the accepted modality to assess metabolite changes associated with microbial production in the gut.^{128, 129} Whether the excretory products are representative of what is being experienced in the host is unknown. Serum can also be used to investigate which microbial

metabolites reach the systemic circulation, although this presents additional challenges. Are all metabolites relevant for the immune-microbiome axis capable of reaching the systemic circulation? Are titers high enough to be quantifiable? Additionally, do the tissue levels differ significantly from circulating levels of a given metabolite? Because immune cell composition and function has been shown to vary significantly across different GI segments⁵⁹, one would suspect the same is true for metabolites within the tissue. To begin to answer some of the questions mentioned above, having a method to access the microenvironmental space within the GI tract would be of high utility.

SCFA present a unique example of a subset of metabolites which would be of interest at the site-of-action in the gut. The luminal contents of the LI have about 4-fold higher C3 and C4 levels when compared to the SI.¹³⁰ As SCFAs have been documented several times in various disease contexts, many have wondered about the relevant compartment to measure SCFA levels. Interestingly, patients with low abundance of SCFA producing bacteria documented by NGS were found to have increased levels of SCFA in their fecal matter⁷⁸; which perfectly exemplifies the challenge of using excretory products as a read-out. Fecal SCFA levels do not necessarily reflect the SCFA levels within the host, but rather reflects the SCFA generated in the gut which was not absorbed in the intestines. This notion is supported by experimental work in SHR rats, which showed that in hypertension the luminal cecal levels of C3 were increased, but the serum C3 was reduced.¹³¹ This discrepancy in hypertensive rats between the luminal SCFA and serum levels when compared to their non-hypertensive counterparts was attributable to the reduced expression of Slc5a8 transporters which facilitate the entry of SCFA into the GI epithelium.¹³¹ A recent study also showed that while SCFA serum levels were associated with insulin sensitivity and other obesity-related parameters, a link to fecal SCFA was not found.¹³² SCFAs are thought to be rapidly absorbed in the colon¹³³, and through the isolation of colonic epithelial cells, the utilization of C4 as an energy source for metabolism within these cells was demonstrated.¹³⁴ Of note, intestinal SCFAs are much higher compared to portal blood, whereas SCFA are higher in the portal, then hepatic blood, and least in the peripheral blood, suggesting SCFA are substantially taken up by the liver.¹³⁰

Many metabolites mediate the activity of host cells via interactions with surface receptors. G-protein coupled receptors are thought to mediate the interaction between microbially-produced metabolites and various cell types in the lamina propria and are considered the main mediators of nutrient-sensing in the GI tract.¹³⁵ For example, SCFA are also known to interact with immune cells via g-protein coupled receptors GPR109A and GPR43.¹³⁶ Furthermore, amino acids and amino acid metabolites, bile acid

metabolites, and even traditionally intracellular metabolites like succinate can exit the cell and act as signaling molecules via GPCRs in the gut.¹³⁵ Commensal microbes, whether accidentally or by design, are known to produce GPCR ligands which were found to be as effective as human endogenous ligands at regulating glucose homeostasis and metabolic hormone regulation.¹³⁷ Although some important interactions in the gut do involve metabolite entry into the intracellular space, like histone deacetylase regulation by SCFA¹³⁸ or aryl hydrocarbon receptor activity mediation by tryptophan metabolites^{119, 139}, one would nevertheless expect a pool of available microbial metabolites to be found where they have been absorbed in the host in the IF. A graphical representation of the expected interactions between metabolites produced by the gut microbiome and the host immune cells within the GI microenvironment are shown in Figure 3.

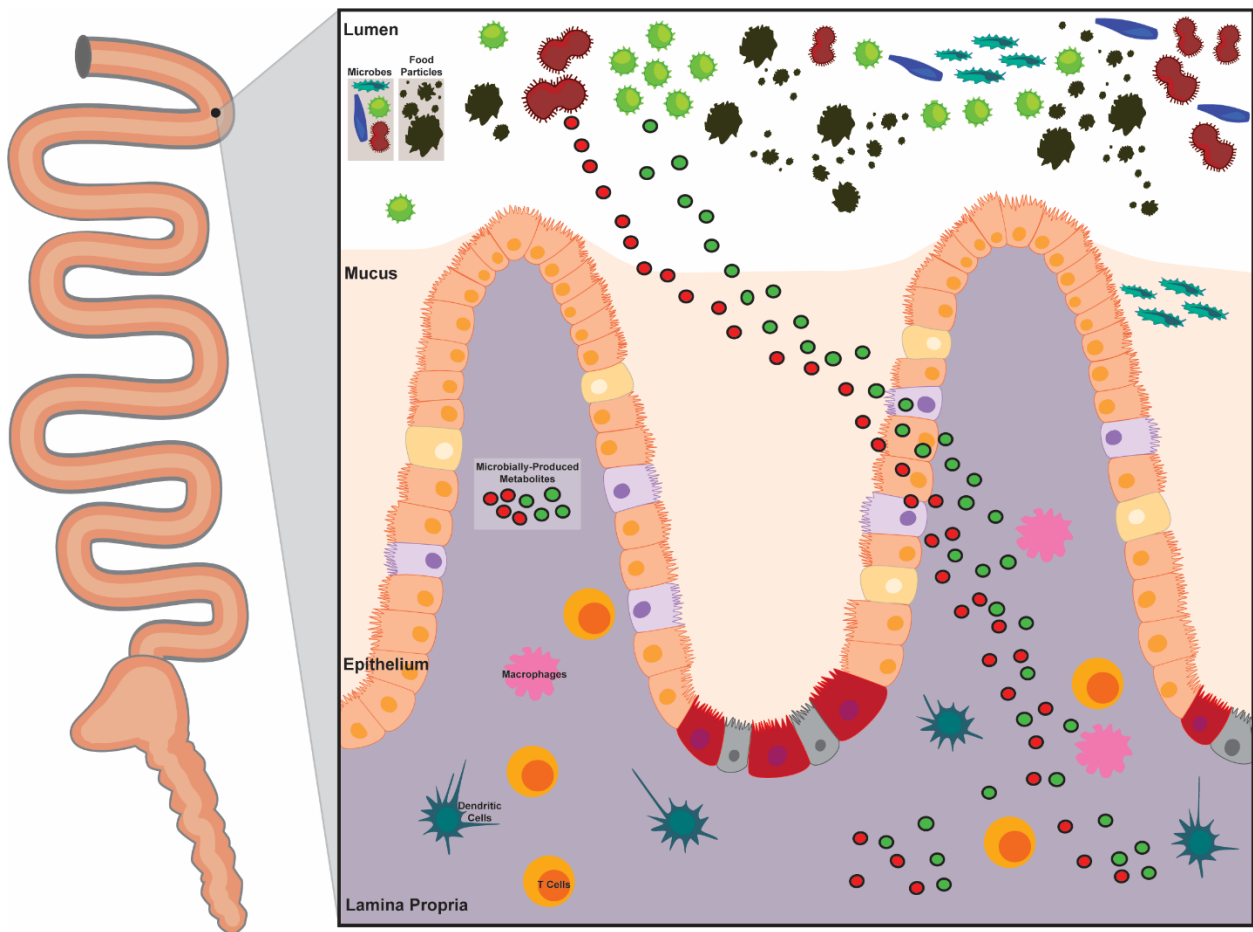


Figure 3. Schematic of the GI microenvironment

On the left, the entire GI tract is shown, on the right, there is a proposed scheme of the microenvironment from that selected subsection of SI. As shown above, the GI lumen is rich in bacteria, and is the compartment housing food particles which in the latter parts of the colon will form into fecal pellets. Metabolites which are produced by microbes have been suggested to pass through the GI epithelium and

enter the host to interact with various types of immune cells. I propose that the extracellular space or IF derived from the GI tissue should be rich in these metabolites and molecules of microbial origin.

1.4.2 Interstitial fluid biology principles and relevance within the GI tract

IF is simply defined as the fluid found in the spaces between the cells of a tissue, the tissue's structural components known as the extracellular matrix (ECM), and the capillaries.¹⁴⁰ The ECM is rich in collagen fibers which provide structure and negatively charged glycosaminoglycans (GAGs) that are important for tissue hydration, whereas the IF has an electrolyte concentration closely resembling that of plasma and a plasma protein concentration ~50% of that of plasma.¹⁴⁰ The IF represents one of the major fluid compartments of the body. The extracellular fluid volume (ECV), is comprised of mostly interstitial fluid volume (IFV), and a small percentage of plasma volume.¹⁴¹ This interstitial space itself varies significantly depending on the tissue of origin. The amount of IF in the skin accounts for almost 50% of the tissue's wet weight whereas muscular tissues are close to around 10%.¹⁴⁰ The high density of structural elements within the IF like GAGs and collagen can make it difficult to access the IF from low-volume spaces.¹⁴⁰ Accessing the IF within different organ systems requires a wide range of methods which both directly and indirectly attempt to quantify IF components.^{140, 142} Conceptually, each of these methods aims to access this space, while leaving the surrounding cells intact and not disturbing the intracellular contents. I pursued IF methods with end-point measurements, which could be applied with minimal risk of tissue injury or destruction. Two of the most common extraction methods are the centrifugation-based and elution-based approach¹⁴², which are technically described in greater detail in section 3.2. To determine the validity of an IF extraction method, i.e. to what extent the method reflects bona fide IF, the concentration of ions relative to the plasma can be measured, though the gold-standard evaluation, especially for the centrifugation-based approach, employs the extracellular tracer ⁵¹Cr-labelled EDTA.¹⁴² The amount of the tracer, which equilibrates only in the extracellular fluid phase and does not pass intracellularly, relative to the plasma concentration gives an approximation of whether the harvested fluid is deriving from the extracellular fluid phase only¹⁴² and is technically described in detail in section 3.2.

IF is often referred to as pre-lymphatic fluid, because interstitial flow is constantly emptying fluid which is filtered from the blood capillaries into the interstitium, and subsequently the IF is taken up and returned to the systemic circulation via the lymphatic vasculature.¹⁴³ The GI tract is dotted with lymph nodes, where draining lymph empties and interacts with immune cells before being drawn into the broader network of lymphatics.⁵⁸ Immunologically, SI and colonic tissues are believed to be distinct compartments, in part

because the draining lymph nodes for these segments are anatomically separated.⁵⁸ Interestingly, in mice the duodenum and the pancreas share draining lymph nodes, and the impact of this co-drainage from multiple organs is not well-understood.^{58, 144} Lymph may be classified as afferent or efferent depending on whether it is transported to or from the lymph node, respectively. The proportions of immune cells (T cells, B cells, DCs) within these lymphatic fractions as well as the lymph node itself have been shown to differ significantly from one another.¹⁴⁵ The lymph undergoes several modifications within the lymph node, as the immune cells and lymph from collecting lymphatics are pooled together from different regions of origin (perhaps even multiple organs) in this compartment.^{58, 140} Accordingly, while prenodal lymph can be considered as representative of the local IF¹⁴⁰, postnodal lymph (which is most frequently sampled) is not representative of the IF or lymph which is native to the original tissue space.¹⁴⁶ While the composition of immune cells in the gut⁴⁷, in the draining lymph nodes¹⁴⁴, and in distal organ systems¹⁶ has been the subject of several investigations, the contents of the IF (i.e. the microenvironment which gives rise to said immune cells) itself has been mostly ignored. Although the IF space within the GI tract is surely of interest to understand the regional interactions between the microbiome and the host (detailed in 1.4.1), to our knowledge, this has not been explored previously.

The importance of tissue specificity is not a new concept, but recent technological advancements have contributed to the growing body of literature suggesting that tissue specific genetic and metabolic information is more informative than broadscale genetic screenings for example.^{68, 147-149} Indeed, tissue-specific genetic signatures are more predictive than unbiased genetic information of cancer outcomes¹⁴⁷ and the side effects experienced in clinical trials¹⁴⁸. Furthermore, a recent study in COVID-19 patients showed that while some disease-specific inflammatory immune cells could be found in both blood and airway samples, the dynamic regulation of immune cells at the site-of-action was only identifiable when comparing these spaces.^{68, 149} Many immune cells never reach the systemic circulation, which stands to reason why during active inflammation, the blood might not be the best place to look for cues about disease activity or progression.⁶⁸ Furthermore, the local signature of T-cells within the airways was predictive of survival and was uniquely identifiable within the airway samples.¹⁴⁹

IF has been used to uncover tissue-specific microenvironmental signatures present in the extracellular space. Proteomic contents of the tumor interstitium have been used to identify potential drug targets or novel early-detection biomarkers in breast, renal, hepatic, and ovarian carcinomas, to name a few.¹⁴² IF in the skin has also been used to demonstrate that following ischemia-reperfusion injury or LPS injection,

there is an immediate increase in inflammatory cytokines $IL-1\beta$ and $TNF\alpha$ in the IF, but not the serum.¹⁵⁰ Measuring serum cytokine expression would have led to the conclusion that no inflammatory stimulus had been experienced by the host¹⁵⁰, demonstrating the importance of measuring the contents of the IF locally in the site where the inflammation occurs. IF extraction from dental pulp has similarly been used to demonstrate how local LPS injection leads to a change in the local inflammatory cytokine signature which was not reflected in the serum.¹⁵¹ Galectin-1 (LGALS1), a protein known to be involved in immune regulation, was also found to be enriched in IF isolated by microdialysis from the human abdominal adipose tissue in type-2 diabetes patients.¹⁵² In summary, the use of IF to identify novel regulators of health and disease has been validated for other organ systems. As the GI tract acts as the interface between the host and its microbial symbionts, the IF is likely to be rich with both host-produced and microbially produced cytokines, metabolites, and proteins. The isolation of GI IF represents a novel route to advance our understanding of the host-microbiome interaction in health and disease.

2. Study aims

2.1 Define the contribution of the gut microbiome in hypertension

The intestinal microbiota has been demonstrated to influence hypertensive end-organ damage, particularly as it relates to the inflammatory component of the hypertensive sequelae. The aim of this portion of my thesis was to determine the overall contribution of the gut microbiome to the pathogenic response to hypertension, using GF mice and colonized (COL) littermate mice with Ang II and 1% NaCl-induced hypertension.

2.2 Develop novel methods for the isolation of interstitial fluid from the GI tract

Stool samples, because they are easily accessible, are often used to analyze the metabolites and microbial bi-products involved in the host-microbiome interaction within the GI tract. However, whether this reflects what is absorbed into the host is still a matter of debate. There remains a logistical problem with measuring the impact of microbially-derived metabolites on the host, in that the expected “site-of-action” is inaccessible. To this end, I aimed to develop and optimize tools to isolate IF from the regional sites-of-interest along the GI tract. Additionally, I sought to examine the IF in comparison with the fecal matter and the serum, to understand how the dynamic interactions between the host and its microbial inhabitants are represented within each of these compartments.

3. Materials and methods

3.1 Germ-free hypertensive mice

3.1.1 Animal Protocol

All animal experiments complied with the German and European law animal protection regulations and were preapproved by the local ethics committee (G0280/13, G0028/21, X9009/18). Mice were provided unlimited access to food and water, and maintained on a 12:12, light: dark cycle throughout the experiment. Wild-type GF C57BL/6J (GF) mice were bred and kept in an isolator system, unless otherwise specified (Metall+Plastic). GF mice used for *in vivo* experiments received sterile water using the Hydropac system (Plexx B.V.). Mice were fed autoclaved standard breeding chow (V1124, Ssniff). Until week 4, all mice were maintained in GF conditions. At 4 weeks, male mice were randomized to either remain GF until week 14 or receive passive bacterial colonization (COL). COL mice were transferred to the regular specific pathogen free (SPF) animal facility. Colonization was initiated by placing formerly GF mice into soiled cages from healthy wild-type male C57BL/6J mice. Because mice are coprophagic, oral consumption of microbes, as well as interaction on the skin surface was possible. After cage transfer, COL mice received sterilized tap water as drinking water. At week 12, COL and GF treatment group mice received Angiotensin II (Ang II, 1.44 mg/kg/d; Calbiochem) by subcutaneous infusion via an osmotic minipump (Alzet) and 1% NaCl (Carl Roth) in the drinking water. For GF mice, 1% NaCl was sterilely injected into the Hydropac system with a syringe and a self-sealing silicon patch (Plexx B.V., Elst, Netherlands). The experimental design is shown in Figure 4. HTN is henceforth used as shorthand for hypertension (Ang II and 1% NaCl) in figures. Minipumps were implanted under sterile conditions and throughout the experiment GF mice remained sterile verified by thioglycolate and 16s PCR, detailed in sections 3.1.5 and 3.1.13, respectively. After two weeks of Ang II + 1% NaCl or sham treatment, all mice were euthanized by isoflurane anaesthesia and blood, spot urine (where possible), feces, and organs were collected. Further experiments performed on these mice or derived from these tissues are listed throughout section 3.1, apart from section 3.1.8 and 3.1.15. Animal handling was executed by animal caretakers at the Max-Delbrück-Center (MDC) or Dr. Nicola Wilck, Gabi N'diaye, and Dr. Hendrik Bartolomaeus as members of the Mueller/Dechend Lab at the Experimental and Clinical Research Center (ECRC) in Berlin-Buch.

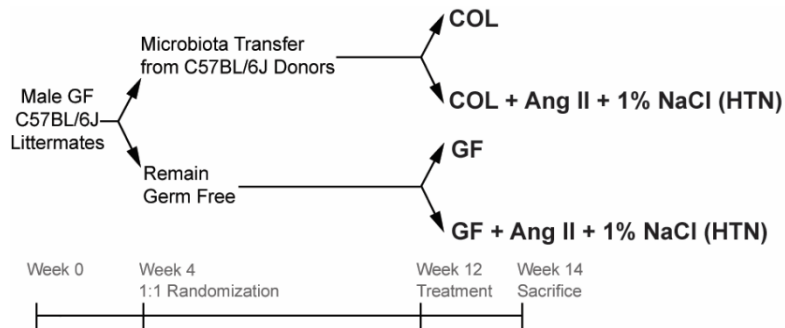


Figure 4. Schematic of GF project experimental design

GF littermates were randomized at 4 weeks to be colonized with SPF microbiota (COL) or kept under GF conditions. At 12 weeks, we induced hypertension by subcutaneous Ang II infusion and 1% NaCl-supplemented drinking water (abbreviated as HTN in figures). Throughout n numbers are as follows; GF Sham n = 5, GF + HTN n = 12, COL Sham n = 5, COL + HTN n = 12. After 14 days, mice were sacrificed, and data was collected to analyze hypertensive end-organ damage. Dr. Nicola Wilck, Dr. Dominik N. Mueller and Dr. Hendrik Bartolomaeus contributed the animal protocol. Animal handling for these experiments was performed by Dr. Hendrik Bartolomaeus, Dr. Nicola Wilck, and Gabriele N'diaye (ECRC, Berlin).

3.1.2 Echocardiography

Echocardiography was performed in week 14 as described by Markó et al.¹⁵³ at the MDC Animal Phenotyping Technology Platform (Dr. Martin Taube; MDC, Berlin). All measurements were performed by an experienced reader blinded to the experimental protocol. Mice were anesthetized with isoflurane and examined on the VisualSonics Vevo 2100 system using a 30 MHz-Transducer (MS-400, VisualSonics). Left ventricular wall thickness was analyzed using M-mode images from the parasternal short-axis view.

3.1.3 Splenic immunophenotyping

After mice were euthanized, spleens were removed and kept at 4 °C in a buffer comprised of PBS (Gibco), 0.5 % bovine serum albumin (BSA, Sigma Aldrich), and 2 mM EDTA (Sigma Aldrich). Single-cell suspensions were obtained using 70 µm strainers, followed by erythrocyte lysis, and were then filtered through a 40 µm mesh. Cells were counted under a microscope using trypan blue and 10⁶ live cells were taken per sample for staining with each respective multicolor flow cytometry panel. All measurements included dead cell exclusion using Live/Dead Fixable Aqua Dead Cell Stain Kit, for 405 nm excitation (Thermo Fisher). Cells were stained with surface antibodies in the PBS + 0.5 %BSA + 2 mM EDTA buffer, together with Fc blocking reagent (Miltenyi) for 30 min at 4 °C. Intracellular antigens were stained using FoxP3 Staining Buffer Kit (eBioscience). Respective intracellular antibodies were incubated for 30 min on ice. All antibodies used for analysis are listed in Table 2 (found in section 3.1.15). Data was recorded on a BD FACS

Canto II (BD Biosciences) using BD FACS Diva software (BD Biosciences). Antibody panels were designed by Hendrik Bartolomaeus and staining was performed by Hendrik Bartolomaeus and Nicola Wilck (ECRC, Berlin). I performed the analysis of immunophenotyping data in FlowJo (TreeStar).

3.1.4 Urine analysis

Spot urine was collected from a subset of experimental mice upon sacrifice. All parameters were measured with the AU480 clinical chemistry analyzer (Beckman Coulter) according to the manufacturer's instructions. The measurement of urinary albumin was done by a turbidimetric approach, where absorption of light is proportional to the albumin concentration. The measurement of creatinine was done by an enzymatic conversion of creatinine and colorimetric quantification of the reaction at the Animal Phenotyping Platform (MDC, Berlin).

3.1.5 Bacterial growth in thioglycolate medium

To verify the GF status of GF mice upon sacrifice, fecal pellets were collected on the last day of life and placed immediately into thioglycolate medium in a 5 mL tube. Thioglycolate medium allows for the growth of obligate aerobes, obligate anaerobes, facultative anaerobes, microaerophiles, and aerotolerant organisms; and thus represents a simple way to identify colonizing microorganisms within fecal matter. After 96 hours of incubation, bacterial growth was examined by eye and compared to a positive control, which were pellets from colonized C57BL/6J mice with a full range of SPF bacteria. Negative control used was a filled thioglycolate tube with no fecal pellet inside.

3.1.6 Histological analysis of renal and cardiac tissue

Upon sacrifice, heart and renal tissues were immediately frozen in -40 °C isopentane and stored at -80 °C for further use. Staining was performed on 5 µm cryosections fixed in -20 °C acetone for 10 minutes. Unspecific binding was blocked with 10 % normal donkey serum (NDS) for 2 hours.

Cardiac cryosections- Primary antibodies were diluted in 10 % NDS (anti-CD4 (H129.19), BD Pharmingen, 1:75; anti-CD8a (53-6.7), BD Pharmingen, 1:100; anti-CD3-A647 (17A2), BioLegend, 1:50; anti-F4/80 (A3-1), Abcam, 1:100; anti-type I collagen (polyclonal), Southern Biotech, 1:100; anti-fibronectin (polyclonal), Abcam, 1:400) and incubated overnight at 4 °C in a humid chamber. Cy3-conjugated secondary antibodies were diluted in PBS for 2 hours at room temperature (RT) (anti-goat-IgG-Cy3 (polyclonal), Jackson

ImmunoResearch, 1:300; anti-rabbit-IgG-Cy3 (polyclonal), Jackson ImmunoResearch, 1:400; anti-rat-IgG-Cy3 (polyclonal), Jackson ImmunoResearch, 1:200) and incubated at room temperature for 2 hours. Cardiac interstitial fibrosis was analyzed from fibronectin staining, by examining the Cy-3 positive area in five representative high-power fields (HPF, 40x) of crosscut cardiomyocytes per heart slide using ImageJ software (open source) with a mean threshold for the Cy3-positive area. Cardiac perivascular fibrosis was quantified using type I collagen immunofluorescence. Cy3-positive fibrosis area was measured using CaseViewer software (3D Histech) and normalized to the mean vessel area. Representative images of interstitial and perivascular fibrosis were taken at 80x magnification in CaseViewer. CD4- and CD8-specific antibodies were used to quantify these immune cells per heart slide in CaseViewer, by identifying the fluorescence of each antibody found in close association with a DAPI-positive nuclei. F4/80 and CD3-positive (with DAPI-positive nuclei) cells were counted and quantified in five high-power fields (HPF, 40x) per heart section using CaseViewer.

Kidney cryosections- Primary antibodies were diluted in 10 % NDS (anti-CD4 (H129.19), BD Pharmingen, 1:100; anti-CD8a (53-6.7), BD Pharmingen, 1:100; anti-F4/80 (A3-1), Abcam, 1:100; anti-CD45 (D3F8Q), Cell Signalling, 1:200; anti-CD3-A647 (17A2), BioLegend, 1:50; anti-Nephrin (polyclonal), RD Systems, 1:20) and incubated overnight at 4 °C in a humid chamber. Cy3-conjugated secondary antibodies were diluted in PBS (anti-goat-IgG-Cy3 (polyclonal), Jackson ImmunoResearch, 1:300; anti-rabbit-IgG-Cy3 (polyclonal), Jackson ImmunoResearch, 1:400; anti-rat-IgG-Cy3 (polyclonal), Jackson ImmunoResearch, 1:200) and incubated at room temperature for 1-2 hours. For the analysis of Nephrin, five evenly distributed HPF (20x) from the cortical region were taken per sample in CaseViewer. Image analysis for Nephrin was subsequently performed using FIJI software (open source), and only Glomeruli that had their main body in the section plane (round, comparably sized) were chosen for analysis. Glomeruli were manually selected, and the mean fluorescence intensity was measured within the area of each glomerulus. Representative images of one glomerulus per group was taken with an 80x magnification in Caseviewer and equally color adjusted in FIJI. Infiltrating immune cells were counted as CD4-, CD8-, F4/80-, CD45- and CD3-positive (with DAPI-positive nuclei) cells and quantified in five high-power fields (HPF, 40x) equally dispersed in the cortical region of each kidney section using CaseViewer software (3D Histech). Kidney tissue was additionally fixed in 4% formalin PBS solution, washed after 24 to 72 hours in PBS, and then embedded in Paraffin and cut to 3 µm. Formalin fixed tissue was stained with Masson's trichrome using standard protocols. Perivascular fibrosis of the kidney was quantified as described above using Masson's trichrome staining.

All histological stainings were scanned using a Panoramic MIDI II slide scanner (3D Histech). Ariana Rauch and Dr. Hendrik Bartolomaeus assisted with kidney nephrin analysis and T cell quantification in the kidney (ECRC, Berlin), and I performed all other heart and kidney histological analyses.

3.1.7 Quantitative real-time RT-PCR of renal and cardiac tissue

Half of one kidney and the apex of the heart were shock-frozen in liquid nitrogen and stored at -80 °C upon sacrifice. RNeasy Mini Kit (QIAGEN) was used for isolation of RNA following the manufacturer's protocol. RNA concentration and quality were determined using a NanoDrop-1000 Spectrophotometer (PeqLab). cDNA was synthesized from 2 µg RNA using the Applied Biosystems High-Capacity cDNA Reverse Transcription Kit (Thermo Fisher). TaqMan or SYBR Green assays were used to quantify target gene expression using the standard curve method on a QuantStudio 3 (Thermo Fisher). Target mRNA expression was normalized to the *18S* housekeeping gene, which was evaluated for its appropriateness compared to other housekeepers prior to use. All primers and probes were designed and validated in the Mueller/Dechend lab (ECRC, Berlin) prior to use. Primers and Probes were designed using PrimerExpress 3.0 (Applied Biosystems) and synthesized by BioTeZ Berlin-Buch GmbH. All primer and probe sequences are provided in Table 1.

Table 1. qPCR primer and probe information

Gene		Sequences (5'→3')
18s	for	ACA TCC AAG GAA GGC AGC AG
	rev	TTT TCG TCA CTA CCT CCC CG
	probe	FAM – CGC GCA AAT TAC CCA CTC CCG AC – TAMRA
Havcr-1	for	CTG GAG TAA TCA CAC TGA AGC AAT C
	rev	GAT GCC AAC ATA GAA GCC CTT AGT
	probe	FAM – CTC CAG GGA AGC CGC AGA AAA ACC – TAMRA
Lcn2	for	TGA TCC CTG CCC CAT CTC T
	rev	GGA ACT GAT CGC TCC GGA A
	probe	FAM – TCA CTG TCC CCC TGC AGC CAG A – TAMRA
S100a8	for	TCA CCA TGC CCT CTA CAA GA
	rev	CCA ATT CTC TGA ACA AGT TTT CG
S100a9	for	TCA GAC AAA TGG TGG AAG CA
	rev	GTC CAG GTC CTC CAT GAT GT
Col1a2	for	CTA CTG GTG AAA CCT GCA TCC A
	rev	GGG CGC GGC TGT ATG AG
	probe	FAM – CCC ACC CTG TAA ACA CCC CAG CGA AG – TAMRA
Col3a1	for	CTC ACC CTT CTT CAT CCC ACT CTT A

	rev	ACA TGG TTC TGG CTT CCA GAC AT
Tgfb1	for	CCC GAA GCG GAC TAC TAT GC
	rev	TAG ATG GCG TTG TTG CGG T
Vcam1	for	CTA CAA GTC TAC ATC TCT CCC AGG AA
	rev	CAC AGC ACC ACC CTC TTG AA
	probe	FAM – ACA ACG ATC TCT GTA CAT CCC TCC ACA AGG – TAMRA
Icam1	for	CAG TCC GCT GTG CTT TGA GA
	rev	CGG AAA CGA ATA CAC GGT GAT
	probe	FAM – CTG TGG CAC CGT GCA GTC GTC C – TAMRA
Tnfa	for	CGT CCC CAA AGG GAT GAG AA
	rev	TGA GGG TCT GGG CCA TAG AA
	probe	FAM – TTC CCA AAT GGC CTC CCT CTC ATC A – TAMRA
Ccl2	for	GGC TCA GCC AGA TGC AGT TAA
	rev	CCT ACT CAT TGG GAT CAT CTT GCT
	probe	FAM – CCC CAC TCA CCT GCT GCT ACT CAT TCA – TAMRA
Il1b	for	CGT GGA CCT TCC AGG ATG AG
	rev	GAG GAT GGG CTC TTC TTC AAA G
Il6	for	GTT GCC TTC TTG GGA CTG ATG
	rev	GGG AGT GGT ATC CTC TGT GAA GTC T
	probe	FAM – TGG TGA CAA CCA CGG CCT TCC C – TAMRA
Fn1	for	GGA CCT GCA AAC CTA TAG CTG AGA
	rev	CTC CCC CAC GAC GTA GGA
	probe	FAM – TGT TTT GAT CAT GCT GCT GGG – TAMRA
Nppb	for	GAA AGT CTC CAG AGC AAT TCA
	rev	GGG CCA TTT CCT CCG ACT T
Nppa	for	AGG AGA AGA TGC CGG TAG AAG A
	rev	GCT TCC TCA GTC TGC TCA CTC A
	probe	FAM – AGG TCA TGC CCC CGC AGG C – TAMRA
Myh6	for	GCC AAG ACT GTC CGG AAT GA
	rev	TGG AAG ATC ACC CGG GAC TT
Myh7	for	CAA TGC CAG GAT TGA GGA TGA
	rev	CGT GCC TGA AGC TCC TTG AG
Ccn2	for	CAA CCG CAA GAT CGG AGT GT
	rev	CAC CGA CCC ACC GAA GAC
	probe	FAM – CAC TGC CAA AGA TGG TGC ACC CTG – TAMRA
Acta2	for	TCC TGA CGC TGA AGT ATC CGA TA
	rev	GGT GCC AGA TCT TTT CCA TGT C
	probe	FAM – AAC ACG GCA TCA TCA CCA ACT GGG A – TAMRA

For: forward primer, rev: reverse primer, probe: Taqman probe.

3.1.8 *In vivo* BP measurement and Ang II pressor response

In vivo BP measurements were performed in collaboration with Dr. Mihail Todiras and Dr. André Felipe Rodrigues from the Bader lab (MDC, Berlin). For these animal experiments, GF mice were maintained until 4 weeks, randomized, and COL mice were newly colonized and handled as described in section 3.1.1 until 12 weeks of age (approval number: G0028/21). Acute mean arterial pressure (MAP) was measured in unrestrained conscious GF and COL mice. Basal cardiovascular parameters as well as Ang II pressor response were obtained over the course of 4 hours. To record BP and infuse Ang II intravenously, laboratory-adapted vascular catheters were used.¹⁵⁴ Subcutaneous injection of Carprofen (5 mg/kg) was administered to all mice for pain management prior to surgery. For catheter implantation, mice were anesthetized with isoflurane (4-5% for induction; 1-2% for maintenance), and the surgery was performed on a thermo controlled table as described previously.¹⁵⁵ A small incision over the femoral triangle was made to expose the femoral artery and vein in which heparin/saline filled (100 units/mL) catheters were introduced proximally to about 1.5 cm, reaching the abdominal aorta and vena cava, respectively. The catheters were tunneled subcutaneously, exteriorized, and secured between the scapulae with a silk suture 3/0. Post-surgery, mice recovered from anesthesia individually in a cage placed on a thermo controlled plate at 37 °C. After regaining consciousness, the arterial catheter was connected to a pressure transducer (AD instruments #MLT0699) to record baseline cardiovascular parameters beat-by-beat for approximately 30 minutes. Data was acquired using the PowerLab data acquisition system (PowerLab/4sp) and LabChart software v5. Once baseline parameters were recorded, the maximal pressor response to increasing doses of Ang II (0, 50 and 500 ng/kg) were calculated by the difference between the peak MAP response and the averaged immediate (approximately 1 minute before Ang II infusion) baseline MAP. Ang II (Calbiochem) was injected intravenously as a bolus by connecting a 100 µL Hamilton syringe (Hamilton) to the intravenous catheter. Aliquots of Ang II were prepared to inject the volume of 0.5 µL/g body weight. Each Ang II bolus injection consisted of total final volume of 100 µL, containing the Ang II solution followed by a saline washout. Ang II doses were administered with 10-minute intervals in between, during a period when minimal physical activity was observed.

3.1.9 Serum metabolomic measurements using MxP Quant 500

Serum Metabolomics measurements from GF mice were done in collaboration with the BIH Metabolomics Core Facility (Dr. Raphaela Fritsche, Dr. Jennifer Kirwan; Berlin). All reagents, internal and calibration standards, quality controls, and a patented 96-well filter plate required for MxP Quant 500 analysis were

included in the kit provided by Biocrates Life Science AG. The MxP Quant 500 kit from Biocrates Life Science AG is a kit-based assay based on phenylisothiocyanate (PITC) derivatization of the target analytes using internal standards for quantification. The MxP Quant 500 kit is a targeted metabolomics assay which can theoretically quantify 630 metabolites in total, from 26 analytical classes including small molecules (1 alkaloid, 1 amine oxide, 20 amino acids, 30 amino acid related compounds, 4 bile acids, 9 biogenic amines, 1 carbohydrate, 7 carboxylic acids, 1 cresol, 12 fatty acids, 4 hormones, 4 indoles and derivatives, 2 nucleobases and related and 1 vitamin) and lipids (40 acylcarnitines, 76 phosphatidylcholines, 14 lysophosphatidylcholines, 15 sphingomyelins, 28 ceramides, 8 dihydroceramides, 19 hexosylceramides, 9 dihexosylceramides, 6 trihexosylceramides, 22 cholesteryl esters, 44 diglycerides and 242 triglycerides).

Plate preparation with serum samples from GF and COL mice was done according to the manufacturer's protocol. Briefly, 10 μ L of serum was transferred to the upper 96-well plate and dried under a nitrogen stream. Thereafter, 50 μ L of a 5% PITC solution was added. After incubation, the filter spots were dried again before the metabolites were extracted using 5 mM ammonium acetate in methanol (300 μ L) into the lower 96-well plate for analysis after further dilution using water. Internal standards were present in the plate prior to analysis. Calibration standards at different dilutions (Cal 1 to Cal 7) were also included on the same plate as recommended. Biocrates quality control (QC) samples were run every 20 samples. One pooled QC sample was measured at the beginning, two in the middle and one at the end. Prior to plate measurement, evaluation of the instrument performance prior to sample analysis was assessed by the Biocrates recommended system suitability test (SST). Separate test mixtures were provided with the kit for liquid chromatography-mass spectrometry (LC-MS) and flow injection analysis-mass spectrometry (FIA-MS) SST evaluation. Pass/Fail criteria were according to Biocrates recommendations.

The LC-MS system was comprised of a 1290 Infinity UHPLC-system (Agilent) coupled to a 5500 QTrap with SelexIon (AB Sciex Germany GmbH) in electrospray ionization (ESI) mode. Acquisition method parameters are available upon request. Two LC methods and two FIA methods were used to analyze the same set of samples. Raw data was assessed and manually curated in Met/DQ version Nitrogen (Biocrates Life Science AG). Compounds were identified and quantified using isotopically labeled internal standards and pre-determined multiple reaction monitoring (MRM) transitions for LC and by their accurate mass for FIA, as according to the Biocrates protocol.

3.1.10 Serum metabolomic analysis

Pre-processing and peak integration was performed by Dr. Raphaela Fritsche, and all further data analysis I created my own analysis pipeline using R statistical software with guidance from the Kirwan lab (BIH, Berlin). The *MetIDQ* software is provided by Biocrates and is usually used for data processing and normalization. Normalization was done on median of Biocrates QC level 2 in 4 replicates. The concentrations of metabolites that were analyzed by FIA were automatically calculated by the software based on internal standard ratios. The analyte peaks obtained by LC were integrated by the Sciex Analyst version 1.6.3 software and normalized to the internal standards. All quantification was done within *MetIDQ* version Nitrogen. An in-house script (a modified version of *Metaquac*¹⁵⁶) was used for data quality analysis and preprocessing. The modification enabled the retention of metabolites considered above the limit of detection but below the limit of quantification by Biocrates software. The median relative standard deviation (RSD) for pooled QC samples was 8.35 % for FIA and 8.81 % for LC (accepted as the upper RSD limit is 15%).

For final metabolite identification, metabolites were considered valid when they appeared in a minimum of 70% of biological replicates. Only analytes with values above the limit of detection (LOD) were considered. The LOD for individual analytes was defined as three times the median peak area in the blank samples (peak intensity was used for FIA data) and a minimum intensity of 1 000 count per second (cps). Analytes below the LOD were rejected. Each analyte was subsequently normalized to its respective labeled internal standard. Data was quality checked among other things for technical reproducibility, missing values and batch effects, as detailed previously.¹⁵⁶ Outliers were removed where a drastically low number (less than 70% of the overall average metabolite count) of metabolites were capturable (likely an issue occurred during sample preparation), or where there was consistently greater than 2 standard deviations between a given sample and the mean for its respective biological group. The filtered and quality checked dataset was used for subsequent statistical analysis. Where necessary, imputation of the group-specific mean value for individual metabolites was used, although this was rare as 98.7% and 99.1% of data points were available in the final selection of GF and COL data, respectively.

3.1.11 DNA isolation and extraction for microbiome analysis

DNA isolation and extraction was performed with technical assistance from Theda U.P. Bartolomaeus (ECRC, Berlin). All laboratory procedures were conducted under a hood with laminar flow (LabGarda ES

Energy Sever Classe II Laminar Flow, NuAire Inc.) to limit environmental contamination. Total DNA was extracted from all stool samples using the ZymoBIOMICS DNA Miniprep Kit (ZYMO Research Europe GmbH). Using 20-50 mg aliquots from the previously frozen stool and cecum content, DNA extraction was performed by following the manufacturer's recommendations with slight modifications for better mechanical disruption. The samples were added to the PeQLab vial containing the ZR BeashingBead Lysis Tube beads (0.1 & 0.5 mm), and after adding 750 μ L ZymoBIOMICS Lysis Solution, the vial was capped tightly. Samples were mechanically disrupted twice using a PeQLab Precellys 24 (Bertin Corporation) for 2 x 15 seconds at 5500 RPM, with a 5-minute rest period in between. The remaining steps of the DNA extraction procedure followed the manufacturer's protocol by ZYMO Research Europe GmbH, the final elution of DNA was performed with 100 μ L ZymoBIOMICS DNase/RNase Free Water. The samples were stored at -20° C before being shipped on dry ice to Novogene for sequencing. The extraction protocols were also performed on positive controls (stool samples from C57BL/6J CONV mice) and with a blank sample (RNase-, and DNase-free, genomic DNA-free water). A 75 μ L blank and 20-50mg positive controls were used for extraction.

3.1.12 Microbiome sequencing data processing and analysis

NGS data was generated by Novogene. Microbiome data was processed and analyzed in collaboration with the Forslund lab at the ECRC (Dr. Ulrike Löber, Dr. Sofia Forslund; Berlin). Shotgun sequencing data were processed using *ngless*.¹⁵⁷ Quality control was performed by trimming reads with phred score below 25, while trimmed reads shorter than 45 bp were discarded. Taxonomic classification was assessed by aligning the quality trimmed reads to *mOTUs*¹⁵⁸ (v2.5) using *bwa*¹⁵⁹ (v0.7.17) with default parameters. Mouse genome GRCm38.p6 was masked with the sequences retrieved from *SILVA*¹⁶⁰ database V138 using *bbtools* (<https://sourceforge.net/projects/bbmap/>). The reads which passed quality control were mapped to the masked mouse reference using *bwa* within *ngless*. Sequences matching the mouse genome were considered off-targets and discarded. Reads which mapped to multiple genes in the reference database were handled using the "dist1" method and normalized using the "scaled" mode. The results were parsed by a customized perl script and visualized using the *ggplot2*¹⁶¹ package. Functional annotation was performed mapping the trimmed and filtered reads to the *MouseGutCatalog* (v0.9)¹⁶², while the *dist1* method was used to account for multiple annotations.

3.1.13 Fecal qPCR

For all stool and cecum content samples and relevant controls, PCR was performed using an Applied Biosystems QuantStudio 3 system (Thermo Fisher Scientific) as described in Bartolomaeus et al.¹⁶³. Amplification and detection were performed in 96-well optical plates (Applied Biosystems) with SYBR-Green (Applied Biosystems). For amplification, the standard protocol of the Applied Biosystems QuantStudio 3 system was followed, i.e., an initial cycle at 95°C for 10 min, followed by 40 cycles at 95°C for 15 s, and 1 min at 60 °C. To check for specificity, melting curve (T_m) analysis was performed, increasing the temperature from 60 to 95 °C at a rate of 0.2 °C per second with the continuous monitoring of fluorescence. Standard curves for quantification consisted of ten-fold serial dilutions in the range of 10⁸ – 10⁰ copies of the 16S rRNA gene of the *E. coli* (Invitrogen, C404010) amplified with primers 27F (5'-GTTTGATCCTGGCTCAG-3') and 1492R (5'-CGGCTACCTGTTACGAC-3'). Using universal primers, Univ 337F 5'-ACTCCTACGGGAGGCAGCAGT-3' and Univ 518R 5'-GTATTACGCGGCTGCTGGCAC-3' the total amount of bacterial 16S in stool and cecum content (COL and CONV) and in stool from GF mice, as well as in the blank and positive controls was quantified. Copy numbers per g feces was calculated for each primer set used, as previously described.¹⁶⁴

3.1.14 Comparative analysis with Pluznick study data

Comparison of fecal microbiome data from our study (hereto forth referred to as the “Berlin” data) to the data previously published by Cheema and Pluznick¹⁶⁵ (referred to as the “Pluznick” data) required reannotation of the Berlin shotgun NGS data, into a format comparable to the published 16s sequencing data. Metabolite and microbiome data from Berlin included only male mice, though the Pluznick data included both male and female mice as a part of the analysis (as the Pluznick n number was too low with only males included). Additionally, non-GF mice from the Pluznick study were CONV (as opposed to COL in Berlin study). Raw 16s sequence data from the Pluznick study was downloaded from NCBI Sequence Read Archive (BioProject: PRJNA514044). LotuS 1.62¹⁶⁶ was used for analyzing the 16S amplicons based on SILVA¹⁶⁰, Greengenes¹⁶⁷ and HITdb databases, and resulted in all taxonomic levels of microbiome abundance tables. Subsequently, these abundance tables were rarefied by using RTK.¹⁶⁸ Abundance table on genus level was adopted for the comparison with this study. Principal Coordinates Analysis (PCoA) of microbiome data using Bray-Curtis distances was performed with the vegan package.¹⁶⁹

Metabolites from Pluznick data were curated for overlapping metabolites where there were exact matches for the biochemical name, CAS ID, HMDB ID, and/or PubChem IDs. Multivariate tests including PERMANOVA and PCoA were performed by using *vegan*¹⁶⁹ R package, and Euclidean distance was adopted. Comparison of the changes in metabolites between sham and hypertension groups on individual level were done by first performing Mann-Whitney U test within GF or COL/CONV groups in each study (NAs were removed if any NA resulted from the test). We then compared the directionality of change for each metabolite in the equivalent group from the Pluznick or Berlin data. For the comparison of effect size for each metabolite individually between sham and hypertension groups in either the GF or COL/CONV conditions of the Pluznick or Berlin study, Cliff's delta was calculated by using *orddom* R package.¹⁷⁰ The distances between the effect sizes in GF or COL groups were calculated by taking the absolute value of numerical difference between the two studies. *Ggplot2*¹⁶¹ was used for plotting, and *ggpubr*¹⁷¹ was applied to add Mann-Whitney U test result. I designed the analysis detailed here, I performed the cross-comparison of metabolomics data, Chia-Yu Chen (ECRC, Berlin) re-processed microbiome data from 3.1.12, and we collaborated on the statistical analysis.

3.1.15 *In vitro* Th17 polarization

For supplementary *in vitro* assays to complement the work from the aforementioned experiments, we utilized C57BL/6J GF mice and C57BL6/J CONV mice aged 9-12 weeks (approval number: X9009/18). Cells were isolated from mesenteric lymph nodes of GF or CONV mice. These cells were then sorted using magnetic activation with the CD4+ T Cell Isolation Kit (Miltenyi Biotec) according to the manufacturer's instructions. Isolated CD4+ T cells were collected and resuspended in MACS buffer at 2×10^6 in 50 μ L. For APC-free differentiation, cells were fluorescently stained for 30 min in an antibody cocktail containing anti-CD4–PercyP Vio 700, anti-CD44–PE, anti-CD62L–APC and anti-CD25–PE–Cy5, and subsequently purified by fluorescence-activated cell sorting on a BD FACS Aria II Flow Cytometry Cell Sorter (BD Biosciences). Sorted naïve CD4+ T cells (CD4+CD62L+CD44^{low}CD25⁻) were stimulated by plate-bound anti-CD3 (2 μ g ml⁻¹, 145-2C11, BD Pharmingen) and anti-CD28 (2 μ g ml⁻¹, 37.51, BD Pharmingen) in the presence of Th17 polarizing conditions using IL-6 (40 ng ml⁻¹), rhTGF β 1 (2 ng ml⁻¹) and IL-1 β (10 ng ml⁻¹). To determine the influence of Ang II on Th17 cell polarization in GF or COL, naïve CD4+ T cells were cultured with vehicle used for stock dilution or 50 μ L Ang II for 96 hrs. Cells were stained and measured as detailed above for Th17-specific markers. Antibodies used for all GF experiments (including those from section 3.1.3) are shown in Table 2.

Table 2. Antibodies used for GF immunophenotyping

Antigen	Fluorophore	Clone	Concentration	Manufacturer
CD3ε	VioBlue	17A2	1:10	Miltenyi
CD4	APC Vio770	GK1.5	1:10	Miltenyi
CD8a	PerCP Cy5.5	53-6.7	1:100	eBioscience
CD11b	PE	M1/70	1:150	BD Bioscience
CD11c	PerCP Cy5.5	N418	1:100	BioLegend
CD25	VioBright FITC	7D4	1:10	Miltenyi
CD44	FITC	IM7	1:100	BD Bioscience
CD45R / B220	Alexa Fluor 647	RA3-6B2	1:100	BioLegend
CD62L	APC	MEL-14	1:100	BD Bioscience
CD69	PE Cy7	H1.2F3	1:100	BD Bioscience
γδ-TCR	PE	GL3	1:100	BD Bioscience
F4/80	Pacific Blue	BM8	1:100	BioLegend
FoxP3	PerCP Cy5.5	FJK-16s	1:50	eBioscience
Gr-1	PE Cy7	RB6-8C5	1:150	eBioscience
Helios	Pacific Blue	22F6	1:50	BioLegend
Ki67	PE Vio770	REA183	1:10	Miltenyi
Ly6C	APC eFluor 780	HK1.4	1:10	eBioscience
RORyt	APC	REA278	1:10	Miltenyi
Tbet	PE	REA102	1:10	Miltenyi
CD4	Percyp Vio 700	GK1.5	1:20	Miltenyi
CD44	PE	IM7.8.1	1:20	Miltenyi
CD62L	APC	MEL-14	1:100	BioLegend
CD25	PE-Vio770	PC61	1:100	BD Pharmingen
Il-17A	PE	eBio17B7	1:50	eBioscience
TNFα	APC Cy7	MP6-XT22	1:50	BioLegend

3.2 Interstitial fluid isolation and analytics

3.2.1 Animal protocols

All animal experiments within section 3.2 performed at the ECRC (Berlin) were preapproved by the local ethics committee (C57BL/6J mice: X9009/18, SD rats: Y9004/18) and complied with the German and European legal animal protection regulations. All mouse experiments were carried out using C57BL/6J male mice aged 9-12 weeks. All rat experiments were carried out using SD rats aged 19-22 weeks, and for some experiments both male and female rats were used, which is marked in the corresponding figures. All experiments where sample collection was initiated at the University of Bergen (Norway) were performed by Dr. Helge Wiig and Dr. Tine Karlsen. Experiments performed at the University of Bergen were in compliance with the regulations of the Norwegian State Commission for Laboratory Animals with

approval from the AAALAC International Accredited Animal Care and Use Program at University of Bergen (approval ID #10508 and #13922).

3.2.2 Centrifugation method

The general principle of the centrifugation method is outline in Wiig et al¹⁴⁰, and was adapted for use with GI tissue in both mouse and rat models. Ahead of the experiment, 5 mL Safety cap reaction vessels (Ratiolab) were weighed and prepared with a 9 x 9 cm piece of nylon weaved mesh netting (pore size ~15 × 20 μm, Burmeister AS) for rats, or 7 x 7 cm netting for mice. A schematic can be seen later in Figure 35, showing the arrangement of the netting which primarily acts to suspend the tissue from above while the IF descends into the bottom of the tube. IF should be collected in a humid environment, to avoid evaporation. We utilized an out-of-use incubator as a humid chamber, acquired from the University Clinic in Erlangen. The room temperature humid chamber was brought to 100% humidity, and a water repellant surface is placed inside for sample preparation. Because GI tissue is very delicate, surgical tools were covered in 0.5 mm ROTILABO[®] silicone hose (Carl Roth) to prevent poking holes in or tearing the gut.

After sacrificing the mouse or rat, the entire GI tract was removed from the distal esophagus until the distal colon. GI tissue was placed immediately in a closed petri dish and placed inside the humid chamber. The sectioning approach depends on the goal of the experiment, and the animal model used. For mice, typically 5 segments (colon, cecum, ileum, jejunum, and duodenum) are taken, from the anus to stomach, but in rats as there is significantly more tissue, each non-cecal segment can be split into multiple segments. Each piece of tissue was ligated and cut between the ligations, then placed onto the nylon mesh and pushed down into the 5 mL tube, but still suspended above the bottom of the tube. While preparing one section of tissue, any other pieces were kept inside a closed petri dish to prevent drying. Filled tubes were then centrifuged for 10 minutes at 400 x g. The tissue was then removed and set aside. Tubes containing IF were weighed and ddh2O was added to dilute centrifugation IF, which was then aliquoted and frozen to -80°C. Site-specific fecal matter was removed from the GI tissue segments after centrifugation and collected in Corning[®] cryogenic vials (STEMCELL Technologies) and immediately frozen to -80°C. Where appropriate the tissue itself was used for histological or immunophenotyping analysis.

3.2.3 Elution method

The elution approach has been detailed elsewhere for other types of tissue¹⁴⁰, and we amended this method for use with GI tissue. A schematic detailing this method is found in Figure 24. Briefly, excised tissue was ligated and placed in an isosmotic buffer a 1:10 dilution for a given time, such that highly abundant metabolites and small molecules should travel from a high (within the IF) to low gradient (elution buffer). As detailed above, the humid chamber was used to reduce evaporation of IF from the tissue. The full GI tract was surgically removed from mice or rats as described in 3.2.2. Typically, one section from the colon, cecum, ileum, jejunum, and ileum were excised, although sectioning for elution experiments requires smaller pieces of tissue (~ 2-4 cm) so additional segments were added as needed. As above, coated tools were used to minimize scratching or damage to the gut. Where appropriate, fecal matter from each respective segment was collected into a corresponding cryogenic vial and frozen at -80°C immediately. The inner surface of the GI tract was flushed with elution buffer to remove any remaining fecal contaminants using a 1.7 x 50 mm Vasofix® Safety IV catheter (B. Braun Medical Industries) with the needle removed to leave only the plastic tubing, which was attached to the end of a 5 mL syringe (B. Braun Medical Industries). Tissue was then squeezed gently, ligated, and placed in a pre-weighed 15 mL tube. Isosmotic elution buffer was then added at a 1:10 ratio based on the tissue weight, and this was placed at 4°C on a rocker for between 2 and 48 hours. Once the elution period was over, the GI tissue was removed from the tube, and the elution IF was aliquoted and frozen to -80°C.

Selection of the appropriate elution buffer depends on the intended use for the resultant IF. For example, mannitol buffer is preferable if the intention is to measure ion concentrations after eluting, whereas saline buffer, due to a matrix-effect, is preferred for measurement of SCFA from resultant elution fluid. Saline buffer was pre-prepared isotonic 0.9 % sodium chloride solution for injection (B. Braun Medical Industries). Mannitol buffer was made by adding 5 % pure (99.9999% identity) D-mannitol (Sigma-Aldrich) to double-distilled water (18.2 Ωm) to achieve an osmolarity of between 285-295 mOsm/kg. Glucose-based buffer solution was prepared by adding 5 % pure (≥99.5% identity) D-(+)-Glucose (Sigma-Aldrich) to double-distilled water (18.2 Ωm) to achieve an osmolarity of between 285-295 mOsm/kg. All buffers were tested using the Knauer Semi-Micro Osmometer – Type ML to ensure the osmolarity was consistent with that of plasma.

3.2.4 Ion chromatography

Ion chromatography measurements were performed by the Wiig lab at the University of Bergen (Norway). Sodium and potassium in the eluted tissue solutions and serum were baseline separated in a 10 minutes 7.5-60 mmol/LMSA gradient at a flow rate of 0.2 mL/min by a Dionex IonPac CS 16-4 μ m RFIC analytical column (2 \times 250 mm, P/N 088582) and guard (2x50 mm, P/N 088583) using a Dionex Integrion HPIC System equipped with a CDRS 600 (2 mm) Cation Electrolytic Suppressor and a high pressure EGC 500 methane sulfonic acid eluent generator cartridge. Thereafter ion content was related to tissue wet weight, dry weight, and water content.

3.2.5 ⁵¹Cr-EDTA extracellular tracer – centrifugation method

To validate the capture of IF in our methods, the radiolabeled isotope ⁵¹Cr-EDTA was used as an extracellular tracer. The relative level of the tracer in IF compared to serum allows one to conclude whether the obtained fluid has been diluted by intracellular contents or other extraneous factors. Extracellular tracer experiments were performed at the University of Bergen (Norway) in collaboration with Dr. Helge Wiig and Dr. Tine V. Karlsen (approval ID #10508 and #13922). For centrifugation experiments, the IF/serum ratio of the ⁵¹Cr-EDTA tracer should be close to 1.0 if the method applied has been successful in obtaining IF. Male C57BL/6 mice (n = 7) were anesthetized with 2 % isoflurane in 100 % O₂ before ⁵¹Cr-EDTA (~ 6 million counts in 100 μ L isotonic saline) was injected into the tail vein with an insulin syringe. With the mice under continuous isoflurane anesthesia, the ⁵¹Cr-EDTA was left to equilibrate in the extracellular fluid phase for 1 hour. During the experiment, the body temperature was kept at 37°C with the aid of a servo-controlled heating pad. At the end of the equilibration period a blood sample was obtained by cardiac puncture before the mice were terminated by neck dislocation. Immediately thereafter, the mice were transferred to a humidity chamber keeping 100 % humidity throughout the rest of the harvesting procedure. Blood samples were spun at 10 621 x g to separate serum from erythrocytes. I trained Dr. Tine V. Karlsen prior to performing the experiments, and centrifugation was performed as described in section 3.2.2. A small piece of skin was excised and centrifuged as a reference sample. One hour after collection, isolated gut and skin IF and serum samples were counted in a gamma counter and fraction of IF calculated as the IF/serum count ratio for each sample. The same procedure performed in SD rats (n=8) with minimal modifications and a greater number of segments because of the GI length. Due to the rat's larger body size, they received a higher dose of chromium (~15

million counts in 100 μ L isotonic saline) and the chromium circulated for 2 hours (compared to 1 hour in mice) before sacrificing and harvesting.

3.2.6 ^{51}Cr -EDTA extracellular tracer – elution method

For Elution experiments, ^{51}Cr -EDTA was used to assess how rapidly and reproducibly the tracer could be extracted from the tissue, to estimate the likelihood that metabolites and other small molecules would be detected in the elution fluid after a given period where the tissue was bathed in buffer. These experiments were done in collaboration with Dr. Helge Wiig and Dr. Tine Karlsen from the University of Bergen in Norway (approval ID #10508 and #13922). Male C57BL/6J mice ($n = 6$) were anesthetized with 2 % isoflurane in 100 % O_2 before ^{51}Cr -EDTA (~ 14 mill counts in 100 μ L isotonic saline) was injected into the tail vein with an insulin syringe. With the mice under continuous isoflurane anesthesia, the ^{51}Cr -EDTA was left to equilibrate in the extracellular fluid phase for 1 hour. During the experiment, the body temperature was kept at 37°C with the aid of a servo-controlled heating pad. At the end of the equilibration period a blood sample was obtained by cardiac puncture before the mice were terminated by neck dislocation. Immediately thereafter, the mice were transferred to a humidity chamber keeping 100 % humidity throughout the rest of the harvesting procedure. Elution samples were isolated as described in section 3.2.3, and Dr. Tine V. Karlsen was trained in the procedure prior to initiating these experiments. The samples were placed in a cold room (4°C) on a rocking belly dancer and after 2, 4, 6, 24 and 48 hours a 100 μ L sample were removed from the eluted solution for gamma counting. After 48 hours the gut samples were removed from the mannitol solution and counted. In addition, a serum sample was also counted for each mouse. The eluted fraction with time was determined by dividing ^{51}Cr -EDTA counts in the eluted sample at each time point with total counts in the corresponding gut sample prior to elution. In addition, extracellular fluid volume was found as the plasma equivalent space of ^{51}Cr -EDTA for each gut segment.

3.2.7 Total tissue water determination

To determine the total tissue water (ECV and intracellular volume (ICV)) of a given segment, the GI tissue was removed from the distal colon to the stomach from C57BL/6J mice ($n=7$). Samples were segmented into colon, cecum, ileum, jejunum, and duodenum sections. Each segment was cut lengthwise, and fecal contents were carefully removed. Tissue was lightly rinsed with 1x DPBS (Gibco), and carefully blotted to remove excess water. Cleaned tissues were then weighed and placed in the UF450 drying oven (Memmert

GmbH) to dry for 36 hours at 70°C. Tissues were weighed a second time after 100 hours to ensure that all fluid was dried out of the tissue, and indeed the weight did not change beyond 36 hours, therefore the tissue had been dried completely. The dry weight was divided by the wet weight of the tissue to give the fraction of a given tissue weight which could be attributed to a fluid compartment.

3.2.8 Proteomics analysis

Mouse experiments- Protein concentration of IF and serum samples was measured by BCA assay. Twenty micrograms of protein were digested with trypsin, and 2 micrograms were used as input for IF and serum samples, normalizing the intake material across conditions. 1 volume of SDC lysis buffer was added and samples were heated for 10 min at 95°C. After cooling down to room temperature Endopeptidase LysC and sequence grade trypsin was added at a protein:enzyme ratio of 50:1 and samples were digested overnight 37°C. After adding formic acid (1% final concentration) peptides were cleaned-up (C18 stage tips) and analyzed by reversed phase chromatography (98 min gradient of 2-55% acetonitrile) on a High-Performance Liquid Chromatography (HPLC) system (ThermoFischer Scientific) coupled to an Q Exactive HF-X mass spectrometer for mouse experiments (ThermoFischer Scientific). The instrument was operated in the data-dependent mode with performing full scans (60K resolution; 3×10^6 ion count target; maximum injection time 10 ms), followed by top 20 MS2 scans using higher-energy collision dissociation (NCE of 27; 15K resolution, 1×10^5 ion count target; 1.3 m/z isolation window; maximum injection time: 22 ms). Only precursors with charge states between 2-7 were fragmented. Dynamic exclusion was set to 30 sec. Raw data were analyzed using the MaxQuant software (v1.6.10.43). The internal Andromeda search engine was used to search MS2 spectra against a mouse decoy UniProt database (MOUSE.2019-07) containing forward and reverse sequences. The search included variable modifications of oxidation (M) and N-terminal acetylation, deamidation (N and Q) and fixed modification of carbamidomethyl cysteine. Minimal peptide length was set to 7 amino acids and a maximum of three missed cleavages was allowed. The false discovery rate (FDR) was set to 1% for peptide and protein identifications. The integrated label-free quantification algorithm was activated. Unique and razor peptides were considered for quantification. Retention times were recalibrated based on the built-in nonlinear time-rescaling algorithm and MS/MS identifications were transferred between LC-MS/MS runs with the "Match between runs" option. The resulting text files were used for further analyses using the Perseus software package (v. 1.6.2.1). LFQ (label-free quantification) intensity values were used for quantification. Reverse hits, contaminants and proteins only identified by site were filtered out.

Rat experiments - Protein concentration was measured by BCA assay. Twenty micrograms of protein were digested with trypsin, and 2 micrograms were used as input for IF and serum samples, normalizing the intake material across conditions. 1 volume of SDC lysis buffer was added and samples were heated for 10 min at 95°C. After cooling down to room temperature Endopeptidase LysC and sequence grade trypsin was added at a protein:enzyme ratio of 50:1 and samples were digested overnight 37°C. After adding formic acid (1% final concentration) peptides were cleaned-up (C18 stage tips) and analyzed by reversed phase chromatography (2ug per injection, 98 min gradient of 2-55% acetonitrile) on a HPLC system (ThermoFischer Scientific) coupled to an Q Exactive Plus mass spectrometer (ThermoFischer Scientific). The instrument was operated in the data-dependent mode with performing full scans (70K resolution; 3×10^6 ion count target; maximum injection time 50 ms), followed by top 10 MS2 scans using higher-energy collision dissociation (NCE of 26; 17.5K resolution, 5×10^4 ion count target; 1.6 m/z isolation window; maximum injection time: 250 ms). Only precursors with charge states between 2-6 were fragmented. Dynamic exclusion was set to 30 sec. Raw data were analyzed using the MaxQuant software (v1.6.3.4). The internal Andromeda search engine was used to search MS2 spectra against a rat decoy UniProt database (RAT.2019-07) containing forward and reverse sequences. The remainder of the method (peptide identification, selection, quality control and data analysis) was the same for rats as in mice, detailed above.

Where appropriate, missing values were imputed by random draw from Gaussian distribution with $0.3 \times$ standard deviation and downshift of $1.8 \times$ standard deviation of the observed values per sample. When the percentage of valid values for a given protein was used as an inclusion criterion, unimputed values were exclusively considered for data filtration. For all experiments from rats and mice, similar statistical methodologies were used. Euclidean distances were used for all cluster-based analyses along an axis. Pearson's correlation was used to assess the similarities between given samples either individually or by the group mean. Principal component analysis (PCA) with Euclidean distances was used to assess similarities between samples. An FDR correction of 5% was applied for statistical testing unless otherwise stated. All proteomics experiments were performed in collaboration with Dr. Marieluise Kirchner and Dr. Philipp Mertins from the BIH Proteomics Core Facility (Berlin).

3.3 Shared methods

3.3.1 Metabolomics analysis of short chain fatty acids

SCFA from C57BL6/J GF and CONV mouse feces were isolated and measured towards study aim 2.1 using GCMS exactly as described in Haghikia et al.¹⁷² These experiments were performed in collaboration with the lab of Stefan Kempa with the assistance of Sabrina Geisberger (MDC Proteomics and Metabolomics Platform, Berlin). Modifications were made to the method described in Haghikia et al.¹⁷² to measure SCFA from fecal, serum, and IF samples towards aim 2.2. The full method is therefore described here in detail.

Briefly, 90 μ L of serum or IF samples (with diluent of ddH₂O included where appropriate) were extracted by shaking for 30 min at 25°C in 100 μ L diethyl ether and 10 μ L HCl. Stool samples were extracted with 20 μ L of HCl and 200 μ L of diethyl ether per 10 mg of stool. After centrifugation for 5 minutes at 1500 x g, 50 μ L ether phase was transferred into GC-MS glass vials. Derivatization was performed with 10 μ L MTBSTFA for 30min at 80°C, followed by overnight incubation at room temperature. 100 μ M crotonic acid was spiked in as internal control in all samples. 1000 μ M sodium acetate was added to serum samples to increase signal above background. Pure water, as well as dilution series of Volatile Free Acid Mix (CRM46975, Sigma Aldrich) were prepared and measured in parallel and served as background and calibration curve, respectively. GC-MS analysis was performed on a Thermo Scientific™ Q Exactive™ hybrid quadrupole Orbitrap mass spectrometer, coupled to a Thermo Scientific™ TRACE 1300 Series gas chromatograph and a Thermo Scientific™ TriPlus RSH Autosampler, at a resolution of 60,000, scan range of 65 to 600 m/z and with a split of 1:10. Initial temperature was 68°C, held for 2 minutes, followed by a 7 °C/minute ramp until 150 °C and a final 50 °C/minute ramp until 300 °C, held for 2 minutes. Data was analyzed with Thermo Scientific™ Xcalibur™ Quan Browser Software. If technical failures occurred (e.g., extraction was not successful, internal standards were not measurable) these values were removed from the analysis. For any Elution IF samples which were used for SCFA determination, an isosmotic saline buffer solution was used for isolation. In the initial assessments of SCFA from elution IF, a mannitol-based buffer solution was deemed inappropriate because the standard curve for concentration determination was not linear. The concentration curve in a saline-based buffer was similar to in ddH₂O, therefore this buffer was used for further measurements.

3.3.2 Statistical analysis

Statistical analysis for aim 2.1- Univariate data was analyzed using two-way ANOVA, where the interrogated factors were hypertension and microbiome status. When one or both factors were significant, post-hoc testing with Sidak's multiple comparison test was performed to identify the source of variation. Technical failures were removed from analysis prior to statistical testing. For the assessment of relative change for an individual marker within GF and COL groups, values from hypertensive mice were expressed as a percentage of the mean of the respective sham group. COL and GF were then compared using unpaired two-tailed Student's t-test. $P \leq 0.05$ was considered statistically significant for all tests performed in the aforementioned analysis.

Multivariate principal coordinate analysis (PCoA) and subsequent testing using permutational multivariate analysis of variance (PERMANOVA) was performed in R using the *vegan*¹⁶⁹ package, and Euclidean distance (kidney, heart, and immunome data) or Bray-Curtis distance (microbiome) were used for dissimilarity indices. For heatmaps, hypertensive COL and GF mice were compared to their respective sham group using Mann-Whitney U test. Multiple comparisons were adjusted using Benjamini-Hochberg correction for false discover rate. $Q < 0.1$ was considered statistically significant. Effect size analysis was performed using Cliff's delta in R with *orddom*¹⁷⁰, and visualized with *ggplot2*¹⁶¹ packages.

Statistical analysis for aim 2.2- Statistical methods applied were dependent on the experimental design and are listed alongside each figure. For proteomics measurements, the appropriate statistical methods are detailed in section 3.2.8. Data were considered for paired analysis when sequential measurements were taken from one biological sample; and were tested using repeated-measures one-way ANOVA with Tukey's multiple comparisons test. Ordinary one-way ANOVA with Tukey's multiple comparisons test was used for testing differences between segments in the GI tract. When comparing multiple groups to a reference value, an ordinary one-way ANOVA with Dunnett's post-hoc test was applied. Unpaired two-tailed Student's t-test and two-way ANOVA testing was used as described above where appropriate. $P \leq 0.05$ was considered significant.

Universal- All statistical analyses, unless otherwise stated within a respective method, were performed using either R version 4.0.2 or GraphPad Prism 9.

4. Results

4.1 The contribution of the gut microbiome to hypertensive end-organ damage

4.1.1 Verification of experimental integrity

To address aim 2.1, littermate mice were randomized at 4-weeks to either receive colonization or to remain GF for the duration of the experiment, and at 12-weeks hypertension was induced (see Figure 4). To confirm the reliability of our experiments, the colonization or GF status of experimental mice was assessed at 14 weeks upon sacrifice. GF status is characterized by an enlarged cecum (e.g., megacecum), which disappears upon colonization. Indeed, the megacecum was present in GF mice and did not persist in the mice which received passive colonization at week 4 (COL) (Figure 5A). Fecal bacterial growth in thioglycolate medium was examined from pellets produced on the final day of experimentation, which confirmed the status of GF mice (representative images shown in Figure 5B).



Figure 5. Microbiome status verification from GF experiments

Representative images of GF and COL mouse GI tract from stomach to anus are shown in (A) upon sacrifice. B) Representative images of thioglycolate medium with fecal pellets from GF or COL mice upon sacrifice, compared to a negative control (no fecal pellet). Samples were collected by Dr. Hendrik Bartolomaeus and Gabriele N'diaye (ECRC, Berlin).

To check the comparability of the bacterial load in COL mice compared to classic CONV C57BL/6J mice, 16s rDNA copies per gram stool were measured by qPCR. Additionally, these experiments allowed us to confirm again that the GF mice were indeed GF at sacrifice. Fecal matter was tested from all experimental animals; cecal matter was collected from selected representative animals. All COL and CONV SPF mice had similar levels of 16s rDNA in their cecal and fecal matter, whereas GF mice did not have more 16S rDNA copies than blank samples (Figure 6A). Shotgun metagenomics was used to show the bacterial composition on the phylum and genus level grafted into COL mice with and without Ang II treatment (Figure 6B-C). The goal of sequencing was not to look for shifts in the gut microbiome during hypertensive

treatment, as this has been robustly demonstrated in previous studies (see 1.3.1); but rather to provide the microbiome information to facilitate reproducibility in future studies. Overall, the microbiome status of GF and COL groups was maintained as intended and therefore we proceeded with phenotypic evaluation.

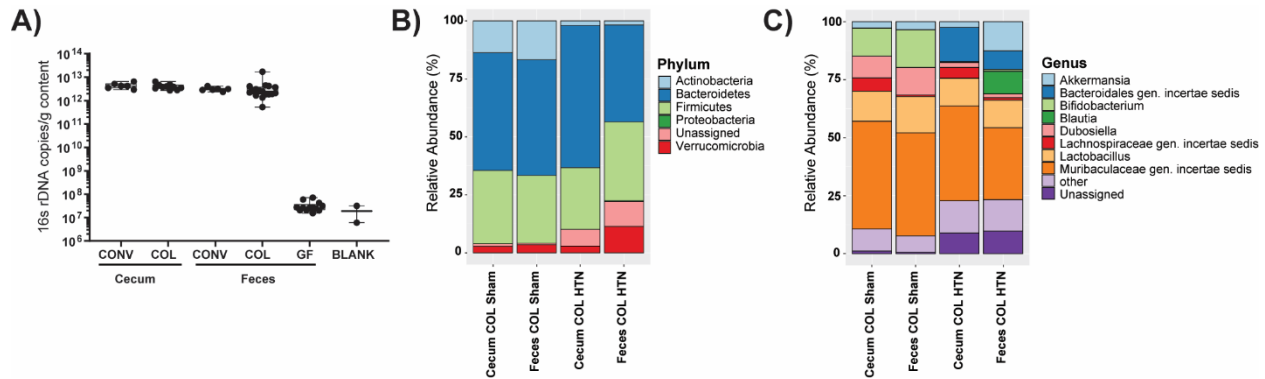


Figure 6. Microbiome status verified by qPCR and shotgun sequencing

For all figures in section 4.1, hypertension induction (Ang II + 1% NaCl) is abbreviated as HTN in figures for brevity. A) 16s rDNA copies per gram of fecal matter from fecal (CONV n= 6, COL n= 17, GF n=13) and cecal content (CONV n= 6, COL n= 10) demonstrates the similarity between CONV and COL mice, and the absence of 16s rDNA in GF samples when compared to buffer alone (Blank n= 2). The mean relative abundance of phyla in cecal and fecal matter from COL mice is shown in (B), and the mean relative abundance of genus (filtered for those with greater than 5% relative abundance in at least one subgroup) are shown in (C) (Cecum COL Sham n = 5, Feces COL Sham n= 5, Cecum COL+ HTN n=5, Feces COL+ HTN n=12). Microbiome sequencing data was annotated by Dr. Ulrike Löber (ECRC, Berlin), and I performed the subsequent analyses.

4.1.2 Hypertensive kidney damage is exacerbated under GF conditions

As detailed in section 1.1.2, uncontrolled hypertension can lead to the development of kidney damage, which is characterized by abnormally high excretion of albumin with the urine (albuminuria), fibrosis, and inflammation. For all analyses of individual disease markers both a two-way ANOVA testing strategy which included all experimental groups, and a relative change assessment was performed. To evaluate relative change for an individual marker within GF and COL groups, values from Ang II + 1% NaCl (henceforth referred to as hypertension) mice were expressed in percent of the mean of the respective sham group. Hypertension induction without uninephrectomy led to a slight increase in albuminuria in COL mice (Figure 7A), similar to what has been previously published.¹⁷³ Interestingly, GF mice developed a greater degree of albuminuria upon hypertension induction, which is abundantly clear when comparing the relative increase of GF and COL mice compared to their respective sham groups (Figure 7A). Lipocalin-2 (*Lcn2*) a known marker for renal injury, was increased significantly in GF mice and not COL mice by two-

way ANOVA (Figure 7B), though the relative change in this marker was not different between GF and COL. Nephrin deficiency in hypertension has been associated with reduced function of the glomerular filtration barrier and the development of proteinuria.¹⁷⁴ A significant decrease of nephrin immunofluorescence in GF mice was evident, where COL mice exhibited a similar but insignificant trend (Figure 7C-D).

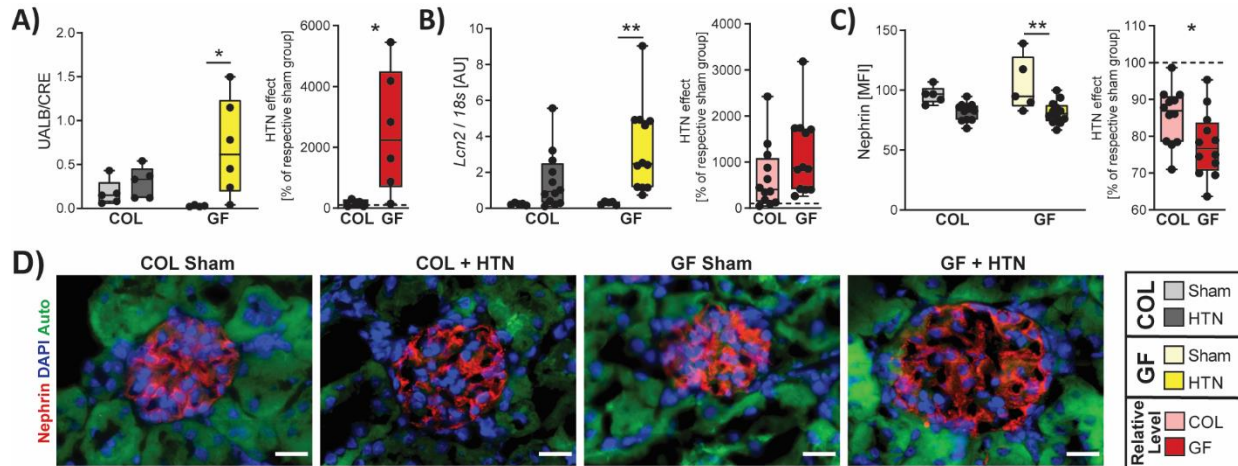


Figure 7. Hypertensive kidney dysfunction is exacerbated in GF mice

A) Urinary albumin-to-creatinine ratio from spot urine collected upon sacrifice from a subset of mice (COL $n = 5$, COL + HTN $n = 5$, GF $n = 4$, GF + HTN $n = 6$). B) *Lcn2* gene expression was measured from kidney tissue by qPCR. C) Nephrin immunofluorescence was quantified as mean fluorescence intensity (MFI) in the glomerular space, averaged per mouse. D) Representative glomeruli are shown from histological kidney sections stained for nephrin. The scale bar represents 20 μm . Throughout the rest of the analysis, n numbers are as follows; GF Sham $n = 5$, GF + HTN $n = 12$, COL Sham $n = 5$, COL + HTN $n = 12$, unless otherwise indicated. In A-C, the left graph was tested using a two-way ANOVA and post-hoc Sidak multiple comparison's test and depicts the raw values for each variable. For A-C, hypertension was identified as the source of variation using two-way ANOVA, and post-hoc multiple comparison between sham and hypertension within each group revealed that the GF comparison was the source of variation. The right plot in A-C depicts the relative change induced by hypertension in comparison to the respective sham group, tested using an unpaired two-tailed T-test (no change (100%) represented by the dotted line). For all plots, p -values are as follows; * $P \leq 0.05$, ** $P \leq 0.01$. Ariana Rauch analyzed the nephrin staining. I performed the analysis of urinary albumin-to-creatinine, as well as the quantification of *Lcn2* expression, and all subsequent analysis.

Differences in kidney inflammation were also evident in GF and COL mice. As expected, the overall number of leukocytes (CD45+ cells) within the kidney was increased in GF but not COL in hypertension (Figure 8A). Hypertension resulted in a significant increase in macrophages (F4/80+ cells, Figure 8B) in the kidney of GF mice but not COL. In line with this, we found that the expression of CC-chemokine ligand 2 (*Ccl2*, Figure 8C) increased in only GF mice. Local *Ccl2* expression is associated with macrophage infiltration in hypertension and contributes to the development of fibrosis in target organs.¹⁷⁵ Infiltrating T cells (CD3+,

Figure 8D) and cytotoxic T cells (CD8+ cells, Figure 8E) were likewise increased in the GF group and not COL upon hypertension. While T helper cells (CD4+ cells) were found to increase in both GF and COL mice, though the relative change in GF mice was significantly different than COL (Figure 8F). Indeed, the change in hypertension relative to sham was consistently exacerbated in GF compared to COL for all immune populations which were examined in the kidney.

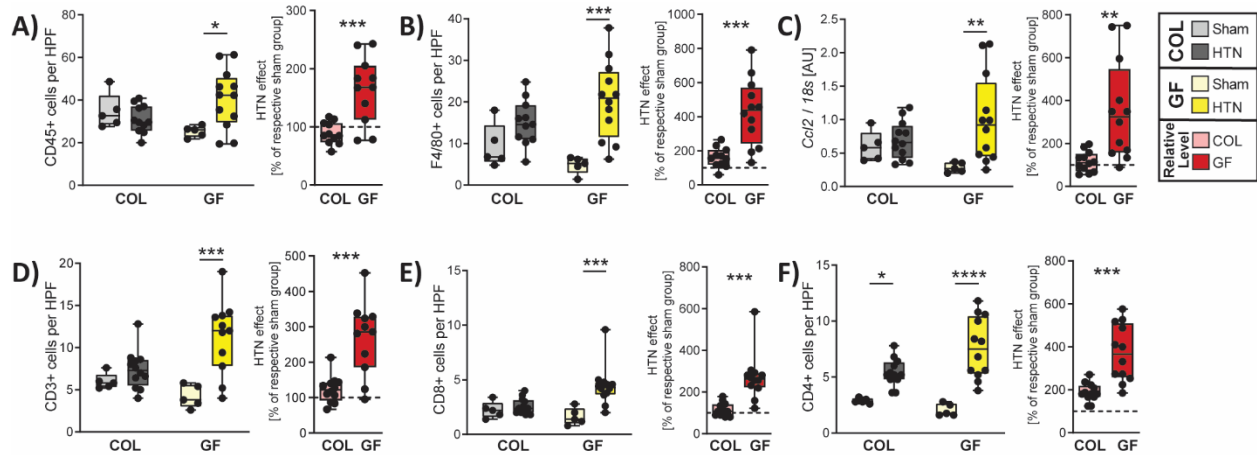


Figure 8. Hypertensive renal inflammation is worsened under GF conditions

A) CD45+ cells, B) Macrophages (F4/80+), D) CD3+ T cells E) CD8+ T cells, and F) CD4+ T cells from kidney sections were counted from 5 representative high-power fields within the cortex. Dr. Hendrik Bartolomaeus assisted with the analysis shown in (D-F). C) Ccl2 expression measured by qPCR from kidney tissue. For (A-F), the left plot was tested using a two-way ANOVA and post-hoc Sidak multiple comparison's test. In (A-E), hypertension was identified as the source of variation using two-way ANOVA, and post-hoc multiple comparison between sham and hypertension within each group revealed that the GF comparison was the source of variation. In (F), hypertension was identified as the source of variation using two-way ANOVA, and post-hoc multiple comparison between sham and hypertension within each group revealed that both the GF and COL comparisons were significant. The plot on the right in (A-F) shows the relative change induced by HTN in comparison to the respective sham group, tested using an unpaired two-tailed T-test. No change (100%) is depicted with a dotted line. For all plots, p-values are as follows; * $P \leq 0.05$, ** $P \leq 0.01$, *** $P \leq 0.001$, **** $P \leq 0.0001$.

Lastly, we investigated kidney fibrosis. Expression of *Col3a1*, a typical marker for fibrosis, significantly increased only in hypertensive GF mice (Figure 9A). Perivascular fibrosis analyzed by Masson's trichrome staining was accentuated in GF mice but not statistically different between the groups using two-way ANOVA; although when comparing the relative increase from sham to hypertension, there was a significant difference between GF and COL (Figure 9B-C). A previous study examining the impact of GF status on the progression of kidney injury demonstrated that sham-treated GF mice tended to have lower baseline values for putative kidney damage markers when compared to COL¹⁷⁶, and a similar (albeit

statistically insignificant) pattern could be seen for some markers in our mice. Overall, renal pathology upon hypertension induction was greater in GF mice when compared to their COL littermates.

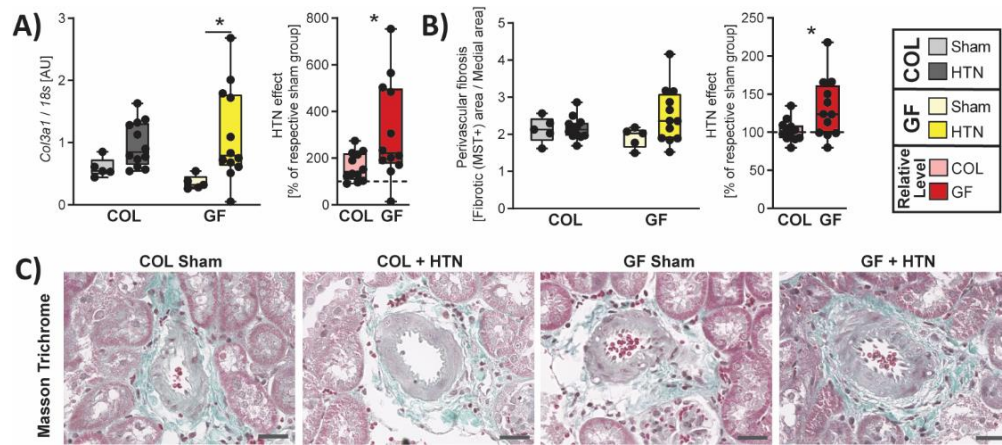


Figure 9. Hypertensive kidney fibrosis is increased in GF mice relative to COL

In (A), *Col3a1* expression was measured by qPCR from kidney tissue. Perivascular fibrosis from Masson's Trichrome Staining histological evaluation, measured as the fibrosis positive area divided by the medial area of the vessel, quantified in (B) and representative images are shown in (C). The scale bar represents 20 μ m. For (A-B), the left graph was tested using a two-way ANOVA and post-hoc Sidak multiple comparison's test. In (A), hypertension was identified as the source of variation using two-way ANOVA, and post-hoc multiple comparison between sham and hypertension within each group revealed that the GF comparison was the source of variation. In the right plot for panels (A-B), the relative change induced by hypertension in comparison to the respective sham group was tested using an unpaired two-tailed T-test. No change (100%) depicted as dotted line. For all plots, *p*-values are as follows; * *P* \leq 0.05.

4.1.3 Hypertensive heart damage is impacted by microbiome status

Cardiac dysfunction and hypertrophic remodeling are hallmarks of hypertensive pathogenesis. Cardiac hypertrophy was calculated as the heart weight-to-tibia length ratio (Figure 10A), which was only increased in hypertensive GF mice relative to their control. Left ventricular weight was estimated from echocardiography relative to the tibia length (Figure 10B) and similarly showed an increase in GF but not COL hypertension-treated mice. Cardiac *Nppb* expression (natriuretic peptides B, a known regulator of cardiorenal homeostasis; Figure 10C) confirmed this pattern. At later stages in cardiac dysfunction, systolic heart failure often develops, which is measured as a reduction in the ejection fraction. Neither the hypertensive GF nor COL mice had a reduced ejection fraction relative to their sham controls (Figure 10D).

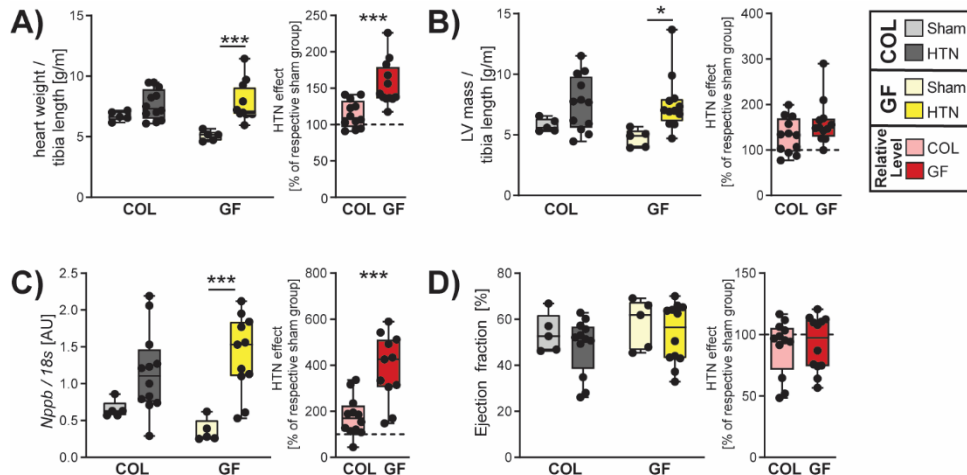


Figure 10. Cardiac dysfunction is moderately increased in GF mice

In (A), the heart weight normalized to tibia length [g/m] was taken at sacrifice. B) Left ventricular (LV) mass was estimated using echocardiography and normalized to the tibia length [g/m]. C) Cardiac ventricular natriuretic peptide gene expression (*Nppb*) was measured by qPCR. D) Echocardiography prior to sacrifice revealed no change in the ejection fraction in GF or COL mice. Echocardiography for (B) and (D) were performed in collaboration with the MDC Animal Phenotyping Technology Platform. Two-way ANOVA and post-hoc Sidak multiple comparison's test were used to test significance in the left plot in (A-D). In (A-C), hypertension was identified as the source of variation using two-way ANOVA, and post-hoc multiple comparison between sham and hypertension revealed that the GF comparison was the source of variation. To the right in (A-D), the relative change induced by hypertension in comparison to the respective sham group was tested using an unpaired two-tailed T-test. No change (100%) depicted as a dotted line. For all plots, p-values are as follows; * $P \leq 0.05$, *** $P \leq 0.001$

Disparate to the kidney phenotype, cardiac fibrosis was regulated in both GF and COL mice. Perivascular (Figure 11A and 11C) and interstitial (Figure 11B and 11D) fibrosis were increased in hypertensive GF and COL mice compared to their respective sham group, though using two-way ANOVA, only the GF group reached significance. Interestingly, when assessing the relative increase in hypertension compared to sham for markers of both perivascular and interstitial fibrosis, there was no difference in GF compared to COL mice (Figure 11A-11D).

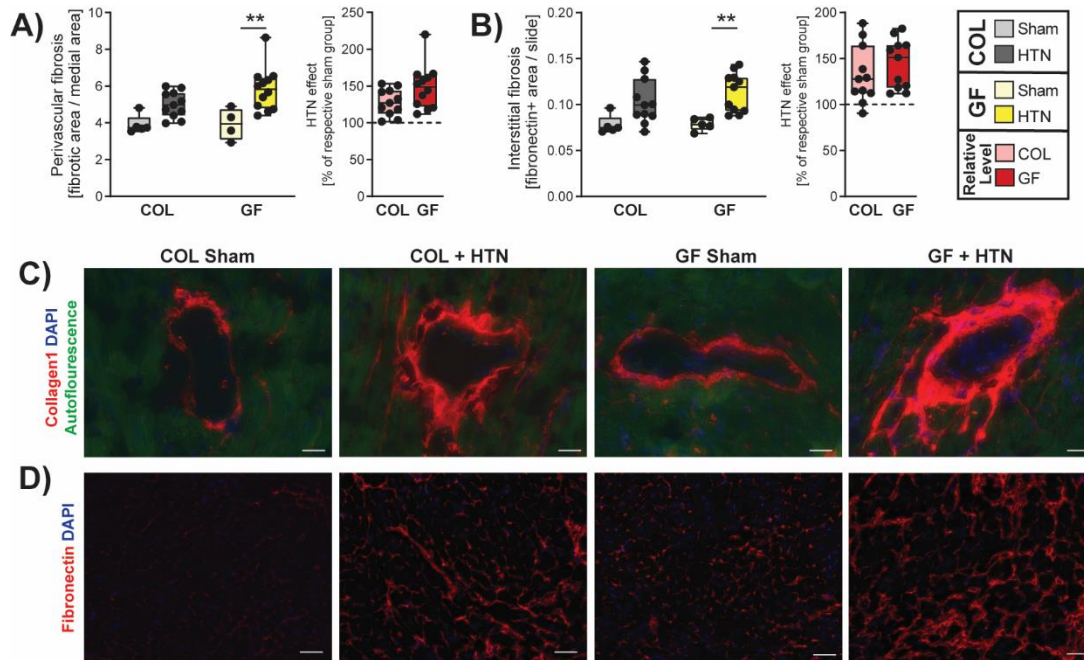


Figure 11. Cardiac fibrosis is regulated in GF and COL mice

Perivascular fibrosis from cardiac vessels, evaluated by measuring the fibrotic area relative to the medial area of vessels from Collagen 1 stained histology slides is quantified in (A) and representative images are shown in (C). B) Cardiac interstitial fibrosis was evaluated as fibronectin positive area proportionate to total area from 5 representative 40x magnification pictures from histological slides, and representative images are shown in (D). In (C-D) the scale bar represents 40 μm . In (A-B), hypertension was identified as the source of variation using two-way ANOVA, and post-hoc testing revealed that the GF comparison was the source of variation. In (A-B), the right plot shows the relative change induced by Ang II + 1% NaCl in comparison to the respective sham group, tested using an unpaired two-tailed T-test. No change (100%) depicted as dotted line. For all plots, p-values are as follows; ** $P \leq 0.01$.

Next, cardiac inflammation was examined. Despite an increase in *Ccl2* expression in GF and not COL (Figure 12A), macrophages (F4/80+) were increased in both GF and COL hearts upon hypertension. The change in overall leukocytes (CD45+) within the heart mimics the changes seen for macrophages (Figure 12C). Furthermore, no significance was reached when comparing CD4+ T helper cell infiltration using two-way anova (Figure 12D), whereas CD8+ cytotoxic T cells increased in both hypertensive GF and COL mice compared to sham (Figure 12E). Nevertheless, the relative comparison between sham and hypertension in GF and COL did reach significance for *Ccl2*, F4/80+, CD45+, and CD8+ cells, where GF was seen to have a greater increase for these inflammatory parameters (Figure 12A-C, E).

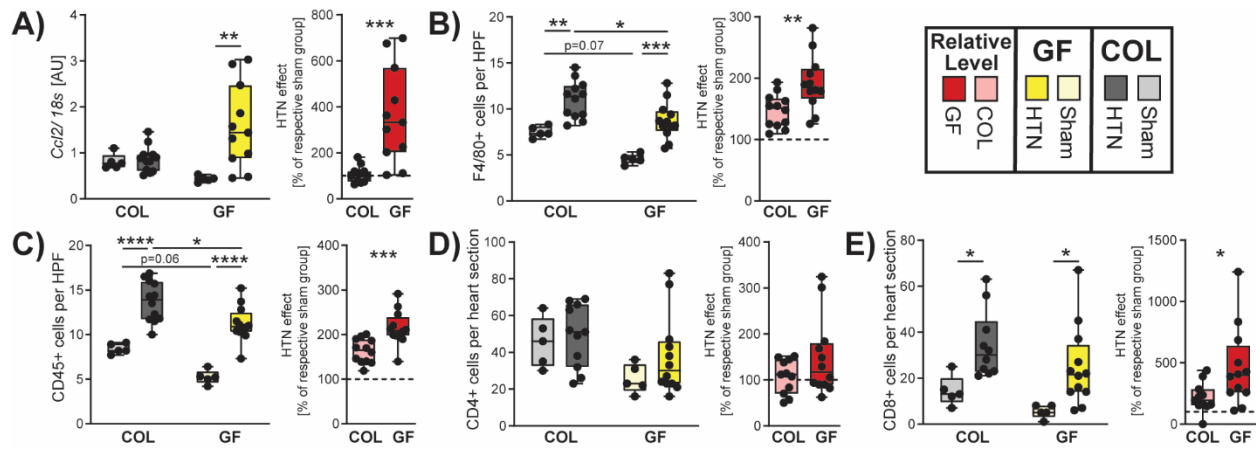


Figure 12. Hypertensive cardiac inflammation is regulated in both GF and COL mice

A) *Ccl2* was measured by PCR from heart tissue. B) Macrophages (F4/80+) and (C) leukocytes (CD45+) were counted from 5 representative high-power fields. CD4+ (D), and CD8+ (E) T cells were counted from whole heart sections. On the left (A-E), two-way ANOVA and post-hoc Sidak multiple comparison's test was used to test relevant comparisons. In (A), hypertension was identified as the source of variation using two-way ANOVA, and post-hoc multiple comparison between sham and hypertension within each group revealed that the GF comparison was the source of variation. In (B-C), hypertension and the microbiome were both identified as sources of variation and all significant post-hoc comparisons are indicated. In (E), hypertension was identified as the source of variation and post-hoc multiple comparison revealed that both the GF and COL within-group comparisons were significant. For (A-E) on the right, an unpaired two-tailed T-test was used to assess the relative change induced by hypertension in comparison to the respective sham group. No change (100%) depicted as dotted line. P-values are as follows; * $P \leq 0.05$, ** $P \leq 0.01$, *** $P \leq 0.001$, **** $P \leq 0.0001$.

4.1.4 The kidney is more sensitive to microbial status in hypertension than the heart

The size of the hypertension-induced effect within each group was additionally assessed by calculating the effect size (Cliff's delta) and fold change for all markers used to examine the phenotype in the kidney (Figure 13A) and heart (Figure 13B). Using this comprehensive univariate testing strategy, the impact of hypertension in GF and COL relative to their respective controls was analyzed and robust false discovery rate (FDR) correction was applied. All the markers which were assessed were grouped into subcategories to see whether any distinct patterns would emerge from these data. Across the subcategorizations of damage, fibrosis, and inflammatory markers in the kidney, the data convincingly suggest that GF mice experienced worsened hypertension-related kidney outcomes compared to COL mice (Figure 13A).

Unlike in the kidney, the distinctions between GF and COL were less evident in the heart (Figure 10-12). Although there was a hypertension effect in COL mice, significance was often not reached within the context of the initial statistical approach (two-way ANOVA) (e.g., cardiac interstitial and perivascular

fibrosis or cardiac *Nppb*). Using the comprehensive univariate testing strategy for the cardiac phenotypic data, considerable overlap between the effects of hypertension in GF and COL were evident (Figure 13B). There is an obvious congruence between the parameters examining hypertension-related cardiac fibrosis (e.g., *Col1a2*, *Col3a1*, and *Acta2* expression) in GF and COL. While several cardiac parameters reached significance here in GF and COL mice, a few markers only reached significance in the GF group (e.g., LV mass-to-tibia length, lung weight-to-tibia length, *Ccl2* and *TNfa* expression). Altogether, these data suggest that the development of hypertension-induced kidney damage is highly sensitive to the host's microbial status. While the cardiac phenotype was influenced by the microbial status to a degree, the development of hypertension-related cardiac dysfunction was not diametrically different in GF and COL mice, unlike what was seen for the kidney.

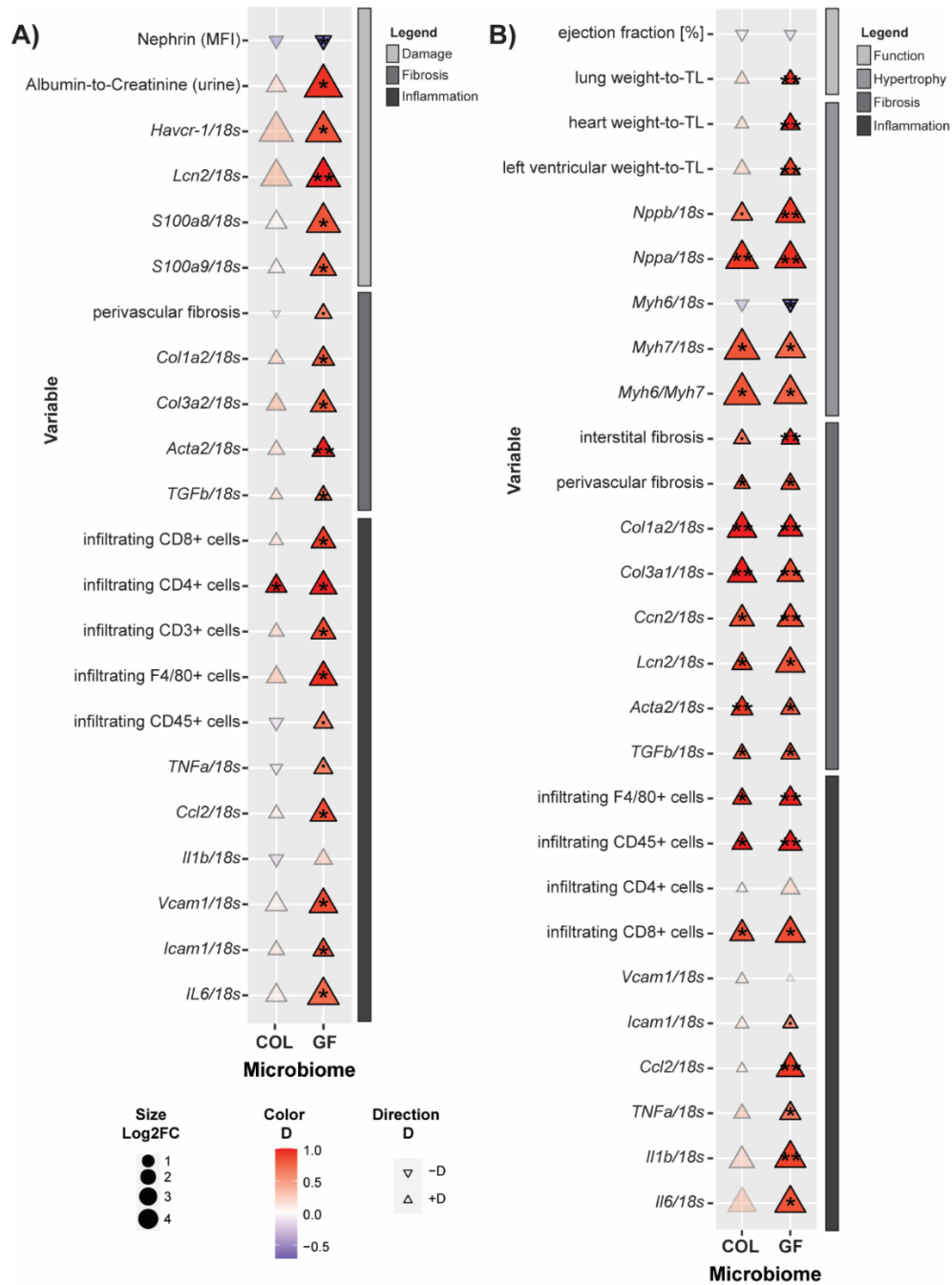


Figure 13. Comprehensive univariate evaluation of the kidney and cardiac phenotype

A) Effect sizes (Cliff's delta [D]) and fold changes were used to assess the effect of hypertension treatment relative to the respective sham group in GF and COL on the kidney phenotype (A) and cardiac phenotype in (B). Color and triangle direction indicates effect size. Size indicates log₂-transformed fold change (Log₂FC) of hypertension compared to the respective sham group. Significance was calculated using the Mann-Whitney U-test and was FDR-corrected with the Benjamini-Hochberg procedure to account for multiple testing. Markers for significant Q-values are superimposed, and transparency indicates non-significant effects. °q ≤ 0.1, *q ≤ 0.05, **q ≤ 0.01. Variables from kidney analysis in (A) are organized by subcategory (Damage, Fibrosis, Inflammation). Variables from cardiac analysis in (B) are organized by subcategory (Function, Hypertrophy, Fibrosis, Inflammation).

PCoA was also used to summarize the overall (dis)similarities amongst all experimental groups from the kidney (Figure 14A) and heart (Figure 14B) phenotypic data. To assess pairwise comparisons of interest, the overall dataset was divided and tested using PERMANOVA (Figure 14A-B). Pairwise PERMANOVA within the kidney revealed a significant distance between sham COL and hypertensive COL mice (P-value=0.012, F-value= 4.8). The impact of the treatment did result in a larger effect within the equivalent GF comparison, as determined by the F-value (P-value= 0.001, F-value= 8.2). In line with our initial univariate analyses (Figure 7-9, Figure 13A), the overall phenotypic change in the kidney in response to hypertension was larger in GF mice than in COL mice. As expected, the pairwise PERMANOVA between hypertension-treated GF and COL groups (P-value= 0.044, F-value= 3.2) was significant. Despite some slight differences within the sham groups (e.g., albuminuria, F4/80+ cells), pairwise comparison of GF and COL sham groups was insignificant (P-value= 0.262, F-value= 1.4).

Pairwise comparisons were also used to assess the trajectory of each group in the cardiac phenotypic space (Figure 13B). Consistent with the findings from the univariate evaluations of the overall cardiac phenotype (Figure 10-12, Figure 13B), the comparison between GF and COL hypertension groups showed significant overlap in the PCoA plot. Likewise, pairwise comparison between GF and COL hypertension groups was not significant (P-value= 0.391, F-value=1.1). Conversely, the difference between sham GF and COL samples was significant, indicating that the basal cardiac phenotype was influenced by colonization (P-value = 0.01, F-value = 5.6). As anticipated, comparison of hypertension to sham from GF (P-value = 0.01, F-value = 4.8) and COL (P-value = 0.046, F-value = 3.2) were both significant. The larger F-value in the GF group does mirror the larger phenotypic shifts in GF mice, most likely driven by significantly different sham groups. Taken together, the univariate and multivariate approaches indicate a larger effect of hypertension in GF mice for the most part, although there is a clear difference dependent on the organ of interest. In the case of the kidney, this increased effect was driven by a stronger adverse response of GF mice to hypertension, whereas in the case of the heart, this effect was driven by phenotypic differences in the healthy groups (sham-treated mice).

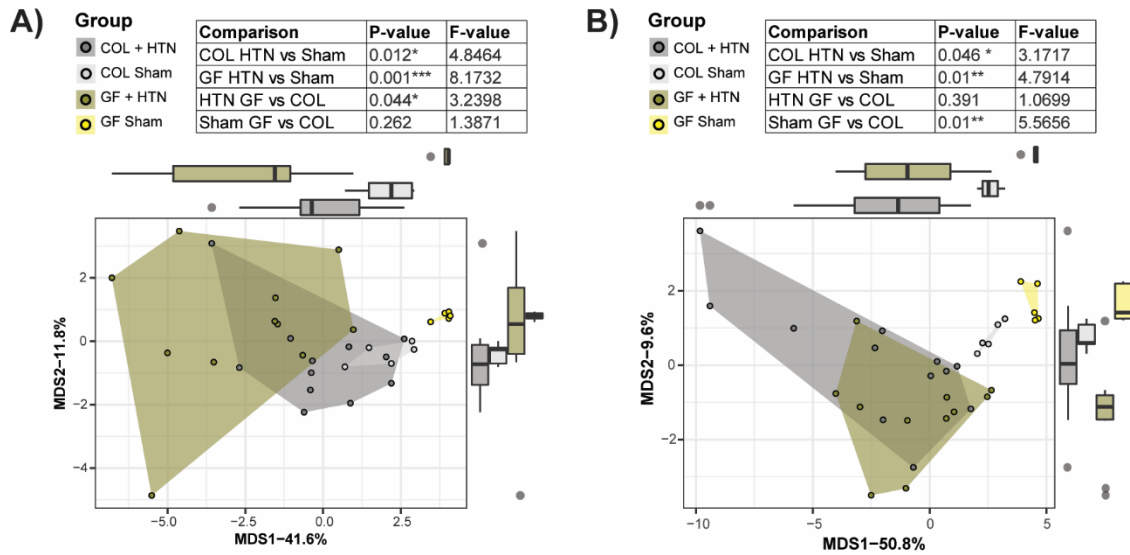


Figure 14. Comprehensive multivariate evaluation of the kidney and cardiac phenotype

PCoA was performed using multi-dimensional scaling (MDS) reduction based on Euclidean distances for (A) kidney and (B) cardiac phenotypic data to demonstrate the dissimilarities between samples from each group. Box plots corresponding to each MDS can be seen along the axes. Select pairwise comparisons between groups were performed using PERMANOVA testing and reported in the inset table.

4.1.5 The impact of the microbiome on vascular reactivity and BP

While the primary aim of this study was to investigate the impact of the microbiome in hypertensive heart and kidney damage, the vascular phenotype in these mice was also of interest. Others have suggested that vascular reactivity and BP homeostasis may be dependent on microbial colonization.^{177, 178} It would have been interesting to confirm the increase in BP associated hypertension induction, alongside the phenotypic shifts in the kidney and heart. It is possible that GF mice and COL mice may have developed differences in their basal mean arterial pressure (MAP) or BP reactivity to Ang II through the colonization process. Although, implantation of telemetry devices for BP monitoring requires microscopic vascular surgery, which was not feasible under sterile conditions in our primary experimental animals. To address the lingering questions about GF and COL vascular reactivity, additional mice were colonized via the same colonization procedure as previously outlined in 3.1.1, and *in vivo* BP measurements using an implanted arterial catheter in freely moving mice were performed. At baseline, GF mice had a significantly higher MAP than their colonized counterparts (Figure 15A). The mean MAP of each group (GF mean value = 118.4 mm Hg, COL mean value = 107.8 mm Hg) was still in a range considered normal for untreated C57BL/6J mice¹⁷⁹, though this does not negate the potential impacts of a nearly 10 mm Hg increase experienced by GF mice. Acute intravenous infusion of Ang II was used to test whether Ang II-dependent reactivity of the

vasculature is similar in these mice. Ang II infusion produced a comparable increase in BP in GF and COL mice (Figure 15B). For the sake of comparison to our primary animal experiments, the chronic infusion rate of the implanted Ang II minipumps is 16.67 ng/kg per second.

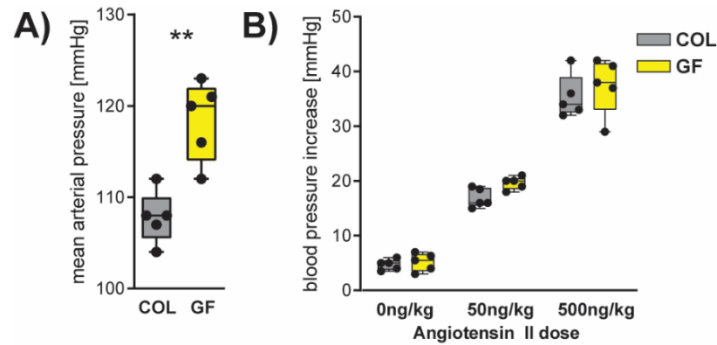


Figure 15. *In vivo* vascular reactivity of COL and GF mice

A) Awake, resting GF and COL mice were implanted with an arterial catheter to measure BP. The difference in baseline MAP was tested using an unpaired two-tailed t-test (** $P \leq 0.01$). B) BP was measured after acute intravenous infusion of a defined bolus of Angiotensin II. No statistical difference between the BP increase in GF and COL mice was found using a two-way repeated measurement ANOVA ($p=0.14$). Ang II dose, as expected, had a significant influence on the rise in BP ($p \leq 0.0001$, not shown). This experiment was done in collaboration with André Felipe Rodrigues and Mihail Todiras of the Bader lab (MDC, Berlin).

4.1.6 Inflammation in hypertension is impacted by the microbiome

Immune mechanisms are known to play a role in the pathogenesis of hypertension (detailed in section 1.3.2) and certain microbially-produced metabolites (e.g., SCFA and ILA) can influence these inflammatory processes (detailed in section 1.3.3). The splenic immune cell composition was used as a surrogate parameter to investigate systemic inflammation in GF and COL mice with hypertension by flow cytometry. In total, of 23 immune cell subsets which were quantified, 12 were differentially affected by hypertension when comparing each treated group to the respective sham.

Table 3. Immune cell subsets measured in GF and COL mice

Category	Variable	P	P	Q	Q	FC	FC	D	D
		GF	COL	GF	COL	GF	COL	GF	COL
Th cell differentiation	Ki67+ % of Treg	0.058	0.014	0.110	0.062	1.742	1.423	0.617	0.767
Th cell differentiation	Th17 % of T helper cells	0.002	0.001	0.017	0.007	5.138	3.797	1.000	0.967
Th cell differentiation	Ki67+ % of Th17	0.646	0.140	0.708	0.268	1.008	0.833	-0.167	-0.483
Th cell differentiation	Th1-like Th17 % T helper cells	0.058	0.101	0.110	0.239	2.842	2.937	0.617	0.533
Th cell differentiation	Ki67+ % of Th1-like Th17	0.013	0.104	0.050	0.239	1.729	1.287	0.800	0.533

Th cell differentiation	Th1 % of T helper cells	0.721	0.506	0.754	0.646	0.942	0.770	-0.133	-0.233
Th cell differentiation	Ki67+ % of Th1	0.023	0.562	0.076	0.660	1.365	1.051	0.733	0.200
T cell overview	T cells % of splenocytes	0.874	0.342	0.874	0.492	1.001	0.963	-0.067	-0.317
Th cell differentiation	Treg % of T helper cells	0.442	0.574	0.508	0.660	0.876	0.818	-0.267	-0.200
T cell overview	T helper % of T cells	0.082	0.013	0.145	0.062	0.942	0.931	-0.567	-0.800
T cell subtype	Central memory % of T helper cells	0.002	0.916	0.017	0.916	0.440	1.134	-0.983	0.050
T cell subtype	Effector memory % of T helper cells	0.246	0.646	0.333	0.675	1.159	1.097	0.383	0.167
T cell subtype	Naive % of T helper cells	0.130	0.234	0.213	0.385	1.069	0.915	0.500	-0.400
T cell subtype	Effector memory % of cytotoxic T cells	0.006	0.130	0.028	0.268	0.578	1.359	-0.833	0.500
T cell subtype	Central memory % of cytotoxic T cells	0.031	0.460	0.088	0.622	1.333	0.928	0.700	-0.250
T cell subtype	Naive % of cytotoxic T cells	0.225	0.646	0.324	0.675	1.034	0.953	0.400	-0.167
T cell overview	gd T cells % of T cells	0.315	0.315	0.382	0.484	0.951	1.067	-0.333	0.333
Innate immunity	gMDSC % of splenocytes	0.001	0.082	0.017	0.235	5.865	1.755	0.933	0.567
Innate immunity	mMDSC % of splenocytes	0.160	0.000	0.245	0.007	1.684	3.000	0.467	1.000
Innate immunity	CD11c low CD11b high % of splenocytes	0.037	0.027	0.093	0.103	0.852	1.667	-0.667	0.717
Innate immunity	CD11c high CD11b+ % of splenocytes	0.057	0.186	0.110	0.329	0.732	0.755	-0.617	-0.433
Innate immunity	CD11c+ CD11b- % of splenocytes	0.292	0.082	0.373	0.235	0.881	1.170	-0.350	0.567
Innate immunity	CD11c- CD11b+ % of splenocytes	0.004	0.006	0.022	0.047	2.795	1.677	0.867	0.833

Univariate analysis from the immune data measured using flow cytometry from sham and hypertensive mice in GF and COL. P represents the raw P-value, and Q represents the P-value after FDR correction. FC is the fold-change of the hypertension effect relative to sham (which was log2 transformed for plotting in Figure 16B). D represents the effect size (Cliff's delta) of the hypertension to sham effect within GF or COL.

The impact of each of the 23 immune parameters on the trajectory of each treatment group multivariately was examined using PCoA (Figure 16A). Because it is known that the immune system of GF mice differs from their colonized counterparts³⁴, it was unsurprising that the pairwise comparison of sham-treated GF and COL mice (P-value = 0.011, F-value = 6.6) was significant. It is indeed intriguing that the 8-week colonization period induced such a shift in the immunome, given that these mice were not separated until their fourth week of life. This difference between COL and GF was also evident in the mice which were hypertension treated (P-value = 0.026, F-value = 2.8). Pairwise comparisons of individual groups using PERMANOVA indicated that the hypertension to sham comparison was significant in the GF group (P-value = 0.006, F-value = 4.8), but not within the COL group (P-value = 0.177, F-value = 1.6) (Figure 16B). Overall, it seems the inflammatory status of GF mice was disturbed to a greater degree by hypertension induction than in COL mice. The effect size and fold change calculation (as shown in 4.1.4) was used to evaluate the changes to the 12 immune cell subsets which were regulated by hypertension treatment in either GF or COL mice, or both (Figure 16B).

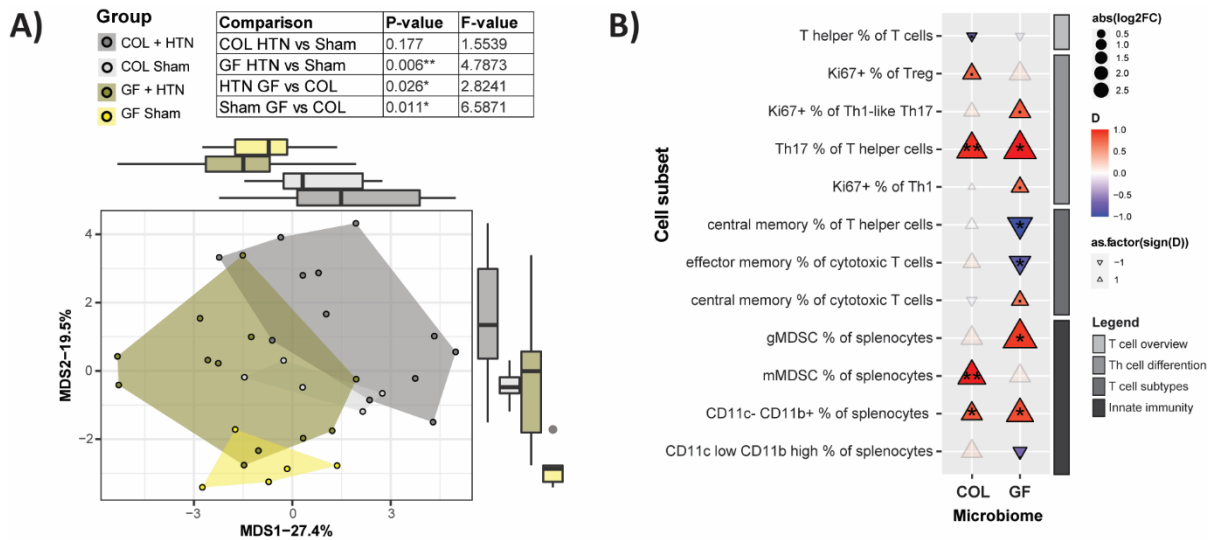


Figure 16. Inflammation is influenced by microbial status

Several unique immune cell subsets were measured from the spleen, as a proxy measure of systemic inflammation. A) Principal Coordinate analysis was performed based on Euclidean distance scaling of immunophenotyping data to demonstrate the dissimilarities between study groups. Pairwise comparisons between groups were performed using PERMANOVA and reported in the inset table. B) Immune cells which were regulated by hypertensive treatment in one or both conditions (GF and COL) are shown. Immune cell subsets are organized by subcategory (Innate immunity and T cell overview, differentiation, and subtypes) and subsets. Effect size (D, Cliff's delta) is shown to demonstrate the effect of hypertension relative to the respective sham group in GF and COL. Color and triangle direction indicates effect size. Size indicates log₂-transformed fold change (Log₂FC) of hypertension induction compared to the respective sham group. Significance was calculated using the Mann-Whitney U test and was FDR-corrected using the Benjamini-Hochberg procedure to account for multiple testing. Markers for significant Q-values are superimposed, and transparency indicates non-significant effects. ° $q \leq 0.1$, * $q \leq 0.05$, ** $q \leq 0.01$. Panel design and staining was carried out by Dr. Hendrik Bartolomaeus and Dr. Nicola Wilck (ECRC, Berlin), and I performed the gating and analysis of immunophenotyping data.

Splenic MDSC are known to increase in hypertension and have anti-hypertensive properties.¹¹¹ Interestingly, there was an increase in monocytic MDSC (mMDSC) upon hypertension, and this increase was only significant in hypertensive COL mice (Figure 17A). Furthermore, for both mMDSC and granulocytic MDSC (gMDSC) (Figure 17B) subtypes, hypertensive COL mice showed a significantly higher frequency of these anti-hypertensive immune cells than hypertensive GF mice. Interestingly, the relative increase in hypertension compared to sham for mMDSC was lesser in GF mice but greater for gMDSC than in COL (Figure 17A-B). The subtleties of whether the relative increase, or absolute number of MDSCs is relevant in hypertension is currently unknown. Th17 cell activity has been previously shown to strongly impact hypertension pathogenesis, BP, and the infiltration of immune cells in target organs.¹⁰⁷ An increase in Th17 cells in was notable in both GF and COL mice, though this effect only reached significance in GF mice by two-way ANOVA (Figure 17C). The relative change in Th17 cells, though insignificant, is higher in

GF compared to COL. This increase could be driven by a slight enrichment of pathological Th1-like Th17 cells, defined by their co-expression RORγT and Tbet (Figure 17D).¹⁸⁰ Whether these findings are causally associated with the hypertensive damage seen in GF and COL mice is indeterminable from these experiments.

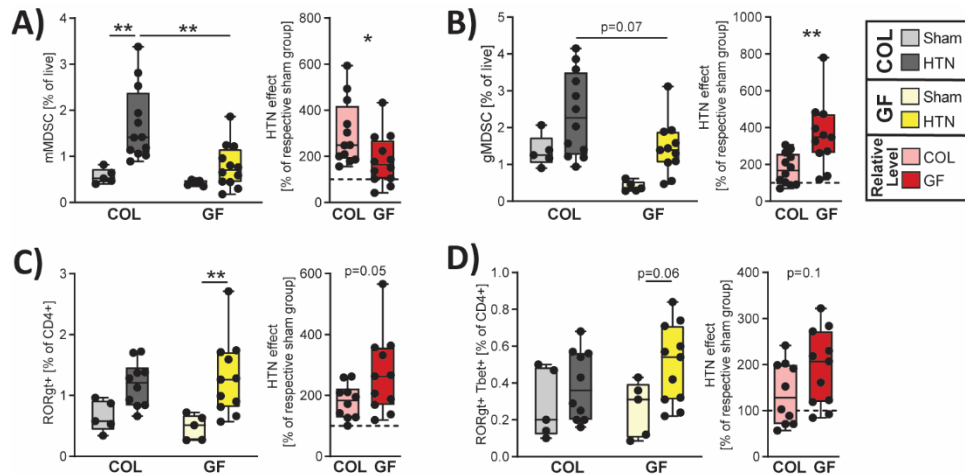


Figure 17. Th17 and MDSC cells are differentially regulated in GF and COL mice

These data are derived from the dataset described in Figure 16. Selected immune cells subsets from splenic immunophenotyping are shown. Monocytic MDSCs (mMDSC, A), granulocytic MDSCs (gMDSC, B), Th17 (C), and Th1-like Th17 cells (D) are shown. To the left in each panel, two-way ANOVA and post-hoc Sidak multiple comparison's test were used. In (A-B), hypertension and the microbiome were both identified as sources of variation and significant post-hoc comparisons of relevance are indicated. In (C-D), hypertension was identified as the source of variation using two-way ANOVA, and post-hoc multiple comparison between sham and hypertension within each group revealed that the GF comparison was the source of variation. To the right, the relative change induced by Ang II + 1% NaCl in comparison to the respective sham group was tested using an unpaired two-tailed T-test. No change (100%) depicted as dotted line. For all plots, p-values are as follows; * $P \leq 0.05$, ** $P \leq 0.01$.

Pre-existing conditions have been shown to impact the downstream effector differentiation of naïve T cell responses.¹⁸¹⁻¹⁸³ Since the conditions of origin for naïve T cells can influence cell fate, I hypothesized that in the absence of microbes and their metabolites, these cells in GF mice may polarize differently than their counterparts from COL mice. *In vitro* Th17 polarization of naïve T cells derived from the mesenteric lymph nodes of GF and CONV mice was performed in the presence or absence of Ang II. Naïve T cells from GF mice more readily polarized towards Th17 cells than cells from CONV mice, particularly in the presence of Ang II (Figure 18A-B). These *in vitro* findings suggest that the pre-conditioning of naïve T cells within GF and COL mice may impact polarization into pro-inflammatory effector T cells.

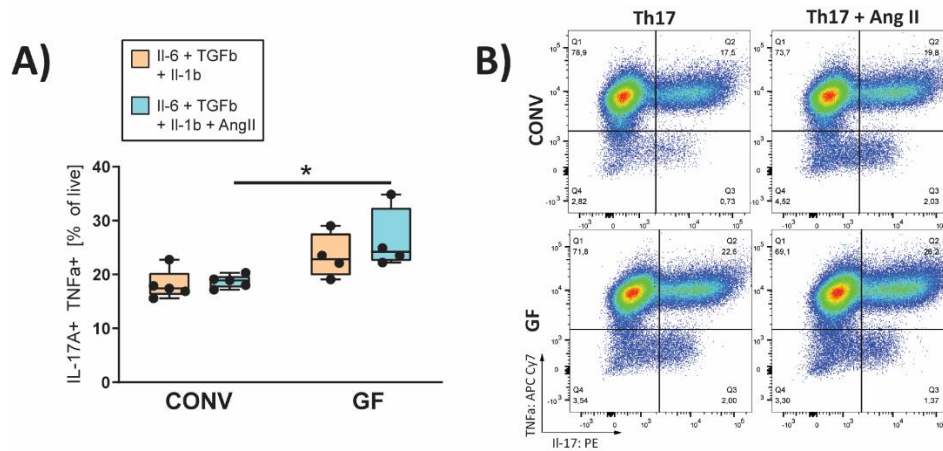


Figure 18. *In vitro* Th17 polarization of naïve T cells from GF and CONV mice in the presence of Ang II

A) Naïve T cells from mesenteric lymph nodes of either GF or CONV mice, polarized *in vitro* towards a Th17 using a cocktail of IL-1 β , TGF β , and IL-6 with or without Ang II (GF n = 4, CONV n = 5), and representative images are shown in (B). In (A) two-way ANOVA and post-hoc Sidak multiple comparison's test was used to test significance and revealed that the microbiome was the source of variation. Post-hoc testing revealed that the Ang II-treated groups within CONV and GF were significantly different (* P \leq 0.05).

4.1.7 Serum metabolome is impacted by microbiome status

As metabolites are known to influence hypertension pathogenesis (see section 1.3.3), the broad-spectrum MxP Quant 500 (Biocrates) kit was used to investigate the serum metabolome. Consistent with the literature¹⁶⁵, GF or COL status affected the hypertension-associated metabolome. Because there were over 300 individually measured metabolites measured using the kit, and hundreds were regulated by hypertension treatment, grouping by metabolite class was used to understand prevailing patterns from these data (Figure 19). There were 15 classes of metabolites where hypertension (compared to the respective sham) had an effect for GF, COL, or both. Four of those metabolite classes (phosphatidylcholines, hexosylceramides, alkaloids, fatty acids) showed similar trajectories in GF and COL mice, suggesting these classes changed in a microbiome-independent manner upon hypertension (Figure 19).

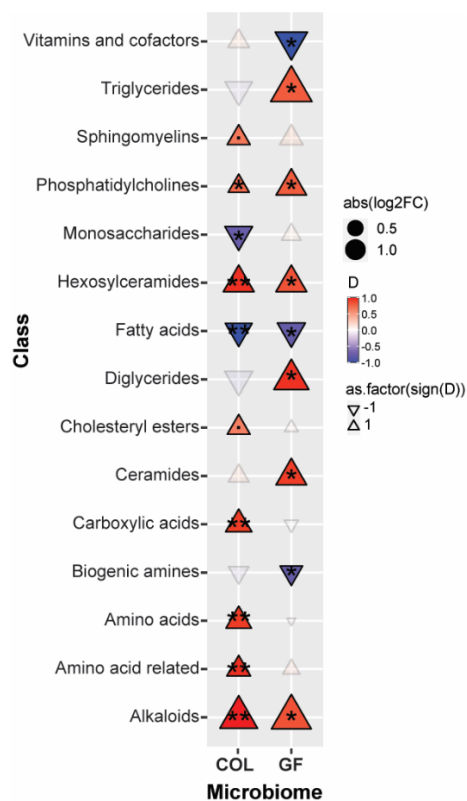


Figure 19. Serum metabolome is impacted by hypertension in GF and COL

Serum metabolites were analyzed from GF and COL mice with and without hypertension by Mass spectrometry with the MxP500 Quant kit (Biocrates). Individual metabolite normalized intensities were grouped by sub-classification within individual samples to assess the overall shifts in metabolism associated with hypertension treatment. Effect size (Cliff's delta [D], indicated by triangle colour and direction) was used to compare hypertension relative to the respective sham group. Triangle size indicates log₂-transformed fold change (Log₂FC). Significance was calculated using the Mann-Whitney U test and was FDR-corrected using the Benjamini-Hochberg procedure to account for multiple testing. Markers for significant Q-values are superimposed, and transparency indicates non-significance. P-values are as follows: °q ≤ 0.1, *q ≤ 0.05, **q ≤ 0.01. Metabolomics data preprocessing and peak integration was performed by Dr. Raphaela Fritsche (BIH Metabolomics Core Facility, Berlin), and I performed data quality analysis based on QC standards, data selection, and all subsequent analyses.

Unsurprisingly, the serum metabolome was significantly impacted by the microbiome status of the host. There were some candidate metabolites, TMAO, 3-indolepropionic acid (3-IPA), and IS, which have been identified as relevant in kidney and heart disease^{126, 184, 185} which could be found only in the samples from COL mice (Figure 20A-C). 3-IPA (Figure 20B) was decreased in hypertensive COL mice, whereas there was a slight but insignificant increase in TMAO (Figure 20A), and an increase in IS (Figure 20C).

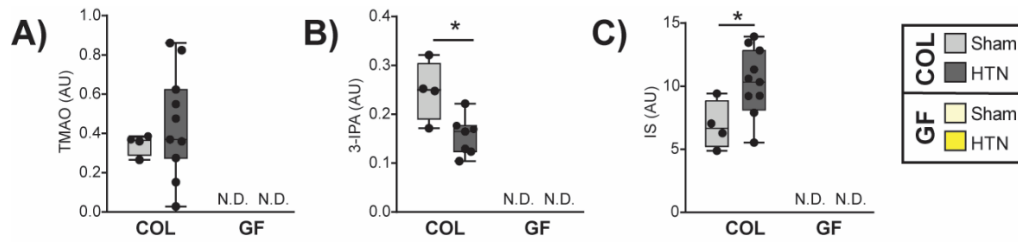


Figure 20. Microbially-produced metabolites TMAO, 3-IPA, and IS are only present in COL mice
*Microbially-produced metabolites of note in CVD measured using the Biocrates MxP500 Quant kit (as described in Figure 19). TMAO (A), 3-IPA (B), and IS (C) were only measurable in the serum of COL and not GF mice. Unpaired two-tailed T-test was used to test for significance in COL values. Significant P-values are denoted as; * $p < 0.05$.*

Although the serum metabolite measurements used here were very comprehensive, they did not cover SCFA metabolites, some of which have potent anti-hypertensive properties (see section 1.3.3). SCFA are highly concentrated within the gut but are lowly abundant and at times undetectable in the systemic circulation, hence the most common mode of measurement is from luminal or fecal matter. Mass spectrometry measurements of fecal C2, C3, and C4 (Figure 21) were performed to assess SCFAs in GF and CONV mice, as a proof-of-principle to demonstrate that our GF colonies are SCFA-depleted. GF mice have long been known to be SCFA depleted¹⁸⁶. I expect that the absence of SCFA in GF mice may have played a role in the phenotypic differences between GF and COL.

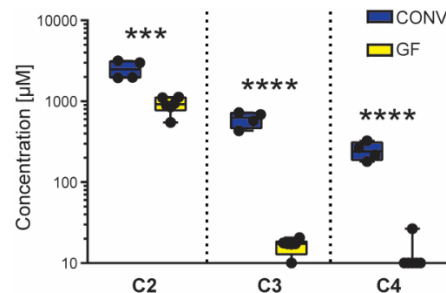


Figure 21. Fecal SCFA in GF and CONV mice
*Fecal short-chain fatty acids (SCFA) from GF or CONV mice demonstrates the significant decrease in C2, as well as the absence of metabolites C3 and C4 in the GF setting (GF n=6, CONV n=4). Significance was tested using unpaired two-tailed Student's t-test for each metabolite individually (*** $p \leq 0.001$, **** $p \leq 0.0001$). SCFA were measured in collaboration with Dr. Stefan Kempa (MDC Proteomics and Metabolomics Platform, Berlin).*

4.1.8 Not all microbiomes in C57BL/6J mice are created equal

Although it is known that microbially-produced metabolites have a potent effect on the pathogenesis of hypertension^{21, 24, 25, 187}, it is unclear whether the putative microbiome from each study can be considered

equivalent or has a similar effect on the metabolome. A recent study from Cheema and Pluznick¹⁶⁵ showed the effect of hypertension on the microbiome and metabolome in GF and CONV mice. Although our experimental set ups were different, I wondered whether the comparison of the microbiome and metabolome data from this study with published data may provide insight into the comparability of microbiomes in different experimental settings. PCoA derived from genus level information from each of the studies showed that with or without hypertension, the microbiome used in these studies did not overlap (Figure 22A). To evaluate whether the implantation of a microbiome would cause a higher level of dissimilarity between the mice with a microbiome compared to the GF groups from both studies; the serum metabolome was curated from both datasets for metabolites which could be measured in all samples. The trajectory of individual metabolites in hypertension compared to sham is shown from GF (X-axis) and COL/CONV (Y-axis) in Figure 22B. Each metabolite is shown twice as there is an equivalent point for both the Pluznick and Berlin dataset. There was significantly less distance between individual metabolites within the serum metabolome of GF mice from these two studies than in the equivalent COL/CONV mice comparison (Figure 22B-C). In other words, the similarity of the hypertension-induced effect on the serum metabolome in GF groups within these two datasets is higher than the equivalent COL/CONV comparison. Either our utilization of littermate mice, or more likely, the obvious differences in the microbiomes used for experimentation, led to incongruities between these two datasets.

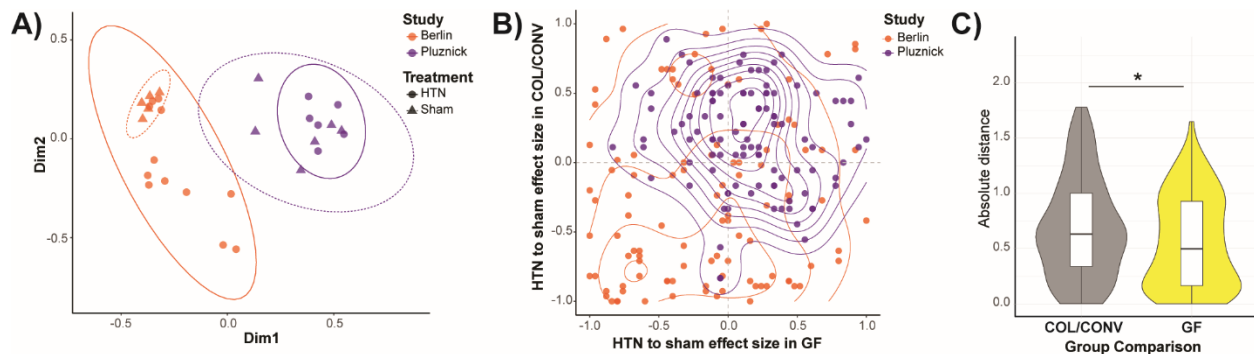


Figure 22. Hypertension in mice with a microbiome elicits divergent metabolome effects

PCoA based on Bray-Curtis distance scaling of microbiome data annotated to the genus level published by Cheema and Pluznick (annotated as Pluznick) and our data (annotated as Berlin) is shown in (A). Colour indicates study group, and ellipses indicate hypertension or sham within each respective study. B) Metabolites which were quantifiable in the serum of GF and COL/CONV mice in both the Pluznick and Berlin study are shown. On the Y-axis the effect size of hypertension compared to sham in COL/CONV mice is shown, and the X-axis shows the effect size of hypertension compared to sham in GF mice. C) Quantification of the distance between the same metabolite along the GF (X-axis) or COL/CONV (Y-axis) from the Pluznick study versus the Berlin study. Significance was tested using the Mann-Whitney U test ($*p \leq 0.05$). I designed the analysis and annotated the metabolomics data from both studies, and Chia-Yu Chen (ECRC, Berlin) assisted with the re-annotation of Berlin microbiome data and generation of graphics.

4.2 Interstitial fluid isolation from the GI tract

4.2.1 Properties of the interstitial fluid reservoir within the GI tract

The variability of immune cells along the gut in concordance with regional changes to the microbiome and its metabolic byproducts is believed to play a role in the development of inflammation in the gut and elsewhere in distal organ systems. The importance of the microbiome in hypertension was detailed in section 4.1; though the exact mechanism by which the microbiome interacted with the host to elicit this differential response is still not well understood. This is partially because the methods currently available are not fully able to capture the host-side of the host-microbiome interface. In section 1.4, IF was presented as a possible window into this compartment. Access to IF from the GI tract would facilitate the assessment of individual substances of interest, to assess whether they are produced locally. To address aim 2.2, I employed known methods within the IF literature to optimize the extraction of IF from GI tissue, to see whether this could be used to directly zoom in to the microenvironment in the GI tract. Initially, healthy CONV C57BL/6J mice were used for experimentation, as mice are the most common model system and would likely be the primary species for implementation of these methods in future. Sectioning the GI tract into smaller subsections for regional examination was a critical part of assay development. For practical reasons, during assay development, not all segments were used for all experiments. Where appropriate, the segments utilized are denoted in an inset schematic for each figure. First, it was important to examine whether there was a meaningful amount of IF within the GI tissue. Unsurprisingly, the ECV of GI tissue was relatively comparable to muscular tissue¹⁴⁰, with an estimated volume of 0.1 to 0.2 mL/g wet weight, depending on the segment of interest (Figure 23). The total tissue water (the ECV and ICV) within a given tissue was also determined from the colon, cecum, ileum, jejunum, and duodenum. There were some very small but significant differences in the total tissue water for individual segments, though this is not likely to be physiologically important. The maximal difference between any two segments was 0.02 mL/g, and mean total tissue water value across all samples was 0.79 mL/g. From these experiments we were able to characterize the properties of the fluid spaces within GI tissue. Given that the wet weight of excised tissue for any one gut segment was maximally 0.2 to 0.3 g from mice, we anticipated that it may be difficult to access the IF from these tissues.

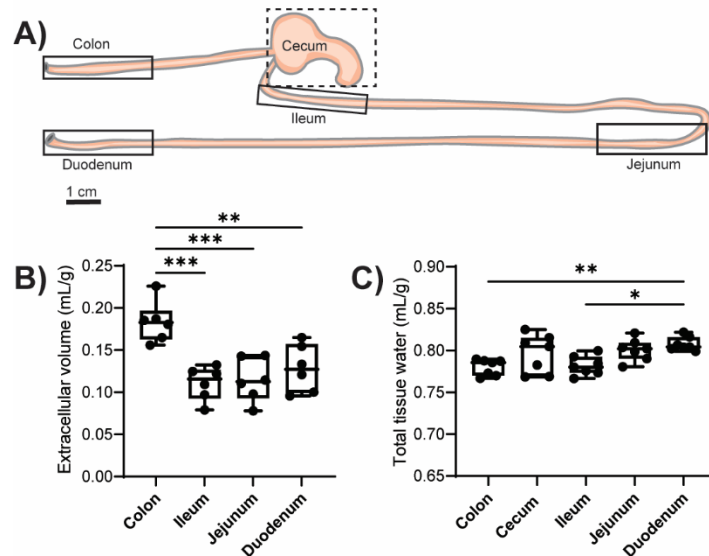


Figure 23. Extracellular fluid volume within the GI tract of C57BL/6J mice

A) Schematic of the segments taken for the analysis from C57BL/6J CONV mice (the cecum was only used in (C)). B) The extracellular fluid volume was determined by counting $^{51}\text{Cr-EDTA}$ for each gut segment in comparison to the plasma equilibration of the tracer ($n=6$). In (C) the total tissue water is shown from C57BL/6J CONV mice ($n=7$). Significance was tested using an ordinary one-way ANOVA with Tukey's multiple comparisons test. P -values are as follows: $*p \leq 0.05$, $**p \leq 0.01$, $***p \leq 0.001$. $^{51}\text{Cr-EDTA}$ extracellular tracer experiments were performed in collaboration with Dr. Helge Wiig and Dr. Tine V. Karlsen (University of Bergen), and I measured the total tissue water in a separate experiment.

4.2.2 Development of the Elution method

Because the IF space from GI tissue in mice was expected to be low-yield, the first method employed to investigate this space was an elution-based method. Elution-based methods have been used previously to isolate IF from tumor tissue and are advantageous because they result in a high-volume fluid which can be used for multiple measurements.¹⁴⁰ The general principle of the method is that the cleaned excised tissue is placed in an isosmotic buffer to maintain tissue integrity and osmotic pressure. Substances from the interstitium should move from their high concentration in the IF into the surrounding buffer. The elution IF will be dilute compared to the original IF within native tissue, though the dilution factor is known and can be accounted for. A schematic detailing how this method was applied is shown in Figure 24.

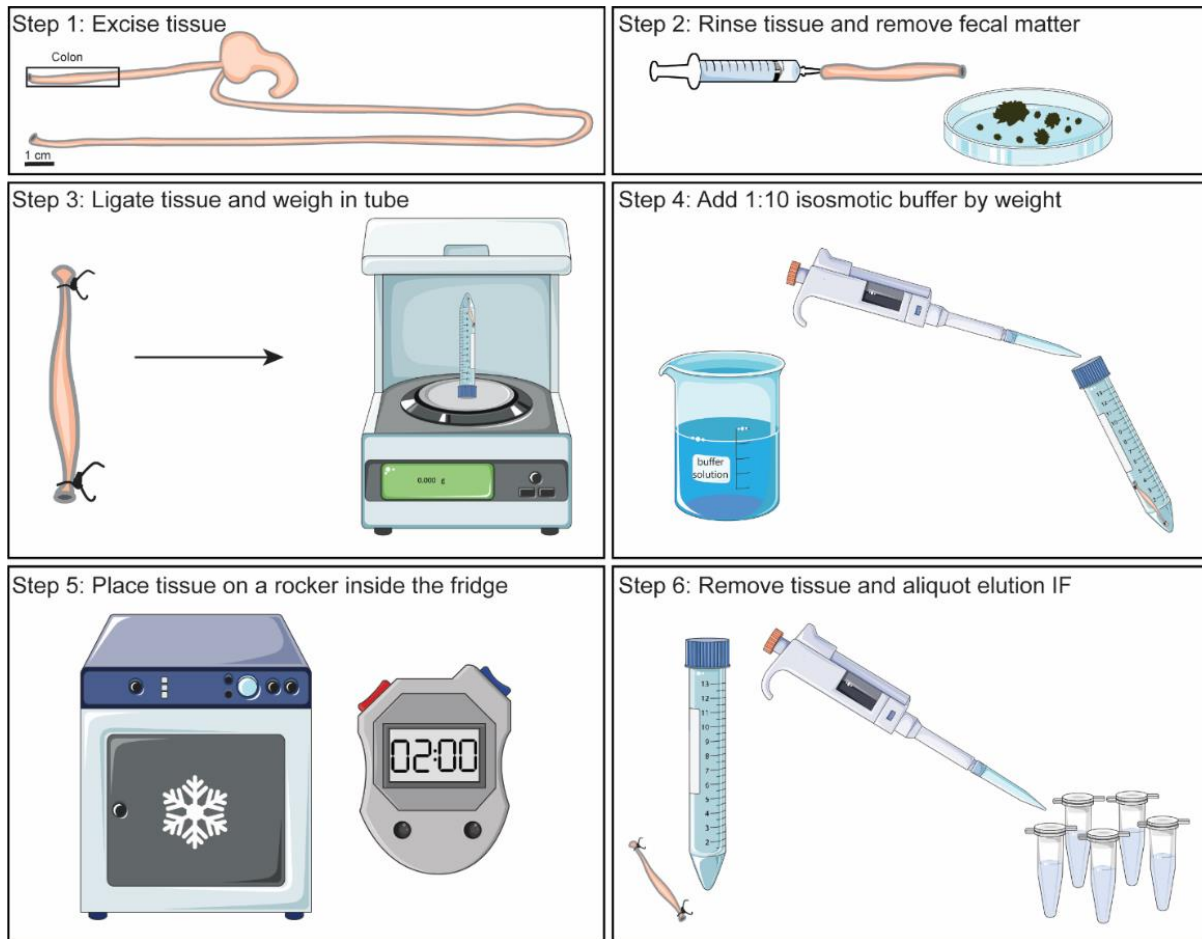


Figure 24. Schematic for the collection of IF using an elution-based method

The GI tract from just below the stomach to the colon was excised. 3 cm pieces of GI tissue were measured, cut and immediately washed from the luminal side using a blunted syringe with approximately 5 ml of isotonic buffer to ensure the removal of any luminal contents. When applicable the fecal matter from the indicated segment was collected prior to rinsing. Then both ends of the tissue were ligated to ensure that if any microscopic luminal contents were still attached to the inner surface of the gut, they would not be extracted into the surrounding buffer. After ligation, tissue was placed in a 1:10 dilution of an appropriate isosmotic buffer solution and placed on a rocker at 4 °C. After the given elution time, tissue was removed, and the eluted fluid was aliquoted and stored at -80 °C for further analysis. Some images were adapted from the Servier Medical Art collection (<https://smart.servier.com>).

In the initial phases of method development, ionic composition from IF was used as a proxy to measure the efficacy of the elution method in different formats.^{140, 142} The ionic composition of IF should be similar to that of plasma^{140, 142}; low in potassium (K^+) and around 140 mmol/L of sodium ions (Na^+). The ratio of IF to serum ideally should be close to one, and K^+ values should be between 3.5-5.0 mmol/L. To optimize the use of elution from GI tissue, the elution timepoint and buffer were varied to see whether this would impact IF isolation (Figure 25B-E). Longer timepoints led to higher K^+ in eluted samples (Figure 25B-C), potentially indicating damage to cells from excised tissue and/or reduced activity of the Na^+/K^+ ATPase.

The impact of different isosmotic mannitol or glucose buffer solutions was also assessed from samples eluted for 8 hours, and minimal differences were observed (Figure 25D-E), and we selected a mannitol-based solution for future experiments arbitrarily. Saline is also a typical isosmotic buffer option for elution, although evaluation of this buffer using ion chromatography is not feasible.

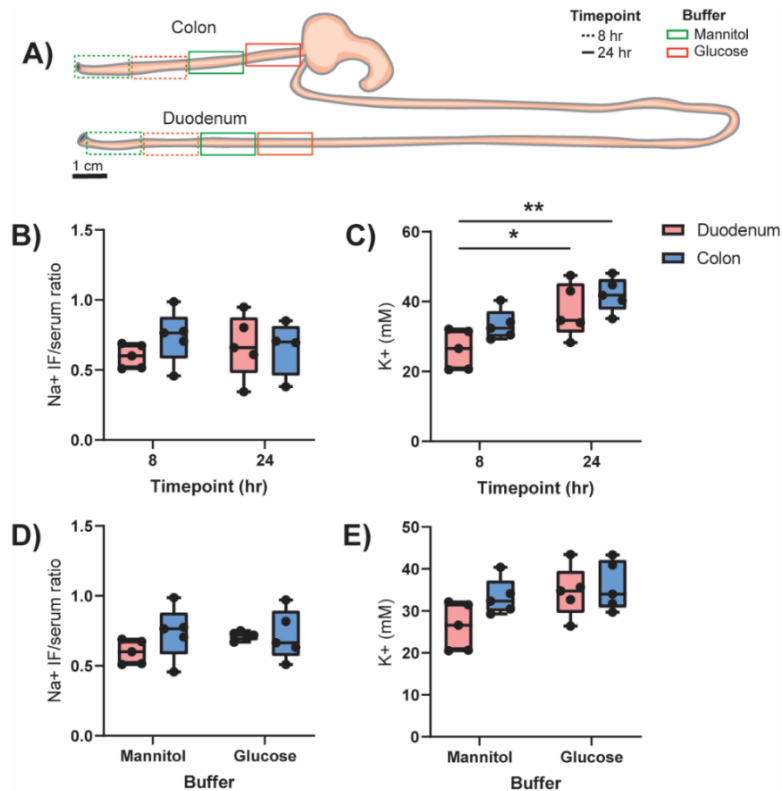


Figure 25. Timepoint but not buffer plays a role in eluted ion composition

A) The scheme above shows the sectioning approach used for GI tissue from C57BL/6J CONV mice in (B-E). 4 segments from each region of the colon and duodenum were taken and were either allocated to be either placed in mannitol or glucose and left eluting for 8 or 24 hours. Comparison of the Na^+ IF to serum ratio (B) and IF K^+ (C) by ion chromatography from samples eluted for 8 or 24 hours in a mannitol-based buffer. Buffer comparison of the Na^+ IF to serum ratio (D) and IF K^+ (E) between samples eluted in a mannitol or glucose solution (please note that some of these values are overlapping with (B-C)). In (B-E) two-way ANOVA and post-hoc Sidak multiple comparison's test was used to test significance. In (B) and (D), no significance was found. In C) both timepoint and segment were found as sources of variation and all significant post-hoc comparisons are plotted. In E) buffer was found as the source of variation but no post-hoc comparisons were significant. $N=5$ for all conditions, and 1 outlier was excluded 24-hour Na^+ IF/serum ratio from the colon. P -values are as follows; * $p \leq 0.05$, ** $p \leq 0.01$. I performed the experiments shown here, and samples were sent for ion chromatography measurement in the lab of Dr. Helge Wiig (University of Bergen).

These initial experiments indicated that shorter elution timepoints may be optimal to reduce cellular breakdown and dilution of elution fluid by intracellular contents. I then repeated this experiment with a

larger number of gut segments and shorter elution timepoints for comparison (2, 4 and 8 hours) and found that across all segments, shorter times for elution resulted in less K^+ deposited in the elution buffer (Figure 26B). The K^+ within any given elution IF sample was still far higher than what could be seen in serum, though this is not unexpected, given the strong gradient of intracellular K^+ and high ICV relative to ECV in the GI tract. To ensure that the preparatory steps used in the elution approach were effective at eliminating fecal matter, 16s rRNA was measured from the elution fluids used in Figure 26. 16s rRNA was not detectable in any of the samples assessed (data not shown), so we do not expect that fecal matter is influencing our results directly.

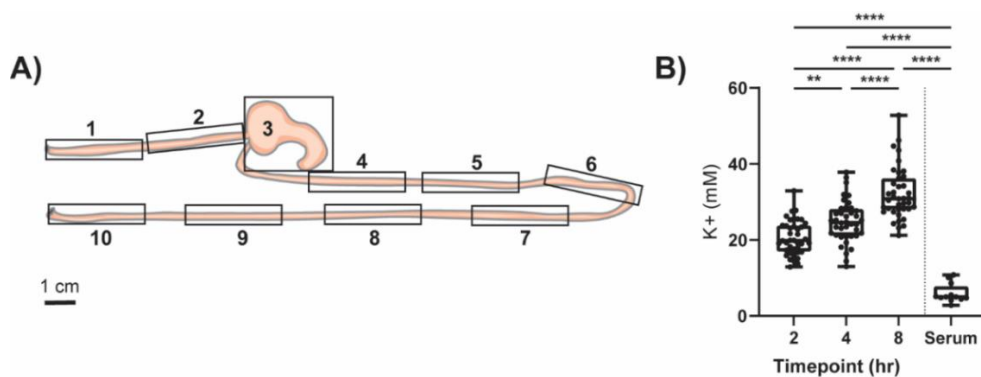


Figure 26. Shorter timepoints result in significantly less K^+ in elution IF

A) The segmentation approach from C57BL/6J CONV mice for the experiment shown in (B). K^+ was measured from elution IF and serum (matched by animal) and compared by timepoint for each segment shown above. Separate animals were processed for each timepoint, $N=4$ for each of the 10 segments at each timepoint. The results from each timepoint were binned, and the results from each segment are shown together. K^+ (mM) for timepoint is plotted in (B), and significance was tested using an ordinary one-way ANOVA with Tukey's multiple comparisons test. P -values are as follows: ** $p \leq 0.01$, *** $p \leq 0.001$, **** $p \leq 0.0001$. I performed the experiments shown here, and samples were sent for ion chromatography measurement in the lab of Dr. Helge Wiig (University of Bergen).

From the aforementioned ion chromatography measurements, the conclusion was made that shorter elution times should be pursued to preserve the tissue integrity. Although, it was important to consider whether the substances-of-interest from the GI tract IF would be extracted efficiently at these lower timepoints. Therefore, a non-native labeled extracellular tracer ^{51}Cr -EDTA was used to assess the amount of time it would likely take for substances of interest (i.e., small molecules/metabolites) to equilibrate with the elution buffer (Figure 27). This tracer approach has the advantage of high sensitivity due to the simple counting of the radioactivity. The presence of the tracer within a given tissue segment was counted upon removal from the mouse prior to placement inside the isosmotic elution buffer, and the recovery of the tracer within the elution buffer was repeatedly measured up to 48 hours after the elution start time.

The amount of tracer within the elution buffer was assessed relative to the total tracer counted in each respective tissue segment. ^{51}Cr -EDTA equilibrated with the surrounding elution buffer very quickly, with most of the tracer eluting after only 2 hours (Figure 27B-E). For the most part, the tracer is not more abundant in samples collected between 4 and 48 hours (Figure 27B-E). In the small intestinal segments, there is more variation in the eluted tracer fraction by animal, which may be because of the lower ECV in the SI (Figure 23B), as it is known that IF is more difficult to mobilize from spaces with a lower IF fraction.¹⁴⁰ Even for the longest time point assessed, a small amount of the ^{51}Cr -EDTA was unrecoverable (eluted fraction unequal to 1); suggesting that there may be unspecific binding of the ^{51}Cr -EDTA within the tissue IF which rendered a fraction of this molecule inaccessible. From these results, it is likely that small molecules from the IF phase in GI tissue are capable of rapidly equilibrating with elution fluid.

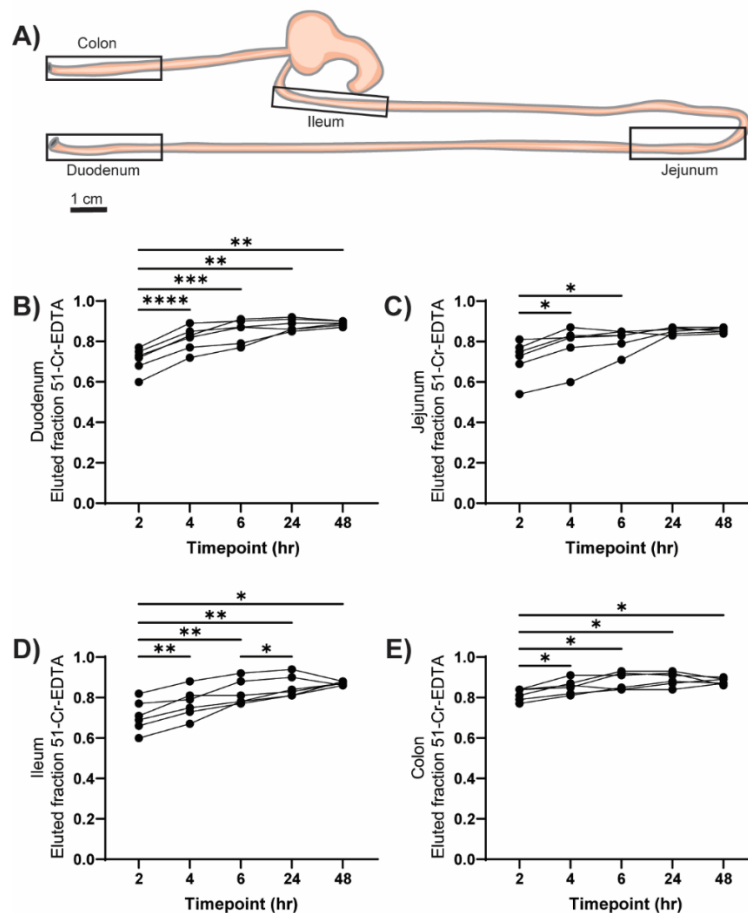


Figure 27. ^{51}Cr -EDTA elution indicates the rapid equilibration of this extracellular tracer with the surrounding elution buffer

A) The scheme above shows the sectioning approach used for GI tissue from C57BL/6J CONV mice for (B-E; $n=6$ for all conditions). The ^{51}Cr -EDTA extracellular tracer was used to determine the rate at which the elution fluid equilibrates with the IF from tissue. In (B-E), at each timepoint, 100 μL sample were removed

*from the eluted solution for gamma counting. The eluted fraction for each segment was determined by dividing counts in the eluted sample at each timepoint with total counts in the corresponding gut sample prior to elution. Data in (B-E) were tested using repeated-measures one-way ANOVA with Tukey's multiple comparisons test and significant post-hoc comparisons are shown. P-values are as follows: * $p \leq 0.05$, ** $p \leq 0.01$, *** $p \leq 0.001$, **** $p \leq 0.0001$. ⁵¹Cr-EDTA extracellular tracer experiments were performed in collaboration with Dr. Helge Wiig and Dr. Tine V. Karlsen (University of Bergen).*

4.2.3 Elution method captures unique IF signature compared to serum

Next, I was interested to examine whether the IF from the GI tract was different from the circulating blood. IF has been shown to hold a unique tissue-specific signature in tumors^{142, 188} and the skin¹⁵⁰, I wondered whether this was similarly evident in the Elution IF. Proteomic characterization of IF isolated using the elution method from breast tumor tissues revealed an abundance of disease-specific protein products which were only abundant in the IF samples and not the serum.¹⁸⁹ In order to better understand the GI microenvironment, shotgun proteomics was used to identify the similarities and differences within the IF. In total, significantly more unique protein IDs were found within the IF compared to the serum (Figure 28B). Expectedly, 1802 proteins were statistically significantly different between elution IF compared with the serum (Figure 28C). While many proteins were overlapping from the serum and IF spaces (Figure 28D), there were 2581 which were unique to the IF space, and 1404 which were shared between the colon and duodenum segments. There was a much larger overlap in the identifiable proteins between these two IF groups than with the serum (Figure 28D). The normalization technique for these data was based on protein amount in the starting material rather than per volume of IF or serum. Because the protein concentration is typically lower in the IF compared to the serum¹⁴⁰, we expect that there may be a slight overrepresentation in the Elution IF of some proteins which are present in equal concentrations across the serum and IF. Nevertheless, proteins which have been documented to be more highly concentrated in the serum like albumin (ALB)¹⁴⁰ did indeed appear to be significantly higher in serum compared to Elution IF (Figure 28C). This fact notwithstanding, because of the increased coverage of proteins from the IF space compared to the serum, IF may be a better route to study proteins relevant for GI health and disease which are not found or are lowly abundant within the serum.

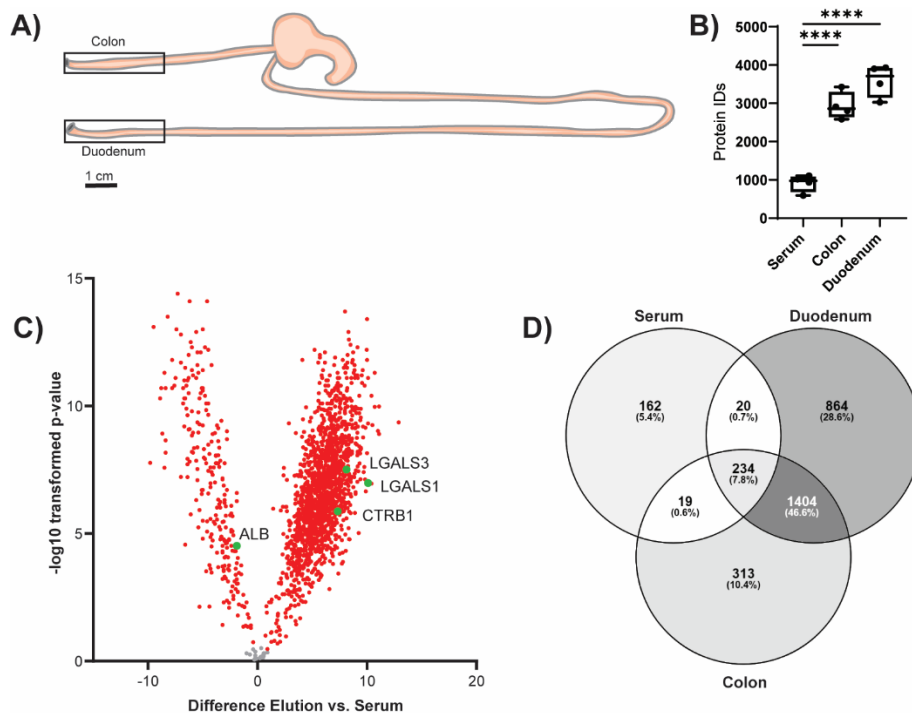


Figure 28. The serum and elution IF proteomes are unique in C57BL/6J mice

A) The scheme for samples which were tested using shotgun proteomics from elution and serum samples of C57BL/6J CONV mice; $n=4$ for each condition. Elution IF was collected for 4 hours in a mannitol-based buffer solution. The mouse Uniprot database 2019 was used for data curation. In B), the total number of protein IDs found in individual samples from the colon, duodenum, and serum. Significance was tested using an ordinary one-way ANOVA with Tukey's multiple comparisons test applied (**** $p \leq 0.0001$). C) Proteins which were found to be significantly different from elution samples compared to the serum. The actual $-\log_{10}$ transformed p -values and the \log_2 difference between elution and serum for a given protein are shown as individual dots, and red dots indicate significant p -values after an unpaired two-tailed T-test with an FDR correction of 5%. The number of overlapping proteins from serum, duodenal and colonic samples are shown in (D). A given protein had to have 100% valid values within at least one group to be included in the comparisons for both (C-D). Shotgun sequencing data and analysis were performed by Dr. Marieluise Kirchner (BIH Proteomics Core Facility, Berlin). I prepared all samples used in these experiments and I created all visualizations shown here with data provided by Dr. Marieluise Kirchner. Venn diagram was produced using the Venny tool (bioinfogp.cnb.csic.es/tools/venny/index.html).

Encouragingly, within the group of proteins which were robustly identifiable from the IF, there were several candidates that have a known biological function in the GI tract such as chymotrypsinogen B (CTRB1)¹⁹⁰, and galectin-1 (LGALS1) and -3 (LGALS3)¹⁹¹ (Figure 28-29). Indeed, LGALS1 has been noted to be more highly expressed in the colon than the duodenum in humans¹⁹², which was recapitulated in the mouse proteomic data (Figure 29B). Each of these candidates are known to be secreted or present in the extracellular space, which stands to reason why they were identifiable in the IF.

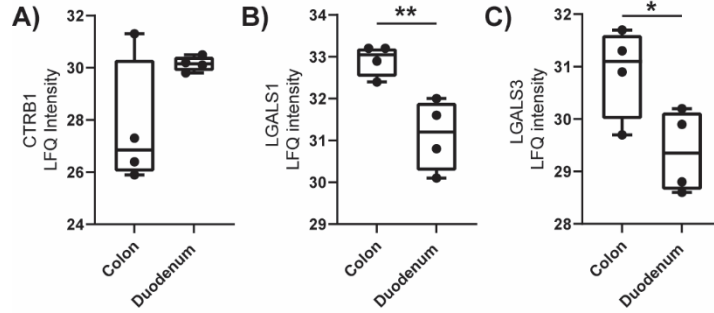


Figure 29. Known proteins of importance within the GI tract were detectable in elution IF

Data shown in (A-C) are derived from the proteomics dataset previously described in Figure 28. The log₂ transformed LFQ intensity values for individual proteins CTRB1 (A), LGALS1 (B) and LGALS3 (C) are shown. Significance was tested using an unpaired two-tailed T test. P-values are as follows: * $p \leq 0.05$, ** $p \leq 0.01$.

The overlap between serum proteins and the elution IF was also of interest; in that the elution IF may contain site-specific information about biomarkers which have already been associated with GI function. For example, if a given protein was identified in the serum as a candidate biomarker for involvement in GI health or disease, the IF could hold additional information about where the protein is derived from (i.e., specific to the colon). To investigate this subgroup, proteins which were robustly identified within the serum data and all IF samples were selected, and intensity within a given sample is shown in Figure 30. Indeed, investigating this group of proteins was proof-of-concept for our experimental set-up. For example, fibrinogen alpha chain (FGA) has been identified as a serum biomarker in Crohn's disease.¹⁹³ Fibrinogen itself has also been identified as a serum biomarker in those with active Crohn's¹⁹⁴, and although fibrinogens are highly multifunctional proteins, they are known to play an important role in defense against microbial pathogens.^{195, 196} This established biomarker was better covered in the samples derived from the elution IF. Additionally, this sub-analysis showed that the interindividual differences between mice were much less influential than the segment of origin within the GI tract (Figure 30).

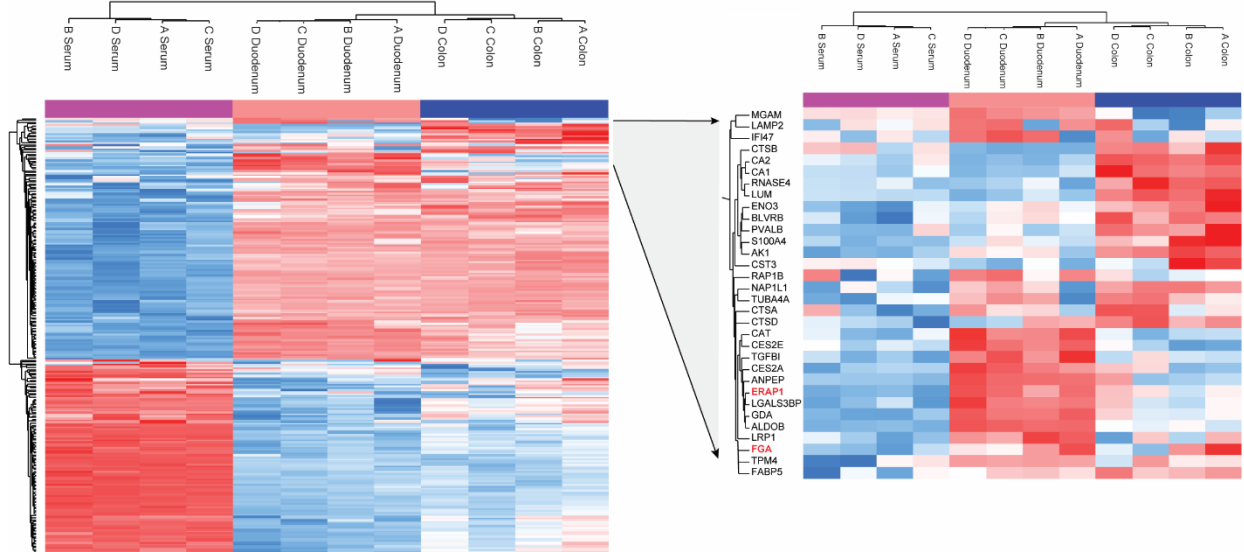


Figure 30. Robustly identified serum proteins and their relationship with elution IF

Dataset described in Figure 28 was used to assess the overlapping proteins within the IF and serum samples. The inclusion criteria for this analysis was 100% valid values for a given protein in all serum and IF samples (total of 234 proteins). An overall z-score across all samples was used to compare between groups for a given protein. On the right-hand side, proteins within this sub-analysis which were differentially regulated between colon and duodenal segments are shown.

Because the preparation requires placement of a given tissue within a buffer solution, I suspected that some degree of intracellular contaminants may be measurable within the elution IF. There were significantly more intracellular proteins annotated to the mitochondrial or ribosomal space in the Elution IF than the serum (Figure 31), although one cannot conclude that this is indeed an “enrichment” effect for the reasons stated above. It is possible that the increased number of intracellular proteins within the elution IF could contribute to the higher protein ID count relative to serum (Figure 28B).

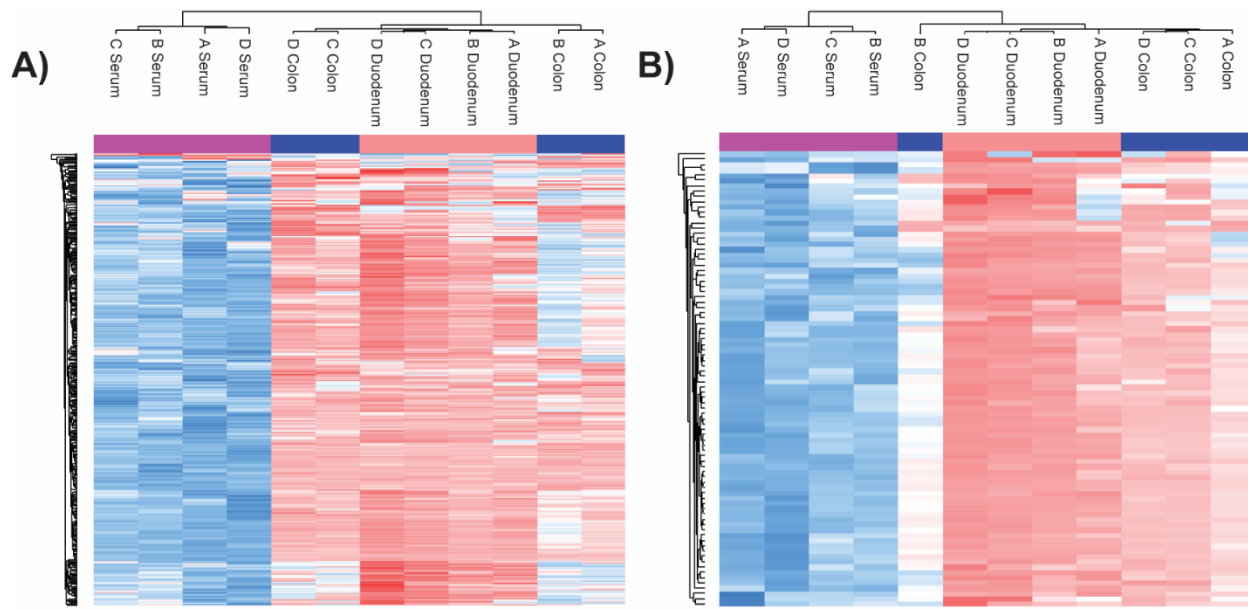


Figure 31. High abundance of intracellular proteins can be found in Elution IF

The dataset described in Figure 28 was used to assess the coverage of (A) mitochondrial and (B) ribosomal proteins within the IF and serum samples. Inclusion criteria for this analysis was 50% valid values for a given protein in elution IF samples, and an overall z-score across all samples was used for comparison.

4.2.4 The impact of time and segmentation on the proteomic elution IF signature

The high number of intracellular proteins in the elution IF led back to the question of whether a shorter elution time would capture a similar overall proteomic signature, such that one could use an even shorter elution time for future experiments. Additionally, as the previous experiment emphasized the segment-specific differences within the elution IF. It was unclear whether these regional dissimilarities would be replicable if the exact location of a tissue selected for analysis would have been slightly different. Another round of proteomics experiments was therefore initiated to evaluate the impact of time and small regional differences on the elution IF (Figure 32A). It was clear that the timepoint minimally impacts the overall proteomic signature, particularly within the colon, where the correlation across timepoints was remarkably high (Figure 32B). The colonic and duodenal subsections clustered together perfectly and correlated highly within these subgroupings, though the correlation was higher between colonic segments (Figure 32B).

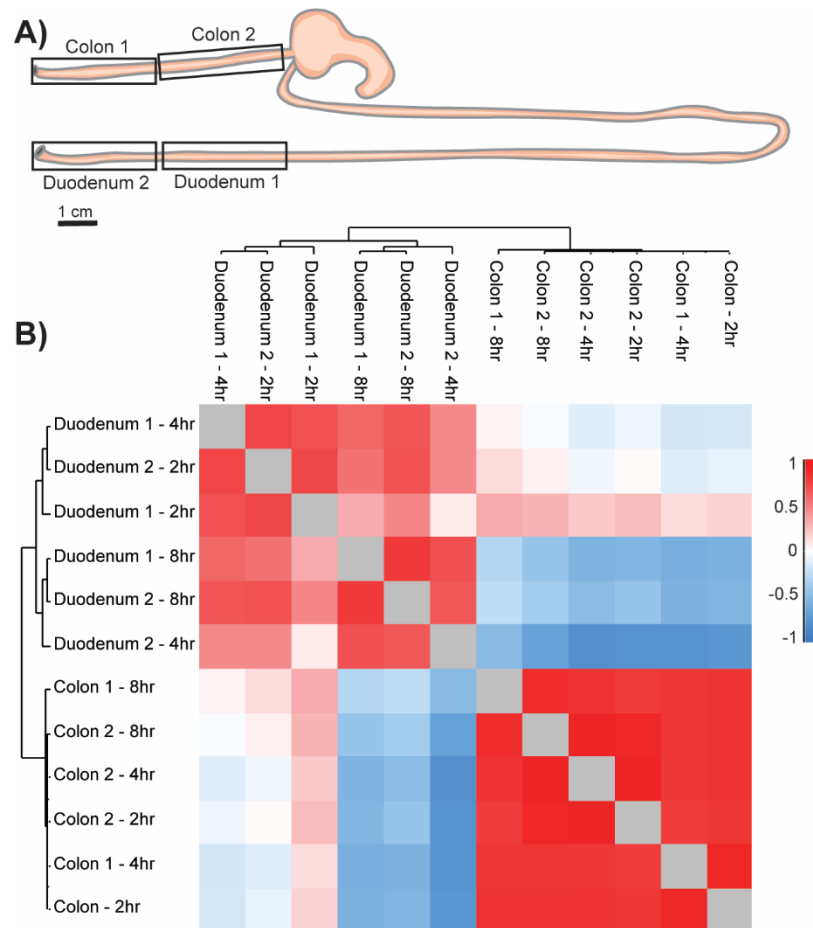


Figure 32. Elution IF samples from the same GI region have a similar proteomic profile

Elution IF was collected from 2 duodenal and 2 colonic segments for 2-, 4-, or 8-hours in a mannitol-based buffer solution from C57BL/6J mice. The collection scheme by segment is shown in (A), and individual timepoints represent separate experimental mice (N=3 for each timepoint and each segment). I performed all experiments shown here. Shotgun proteomics was performed by Dr. Marieluise Kirchner (BIH Proteomics Core Facility, Berlin). The mouse Uniprot database 2019 was used for data curation and the protein FDR was set to 1%. In (B), the mean Pearson's correlation per group from each timepoint and segment was analyzed from all proteins annotated within a given group, and the groups were clustered along the axes based on Euclidean distances.

Between timepoints within each segment individually, the 2- and 4-hour samples were nearly identical (Figure 33), suggesting that these timepoints could be used interchangeably. The only time comparison which had a notable amount of difference within a given segment was for the duodenum 1 segment between the 2- and 8-hour timepoints (Figure 33G).

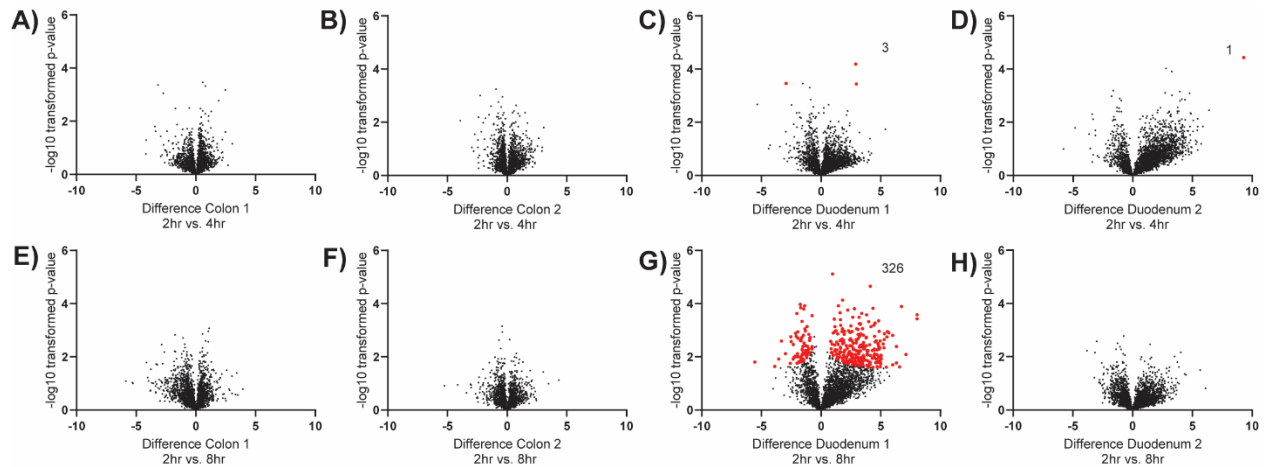


Figure 33. Elution time minimally influences the protein profile within a given segment

These data are derived from the experiment described in Figure 32, refer above for segment collection scheme. Proteins which were found to be enriched in the colon 1 (A), colon 2 (B), duodenum 1 (C) and duodenum 2 (D) between 2- and 4-hour collections. Proteins which were found to be enriched in the colon 1 (E), colon 2 (F), duodenum 1 (G) and duodenum 2 (H) between 2- and 8-hour collections. The $-\log_{10}$ transformed p-values and the \log_2 enrichment between timepoints for a given protein are shown as individual points. Red points indicate significant p-values after an unpaired two-tailed T-test with an FDR correction of 5%, and if any significance was found for a comparison, the number of significant proteins is listed in the top right corner of each panel.

The proteins which were responsible for the discrepancy between the 2- and 8- hour timepoints were mapped exclusively to gene ontology (GO) terms relating to the mitochondria (Table 4). The reason for the increased sensitivity within the duodenum 1 segment is unknown, although it was noted in histological evaluations of GI tissue after elution that there was significantly more cellular edema and damage from small intestinal segments than in the colon (data not shown). Small intestinal segments, even without any unique preparatory methods, often have a higher degree of physical damage visible with histology due to the physical properties of the tissue in comparison to the colon (dialogue with Dr. Robert Klopffleisch, Institute of Veterinary Pathology at the Freie University Berlin). The practicality of a 2-hour timepoint for elution is optimal and because it was so similar to the 4-hour time point for most of the parameters assessed thus far, it was decided on for future experiments.

Table 4. Proteins separating duodenum 1 samples at 8 compared to 2-hour timepoint are mostly intracellularly related

Category column	Category value	Total size	Selection size	Category size	Intersection size	Enrichment factor	P value	Benj. FDR	Hoch.
GOCC name	mitochondrial membrane	3059	326	148	3	0.1902	3.87E-05	0.0096276	
GOCC name	mitochondrial part	3059	326	224	8	0.33512	3.97E-05	0.0096276	
GOCC name	mitochondrion	3059	326	460	28	0.57117	9.61E-05	0.018642	

The differential enrichment between the duodenum 1 segment at 2h and 8h was investigated by mapping the proteins which were significantly different (FDR of 5%) between these timepoints to the corresponding GO terms. All differentially enriched GO terms were mapped to the GO- cellular component (GOCC) biological domain. The total size indicates the number of proteins overall which were identified in these samples; the selection size describes which of these proteins were selected for analysis (the 326 which were significantly different between 2h and 8h). The category size refers to the number of proteins which are attributed to the category value listed, and the intersection size indicates the number of overlapping proteins between the GOCC category and the selection size. The intersection size had to be at least 3 for consideration. The enrichment factor describes the ratio of the observed count to the count expected by chance (intersection size/category size x total size/selection size). The significance of each enriched category was tested using the fisher's exact test and the Benjamini-Hochberg (Benj. Hoch.) FDR correction was applied with an FDR of 2%.

4.2.5 Elution IF contains metabolites known to be locally produced in the GI tract

Our group and others have shown that metabolites of microbial origin play an important role in the mediation of hypertensive disease.^{23-25, 75, 78} Additionally, in section 4.1, the lack of SCFA was suspected to play a role in the increased cardiorenal damage in hypertension seen in GF mice relative to their COL counterparts. Though in section 4.1.7, measurements of SCFA were only achievable from the fecal matter. SCFA levels within the GI tract are typically inferred from fecal levels within the GI tract or from the serum. Using GC-MS, C2, C3, C4 and isobutyrate (isoC4) were measured from elution IF and matched fecal samples, to determine whether the IF reflects fecal SCFA. Because the kinetics of distribution of SCFA within the tissue fluid space were unknown to us and outside the scope of this project, the assumption was made that these metabolites could have been distributed anywhere within the fluid volume of the tissue (extra or intracellularly). Because we could not guarantee that through the elution process, the SCFA from the intracellular spaces would not elute into the elution IF, the total tissue water was considered when determining the SCFA concentration in the tissue. To determine the expected concentration of SCFA within the tissue fluid space (and therefore the IF as well), the following calculations were used:

Step 1: Calculate the concentration of SCFA per gram of tissue ($\mu\text{M}/\text{g}$)

(Concentration (μM) determined in the elution IF x total elution fluid volume (L)) / tissue weight (g)

Step 2: Calculate the concentration of SCFA in the total tissue water ($\mu\text{M}/\text{L}$)

$$\text{Concentration of SCFA in the tissue } (\mu\text{M}/\text{g}) / .00079 \text{ (g/L)}$$

The pattern of enrichment for each metabolite in the feces of healthy male mice under standard chow diet was mirrored in elution IF samples. Furthermore, within the cecum and colon, there was a clear difference in the concentration from IF compared to the serum (Figure 34B-E). One can clearly see that local production by microbial enzymes and tissue uptake is occurring within the LI, as the differential between the serum and IF is negligible from SI segments (Figure 34). This evidence suggests the utility of the elution method to identify metabolites of interest within the tissue.

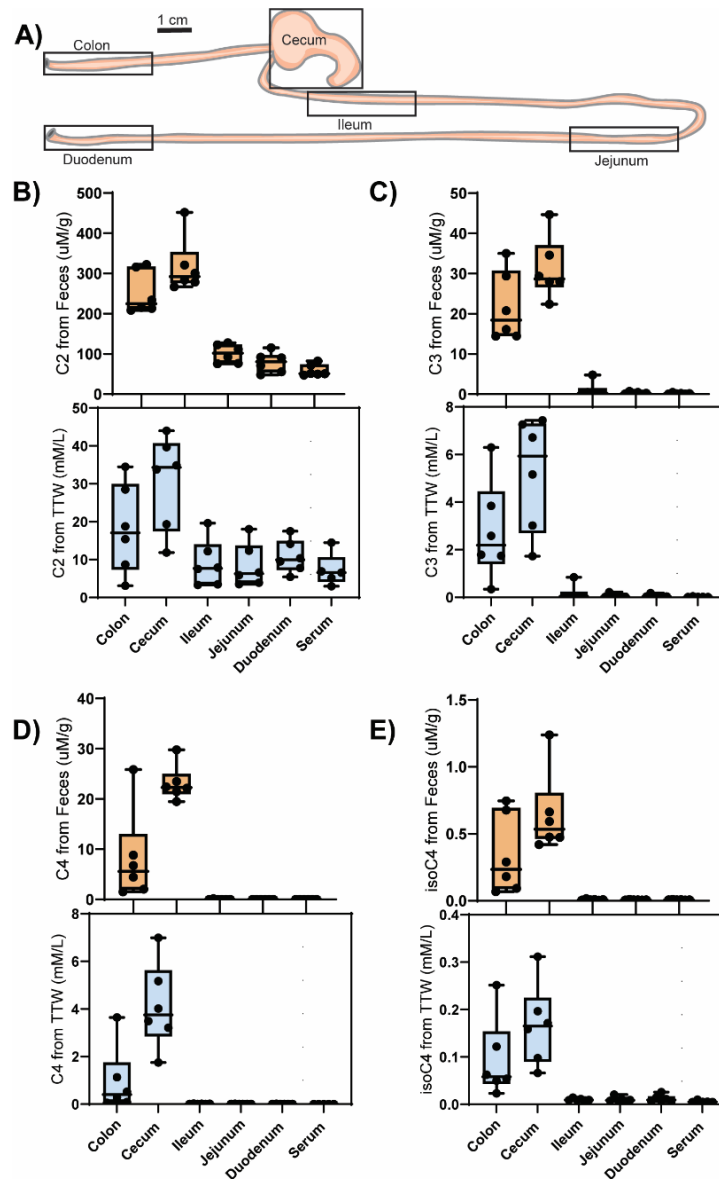


Figure 34. SFCA within IF reflects the enrichment in localized fecal content in the GI tract

A) The scheme for samples which were tested in (B-E) from C57BL/6J CONV mice; n=6 for each condition (one technical failure was removed from the serum). Elution IF was collected for 2 hours in a saline-based isosmotic buffer solution. Elution data was normalized to the elution volume, and the concentration was corrected to the expected total tissue water (TTW) volume to compare with plasma. GC-MS was used to measure C2(B), C3 (C), C4 (D) and isoC4 (E) from fecal (top panel, orange), and IF and serum samples (bottom panel, blue). I performed the experiments and extracted samples with assistance from Dr. Sabrina Geisberger (MDC Proteomics and Metabolomics Platform, Berlin). Dr. Sabrina Geisberger performed GC-MS measurements and peak integration, and I did the subsequent data analysis and calculations.

4.2.6 Centrifugation as an alternative method to capture the IF space

In section 4.2.3 and 4.2.5, we demonstrated using proteomics and metabolomics that elution IF is unique from serum and can provide unique insights into the tissue microenvironment. Because other IF methods have been used in the past to isolate fluid from this compartment, I wondered whether one of these other methods could be employed to confirm the results we obtained from the elution method. The centrifugation method has been used previously to isolate IF from skin and tumor tissues and is often preferred because it allows for the isolation of native material.^{140, 142, 197} Therefore, a centrifugation-based method was pursued as a potential confirmatory method for IF isolation from the GI tissue (Figure 35).

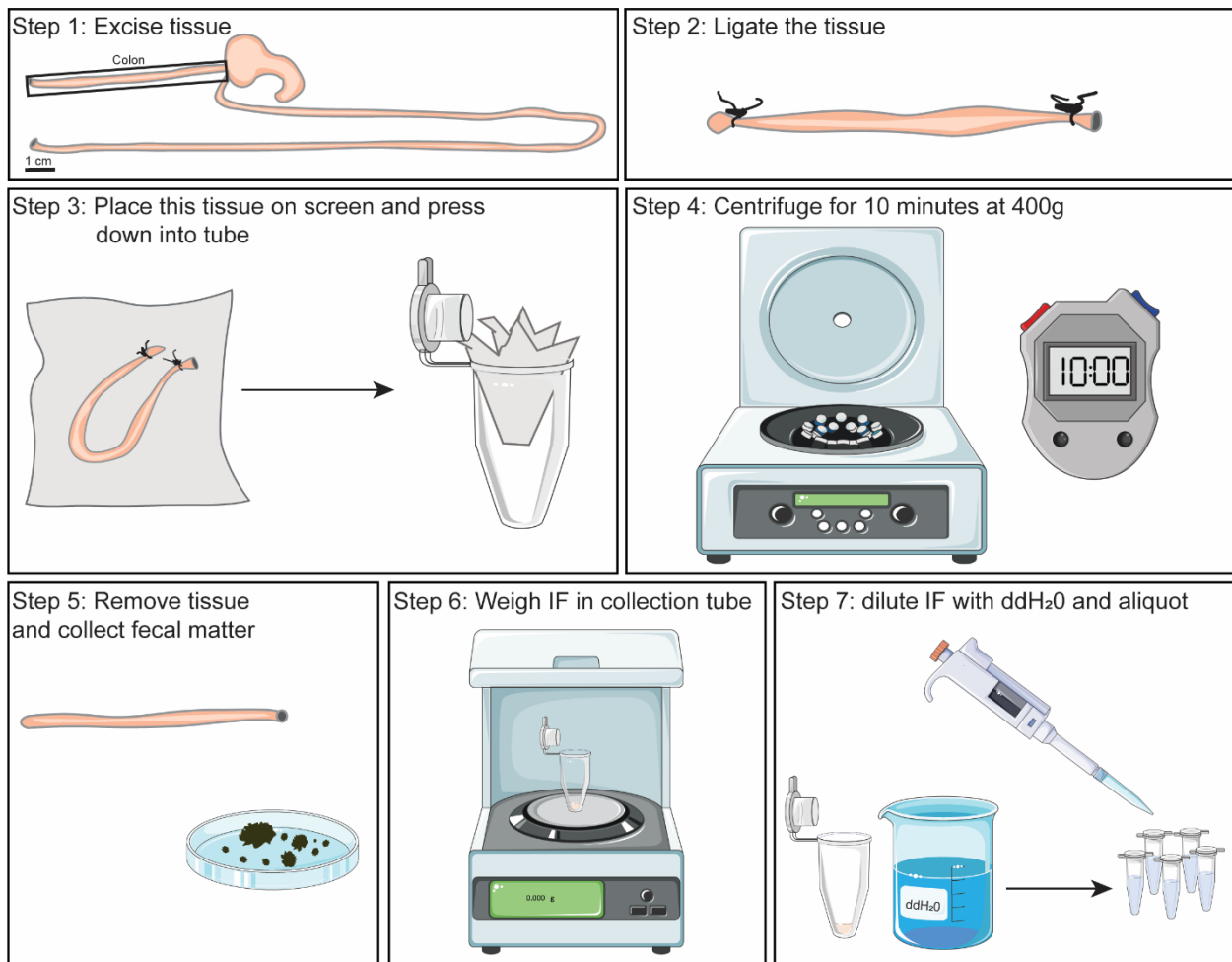


Figure 35. Schematic for centrifugation-based method for IF isolation

The GI tract from just below the stomach to the colon was excised. 7-10 cm pieces of GI tissue were measured, cut and immediately ligated. Tissue was checked for holes, and any fecal matter from the edges of the tissue after the ligation point was squeezed out. Ends of the tissue were trimmed off if needed. Tissue was then placed on a light screen material, folded, and secured inside of a 5 mL Eppendorf tube. Closed tubes were centrifuged for 10 minutes at 400 x g. Immediately upon removal of the tissue, the ligations were trimmed off and fecal matter was collected. IF from within the 5 mL Eppendorf tube was weighed, and diluent was added for aliquotation of Centrifugation IF. IF was stored at -80 °C for further analysis. Some images were adapted from the Servier Medical Art collection (<https://smart.servier.com>).

Optimization of the centrifugation method to compare with elution IF was initiated in mice. Various centrifugation speeds, and segmentation schemes were attempted and tested using ion chromatography before arriving at the method presented in Figure 35 (data not shown). Because our lab also utilizes rats as a model system for experimental hypertension, validation of the centrifugation method was pursued for both species using the ^{51}Cr -EDTA extracellular tracer. The usage of the ^{51}Cr -EDTA extracellular tracer is different between the elution and centrifugation methods; for more details see the methods section 3.2.5 and 3.2.6. In rats and mice, ^{51}Cr -EDTA was used to evaluate the integrity of the centrifugation

preparation. The relative level of the tracer in IF compared to serum allows one to conclude whether the obtained fluid has been diluted by intracellular contents i.e., from a space not containing $^{51}\text{Cr-EDTA}$, or other extraneous factors. For centrifugation experiments, the IF/serum ratio of the $^{51}\text{Cr-EDTA}$ tracer should be close to 1.0. Skin IF isolation by centrifugation has been validated previously, and therefore was used as a reference method for comparison of the GI tissue IF from both mice (Figure 36B) and rats (Figure 36D). While there was significantly more variation in the $^{51}\text{Cr-EDTA}$ tracer isolation from the GI segments than in the skin reference methods in both rats and mice; in both species, the ratio of IF to serum was for the most part close to 1.0. There are some visible differences in capture depending on the segment, which could be due again to the differences in ECV (Figure 23B). Furthermore, because the volumes of native fluid isolated can be quite small, evaporation could have played a significant role (particularly in the values appearing as over a 1.0 ratio). Nevertheless, the $^{51}\text{Cr-EDTA}$ tracer IF to serum ratio in both mice (Figure 36B) and rats (Figure 36D) was not significantly different from the skin reference method.

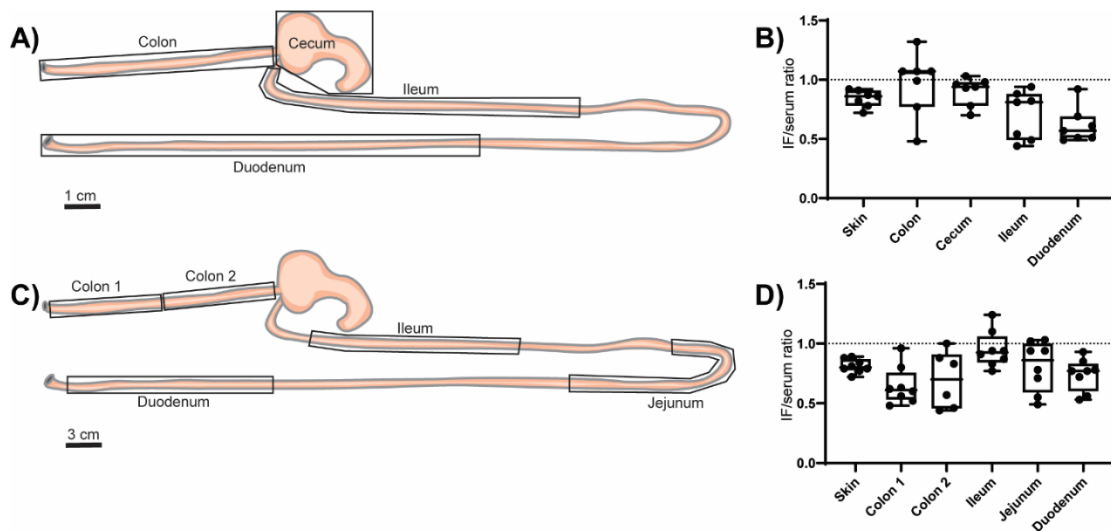


Figure 36. Centrifugation IF isolation efficiency from the gut is not significantly different from skin IF
The $^{51}\text{Cr-EDTA}$ extracellular tracer was used to determine how well the centrifugation method works to isolate IF from GI tissue compared to skin, and the scheme for sample collection is shown in mice (A; n=7) and rats (C; n=8). The IF/serum ratio of $^{51}\text{Cr-EDTA}$ was tallied using a gamma-counter from centrifugation IF in (B) mice and (D) rats. Statistical analysis for (B) and (D) were performed using an ordinary one-way ANOVA with Dunnett's post-hoc test (recommended for comparison to a reference condition) applied to compare the GI tissue segment IF/serum ratio to the skin IF reference method. None of these post-hoc comparisons were significant. Technical failures were removed. These experiments were performed in collaboration with Dr. Helge Wiig and Dr. Tine V. Karlsen (University of Bergen).

The $^{51}\text{Cr-EDTA}$ tracer method, as well as ion chromatography, are very sensitive methods which require only small amounts of biological material. From mice, the Centrifugation IF volume was relatively low for

all segments, averaging between around 0.5 to 4 microliters depending on the segment (Figure 37B). As the purpose of developing the Centrifugation IF was to compare with the Elution IF method, the low fluid volume in mice presented a problem. Both proteomics and metabolite (SCFA) measurements were attempted from mouse Centrifugation IF, though these results were highly variable and not reproducible because the samples were too dilute (data not shown). Because the rat GI tract length and size is far larger, larger volumes of fluid could be obtained, averaging between about 28 to 5 microliters depending on the segment of origin (Figure 37D). The use of the centrifugation method for IF extraction was henceforth pursued in rats to ensure that enough biomaterial could be obtained for analysis. The centrifugation method is therefore appropriate for use with GI tissue depending on the amount of biomaterial which can be used for IF isolation, and the sensitivity and/or specifications of planned analytical techniques.

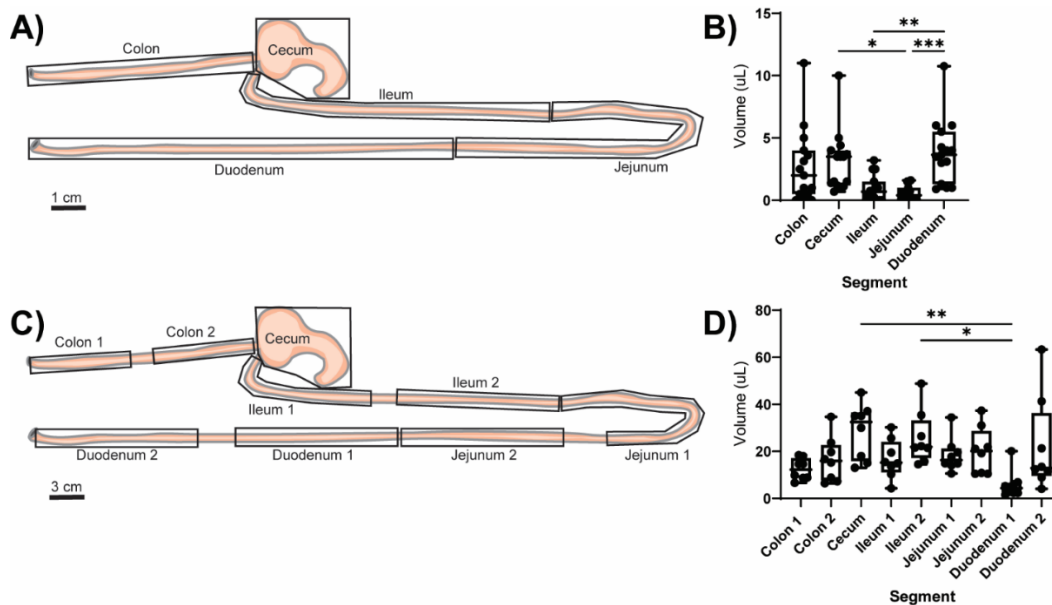


Figure 37. Centrifugation IF volume in mice and rats

The scheme for sample collection for volume determination of centrifugation “native” IF is shown for (A) C57BL/6J CONV mice ($n=15$) and (C) SD rats ($n=8$). Samples were collected per the protocol detailed in Figure 35, and the volume of native IF is shown in mice (B) and rats (D). Data in (B) and (D) were tested using an ordinary one-way ANOVA with Tukey’s multiple comparisons test and significant post-hoc comparisons are shown. P -values are as follows: $*p \leq 0.05$, $**p \leq 0.01$, $***p \leq 0.001$.

4.2.7 Comparability of the proteomic signature from elution and centrifugation IF

Because the tissue from the rat GI tract is so abundant, the elution and centrifugation IF can be compared within one animal for most segments, apart from the cecum because of its unique shape and size (Figure 38A). Elution and centrifugation IF from the colon, ileum, jejunum, and duodenum in rats were compared

using proteomics (Figure 38). Interestingly, in the overall proteomic signature shown by PCA, there are obvious method-specific differences which separate samples along both the X and Y axes (Figure 38B).

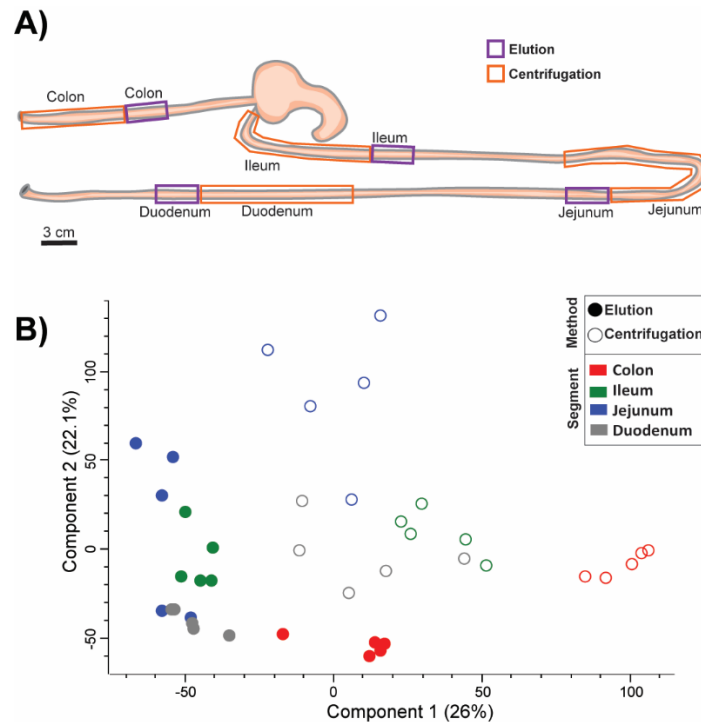


Figure 38. Overall proteomic signature is distinct between the two methods

The scheme for sample collection from male and female SD rats ($n=5$) aged 19-22 weeks is shown in (A), where samples for both elution and centrifugation were collected within each animal. The rat Uniprot database 2019 was used for data curation and the protein FDR was set to 1%. In (B) a PCA of all IF samples included in the analysis is shown; point fill indicate the method and the point colour indicates the segment of origin (colon, ileum, jejunum, or duodenum). I performed these experiments, and shotgun proteomics was performed by Dr. Marieluise Kirchner (BIH Proteomics Core Facility, Berlin).

I expected that part of the separation between methods could be due to intracellular proteins extracted using the elution method. From the centrifugation method, as the preparation was shown to result in the isolation of mostly native fluid (Figure 36), I expected that there would be less intracellular protein enrichment in IF using this technique. To identify what might be driving the differences between methods, an enrichment analysis was performed on each method overall, and the top GOCC terms within the centrifugation and elution methods relative to one another were examined (Table 5). The top differential terms between the two methods were mostly related to intracellular compartments. Interestingly, within both methods there was an enrichment of specific GOCC terms relating to the extracellular space, indicating that overall, some proteins of interest in the IF space are overrepresented in each of the

methods. Based on these data, the method selected for IF isolation will undoubtedly impact the results to some extent in the global untargeted analyses.

Table 5. Differential GOCC enrichment between the elution and centrifugation methods

Enrichment	GOCC Category value	Total size	Selection size	Category size	Intersection size	Enrichment factor	P value	Benj. Hoch. FDR
differential	ribosome	4416	2286	78	12	0.29719	1.41E-11	1.87E-09
differential	cell part	4416	2286	3488	1750	0.9692	6.17E-06	0.0004074
differential	small ribosomal subunit	4416	2286	35	7	0.38635	8.65E-05	0.0038065
differential	ubiquitin ligase complex	4416	2286	43	11	0.49417	0.000287	0.0094856
differential	macromolecular complex	4416	2286	1369	664	0.93695	0.000378	0.009982
Centrifugation	extracellular space	4416	626	351	145	2.9142	1.41E-39	1.86E-37
Centrifugation	intracellular organelle	4416	626	2094	208	0.70071	3.18E-15	1.40E-13
Centrifugation	extracellular region	4416	626	124	47	2.6738	1.84E-11	6.06E-10
Centrifugation	macromolecular complex	4416	626	1369	128	0.65957	6.58E-11	1.74E-09
Centrifugation	ribonucleoprotein complex	4416	626	300	11	0.25866	4.25E-10	9.34E-09
Centrifugation	nucleoplasm	4416	626	448	25	0.39366	7.20E-10	1.36E-08
Centrifugation	extracellular organelle	4416	626	1189	229	1.3587	2.75E-09	4.53E-08
Centrifugation	intracellular non-membrane-bounded organelle	4416	626	641	47	0.51724	3.77E-09	5.52E-08
Centrifugation	intracellular membrane-bounded organelle	4416	626	1750	187	0.7538	1.19E-08	1.57E-07
Centrifugation	protein complex	4416	626	1108	105	0.6685	2.39E-08	2.87E-07
Elution	extracellular space	4416	1660	351	61	0.46232	5.35E-18	7.07E-16
Elution	ribosome	4416	1660	78	8	0.27285	3.50E-08	2.31E-06
Elution	extracellular organelle	4416	1660	1189	375	0.83902	7.16E-08	2.34E-06
Elution	vesicle	4416	1660	1324	424	0.85192	8.86E-08	2.34E-06
Elution	spliceosomal complex	4416	1660	83	53	1.6987	6.05E-07	1.33E-05
Elution	nucleoplasm	4416	1660	448	212	1.2589	2.16E-06	4.08E-05
Elution	extracellular matrix	4416	1660	83	14	0.44872	1.93E-05	0.0002833
Elution	extracellular region	4416	1660	124	27	0.57925	5.58E-05	0.0007363
Elution	intracellular organelle	4416	1660	2094	840	1.0671	0.000111	0.0013399
Elution	proton-transporting two-sector ATPase complex	4416	1660	16	13	2.1614	0.000398	0.0043878

These analyses are derived from the dataset described in Figure 38. The differential enrichment between all IF samples within the centrifugation and elution methods was investigated by mapping the proteins which were differentially enriched (FDR of 5%) within these methods to corresponding GOCC terms. The enrichment categories are either the differentially regulated proteins between the two methods (differential), the proteins enriched selectively within the centrifugation method, or the proteins enriched within the elution method. The total size indicates the number of proteins overall which were identified within all IF samples; the selection size describes the number of proteins enriched within the listed enrichment category. The category size refers to the number of proteins which are attributed to the category value listed, and the intersection size indicates the number of overlapping proteins between the

GOCC category and the relevant selection size. The intersection size had to be at least 3 for consideration, and the top 10 enrichment terms (if more than 10 were found) are shown here. The enrichment factor describes the ratio of the observed count to the count expected by chance (intersection size/category size x total size/selection size). The significance of GOCC category enrichment was tested using the fisher's exact test; and the Benjamini-Hochberg (Benj. Hoch.) FDR correction was applied with an FDR of 2% to root out any spurious findings.

Although there were method-specific differences, the question remained whether findings from one of these methods could corroborate findings from the other, and identify proteins were site-specifically regulated along the GI tract. Indeed, when examining the LFQ intensities for individual proteins of interest, it was clear that although the peak intensity for a given protein did differ between methods, the overall pattern of regulation along the GI tract was roughly similar between the centrifugation and elution methods, especially with regards to the relationship between the colon and the SI (Figure 39-40). Some selected candidates such as CTRB1, LGALS1, and LGALS3 were identifiable within both methods (Figure 39) and were similar to the observations in mouse elution IF for these proteins (Figure 29). LGALS3 did not reach significance in the centrifugation method though was highly significant within the elution method, which could be indicative of a high ICV to ECV gradient for this protein (Figure 39E-F). Additionally, IL18 was capturable with both methods and appeared to be enriched in the colon, though as with the other candidates, the relative level of IL18 within different SI segments did vary between methods (Figure 39G-H). IL18 is of particular interest because it is known to be expressed by enteric neurons and controls goblet cell expression of antimicrobial proteins.¹⁹⁸ The frequency of goblet cells increases from the upper to lower GI tract.⁴⁷

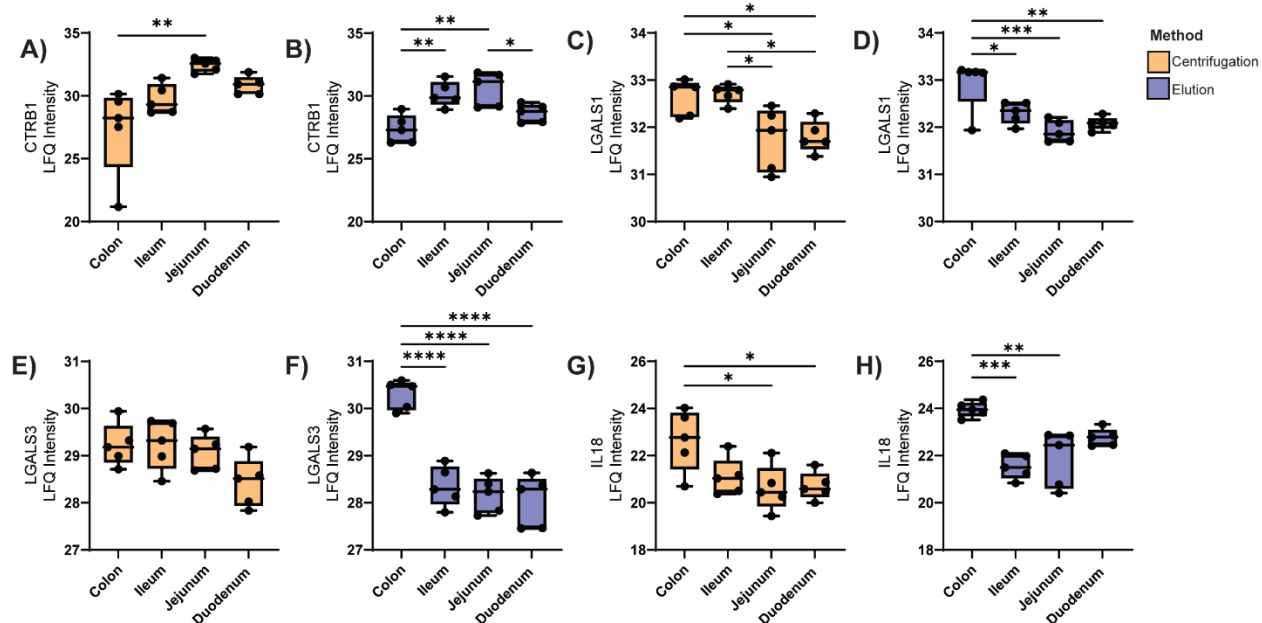


Figure 39. Proteins of interest in rats show a similar enrichment pattern in the GI tract for both methods These analyses are derived from the dataset described in Figure 38. Log₂ transformed LFQ intensities are shown from IF samples collected using either the centrifugation (A, C, E, G) or elution (B, D, F, H) method. CTRB1 (A-B), LGALS1 (C-D), LGALS3 (E-F) and IL18 (G-H) are shown. Significance was tested using an ordinary one-way ANOVA, and when significant, Tukey's post-hoc multiple comparisons test was applied, and all significant comparisons are plotted above. P-values are as follows: * $p \leq 0.05$, ** $p \leq 0.01$, *** $p \leq 0.001$, **** $p \leq 0.0001$.

Although significant similarities between SI segments were observed for various proteins, this was not always the case. For example, regenerating islet-derived protein 3 gamma (REG3G) which is produced by Paneth cells in the ileum through interactions directed by symbiotic bacteria^{199, 200}. REG3G enrichment was highly specific to the ileum and was consistent in both the elution and centrifugation methods (Figure 40A-B).

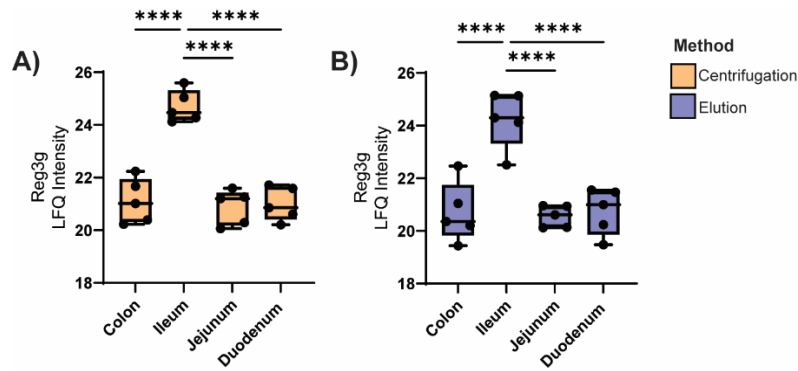


Figure 40. REG3G is selectively enhanced in the ileum in both centrifugation and elution IF

These analyses are derived from the dataset described in Figure 38. Log2 transformed LFQ intensities for the REG3G protein are shown from IF samples collected using either the centrifugation (A) or elution (B) method. Significance was tested using an ordinary one-way ANOVA, and when significant, Tukey's post-hoc multiple comparisons test was applied, and all significant comparisons are plotted above. P-values are as follows: **** $p \leq 0.0001$.

As one could observe from the individual proteins of interest (Figure 39-40), the raw LFQ intensity data may bias the global results significantly because if a protein was more highly concentrated in general using one methodological preparation, the differences between GI sites may be underrepresented in the analysis. Indeed, the enrichment analysis indicated that within both methods there were several proteins annotated to the extracellular space which were enriched in one method relative to the other (Table 5). Importantly, if only one of these methods were used to study regional specificity within the GI tract, would similar conclusions be reached about the enrichment of a given protein of interest relative to the other segments assessed? To answer this question, data were z-scored independently within the elution and centrifugation methods, such that the relative level of a given protein within each method overall would no longer influence our results. Furthermore, a selection filter was implemented to reduce noise and to identify proteins where one could confirm or deny a segment-specific pattern of regulation. If a protein was only identifiable from one method, its absence in the other could be biological, technical, or otherwise, so each protein selected had to appear in both methods. A given protein must have been found within IF samples for at least one segment subspace (colon, ileum, jejunum, duodenum) to be included. Using independent z-scoring and logical data selection, one can see that the differences between methods became significantly less influential and the overlap between segments across methods was much clearer (Figure 41A). Segments from the SI were overlapping to some degree, whereas the colon clusters independently from the rest of the GI tract (Figure 41A). The correlation between segments across methods was much higher than between all segments within a given method (Figure 41B). Interestingly, the most poorly correlated segment between the two methods was the ileum (Figure 41B). Where in the

centrifugation method the ileum correlated with the duodenum, within the elution method this ileal segment correlated better to the jejunum (Figure 41B).

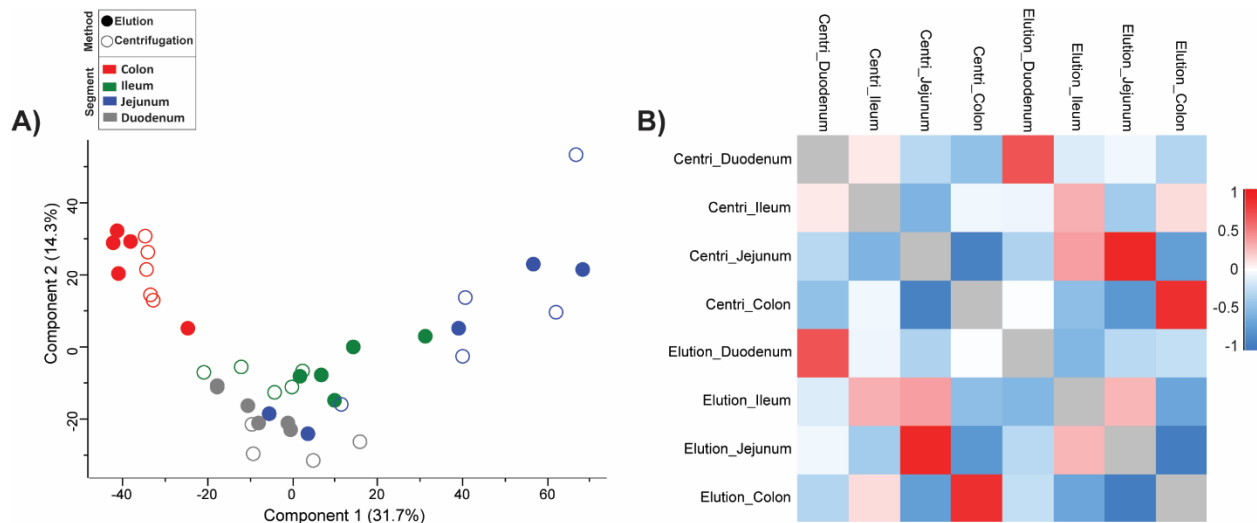


Figure 41. Independent z-scoring by method results in high congruence of the overall proteomic signature from GI segments

These analyses are derived from the dataset described in Figure 38. Independent z-scoring within the centrifugation and elution methods were performed, and only proteins which appeared with 100% valid values in at least one segment irrespective of method were included (in total 3093 individual proteins) for data shown in (A-B). In (A) PCA of all proteomics data post-selection and z-scoring. Point fill indicates the method, and the point colour indicates the segment of origin (colon, ileum, jejunum, or duodenum). In (B), the mean Pearson's correlation for segment within and between methods is shown.

As the principal reason for implementation of the IF methods is to isolate metabolites or molecules within the tissue microenvironment which would otherwise not be capturable, sub-selections of these proteins were made. As the GI tract is rich in immune cells and has an important impact on inflammation throughout the host (see section 1.2.3 and 1.4.1), proteins related to inflammation and immunity were obvious candidates for analysis. I was also interested in proteins annotated to the extracellular space or annotated as secreted, as these are the proteins one might expect to find within IF. Selection of inflammatory response and immune response annotations combined (Figure 42A-B) and extracellular space and secreted protein annotations combined (Figure 42C-D) from the rat Uniprot database resulted in a similar pattern of enrichment as was seen for the overall proteomic signature shown in Figure 41. Given that the PCA plots closely resemble what was seen in the overall PCA in Figure 41, it is likely that both these annotation subgroups have a significant impact on the overall data. In conclusion, the use of an independent z-scoring method revealed an underlying congruency between the proteomic profiles of

individual segments across these two methods. Though, the purposeful selection of only proteins which were identifiable in both methods likely contributed to the similarity between spaces. It is advisable to independently confirm results from either method in some capacity when possible.

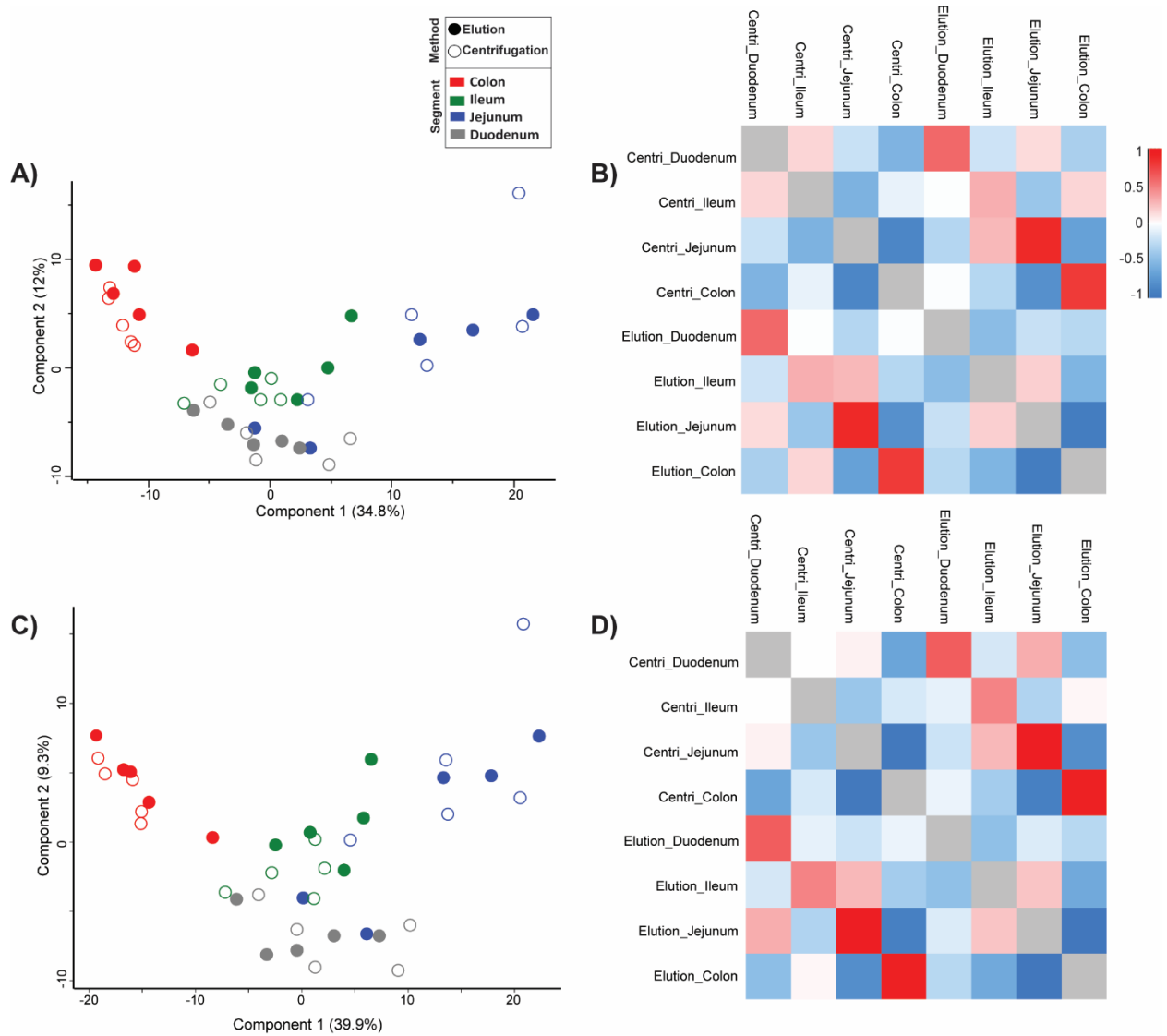


Figure 42. Inflammation-related and proteins expected in IF are similarly enriched in various GI segments in both the elution and centrifugation methods

These analyses are derived from the dataset described in Figure 38. Independent z-scoring within the centrifugation and elution methods were performed, and only proteins which appeared with 100% valid values in at least one segment were included for data shown in (A-D). Selection of inflammatory response and immune response annotations (a total of 285 proteins) from the rat Uniprot database are shown by (A) PCA and (B) Pearson's correlation. Selection of extracellular space and secreted annotations (a total of 354 proteins) from the rat Uniprot database are shown in (A) PCA and (B) Pearson's correlation. In (A) and (C), point fill indicates the method, and the point colour indicates the segment of origin (colon, ileum,

jejunum, or duodenum). In (B) and (D), the mean Pearson's correlation for segments within and between methods are shown.

4.2.8 SCFA from Centrifugation and Elution IF are similarly identifiable in the colon and cecum in healthy rats

Centrifugation IF fluid is rather native and therefore the exact quantification of a given substance in relation to the serum is more intuitive than from the elution method where proteins and metabolites are eluted out of the respective segment IF into a technical solution. Use of the centrifugation method does not require additional information about the kinetics of distribution for a given protein/metabolite within a putative intra- or extracellular space. Because the preparation is short, and relatively gentle, any metabolites or proteins isolated in the IF can be well assumed to be extracellularly derived (refer to Figure 36). I was interested to see whether the results of the SCFA isolation from elution IF would be recapitulated in centrifugation IF. Both the centrifugation and the elution method were applied to isolate IF from the same animals, and site-specific feces were taken from each segment. Because of the cecum's unique shape, it was used only for the centrifugation method, because to separate it would have compromised the integrity of the tissue for IF preparations. The results from elution IF were subjected to the same calculation detailed in 4.2.5. The total tissue water in rats is 0.72 mL/g.²⁰¹ IF isolated within both methods was directly compared for C2 (Figure 43B), C3 (Figure 43C), C4 (Figure 43D), and isoC4 (Figure 43E). One can see that in both methods the enrichment of certain SCFA (apart from C2 which is also non-microbially derived²⁰²) follow a similar pattern (Figure 43). Encouragingly, the results of both methods ended up in a similar micromolar range. Overall, the SCFA's examined in the elution IF appear at lower concentrations than in centrifugation, which was not unexpected given that the elution method is less directly quantitative.

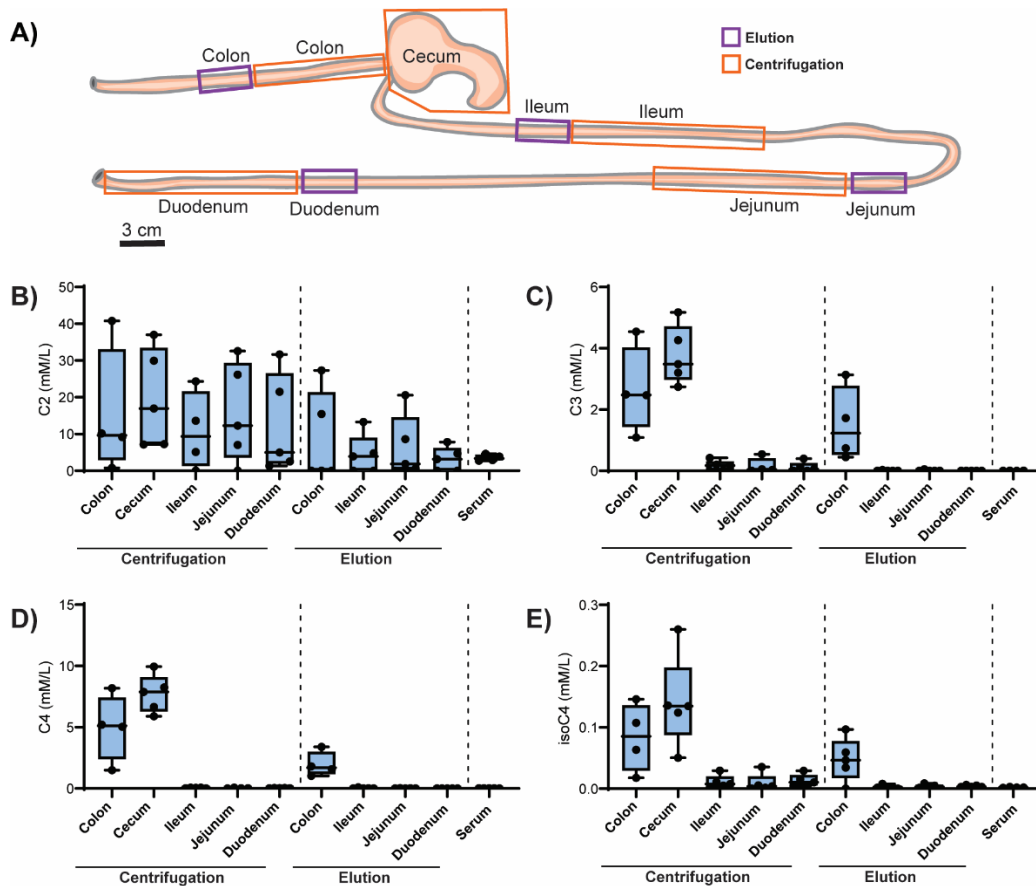


Figure 43. SCFA in IF is similar enrichment along the GI tract in both methods

A) The scheme for samples which were tested in (B-E) from healthy male and female SD rats; $n=5$ for each condition (extraction failures were removed). Centrifugation samples were corrected for dilution factor used to achieve the appropriate volume for injection. Elution IF was collected for 2 hours in a saline-based isosmotic buffer solution. Elution data was normalized to the elution volume, and the concentration was corrected to the expected total tissue water volume to compare with plasma (calculation detailed in section 4.2.5). GC-MS was used to measure C2 (B), C3 (C), C4 (D) and isoC4 (E) from IF and serum samples. I performed the experiments and extracted samples with assistance from Dr. Sabrina Geisberger (MDC Proteomics and Metabolomics Platform, Berlin). Dr. Sabrina Geisberger performed GC-MS measurements and peak integration, and I did the subsequent data analysis and calculations.

Fecal matter was site-specifically collected from each segment which was shown in Figure 44, and SCFA from each of these segments was analyzed. Fecal C2 was unlike what was found in either IF extraction method (Figure 44A). From examining the fecal metabolites C3 (Figure 44B), C4 (Figure 44C), and isoC4 (Figure 44D), one can see that a similar pattern to what was seen in IF was also capturable from the feces, though the overall levels of SCFA from both methods were of course similar because the matrix for measurement was the same. Interestingly, there were some subtle differences in fecal SCFA levels depending on where along the tract the fecal matter was collected (e.g., colon centrifugation and colon elution).

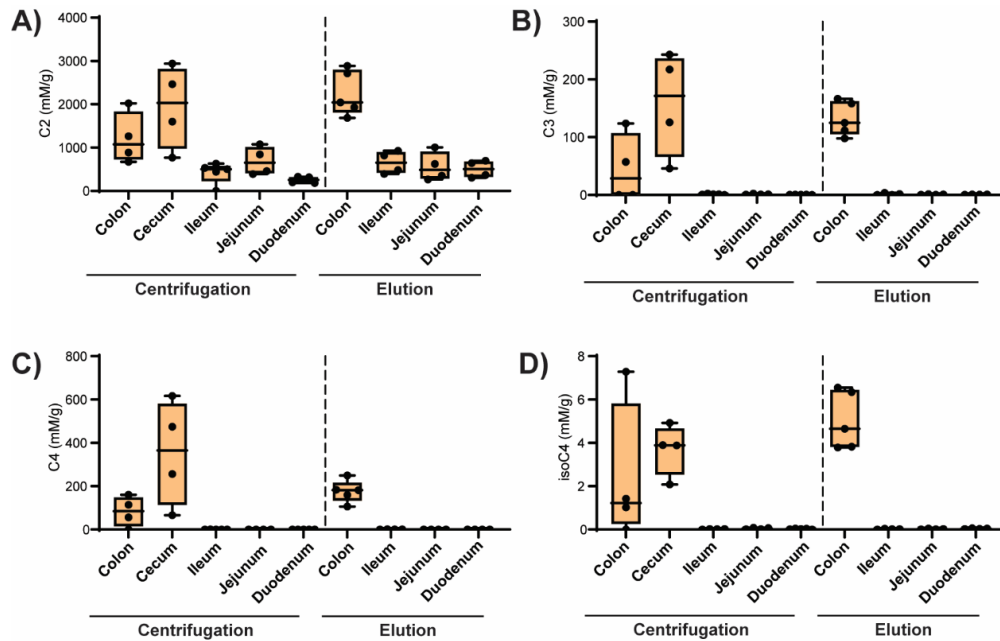


Figure 44. Fecal SCFA enrichment is specific to the colon and cecum in SD rats

GC-MS was used to measure C2 (A), C3 (B), C4 (C) and isoC4 (D) from fecal samples. Each sample was collected from the respective segment area used for IF preparations shown in Figure 44, and the sample collection scheme is shown in Figure 43A. I performed the experiments and extracted samples with assistance from Dr. Sabrina Geisberger (MDC Proteomics and Metabolomics Platform, Berlin). Dr. Sabrina Geisberger performed GC-MS measurements and peak integration, and I did the subsequent data analysis and calculations.

Importantly, using either method, the same conclusion would be reached about the enrichment of C3, C4, and isoC4 within GI tissue IF in the cecum or colon relative to the serum. In conclusion, the centrifugation method can be used as a confirmatory method for results found in the elution method. Indeed, the centrifugation method, when appropriate volumes can be attained, may be advantageous to pursue if the exact concentration within native IF is of interest. In both mice (Figure 34) and rats (Figure 43), the specificity of C3, C4, and isoC4 enrichment within the colon and cecum IF was observed, indicating that this pattern is likely evolutionarily conserved.

5. Discussion

An association between dysbiosis and hypertension has been found in patients^{21, 76} and in rodent disease models.^{21, 76, 90, 92} As the interaction between hypertensive disease and the microbiome has recently been established, much is unknown about the overall contribution of this factor to the mosaic of hypertension. The first aim of my thesis was to define the contribution of the gut microbiome in hypertension using GF and COL littermate mice. I have shown in section 4.1 that the microbiota has a potent effect on hypertension-induced cardiac and renal damage in mice. In a presence/absence scenario, GF mice showed a stronger adverse response to hypertension than their COL littermates. In particular, the kidney seems to be more sensitive to changes in microbial status than the heart. The inflammatory status, the microbiome, and the metabolome was characterized in GF and COL mice, and broadscale phenotypic differences between mice which received colonization was very clear. Because GF mice are known to be lacking in microbially-derived SCFA, I suspect that this played a significant role in the phenotypic response of these mice to hypertension. Further research is needed to investigate the exact mechanisms governing the transition from GF to COL mice, and why the colonization condition offered protection against kidney damage.

On the composite univariately and multivariately, hypertension-associated kidney dysfunction was worse in GF than in COL mice (Figure 7-9, Figure 13-14). While for some kidney damage markers, there were clear quantitative differences between the expression of a given marker in GF and COL hypertensive mice, these results were always interpreted relative to the respective sham group. If the respective sham groups were not considered, and only hypertensive COL and GF mice had been evaluated, for some markers the conclusion may have been that similar levels of kidney dysfunction developed in both groups. For example, nephrin, a surrogate marker for glomerular integrity, in hypertension treated mice from both COL and GF seemed to reach a similar level overall (Figure 7C). Some of the larger effects in our univariate analysis may be related to the slightly lower baseline level of putative markers for kidney damage within sham GF mice compared to sham COL, though these groups do not significantly differ in the overall analyses. Indeed, the comparison of kidney parameters multivariately between sham GF and COL did not reach significance (Figure 14A). However, one might ask why in hypertensive COL mice, kidney damage was not more significant; as kidney damage has been shown several times to develop in C57BL/6J mice during hypertension. The standard model for end-organ damage in our lab includes uninephrectomy to exacerbate the renal phenotype^{108, 203}, which was not included in these experiments because the nature of this procedure would have exposed GF mice to bacterial contamination. Therefore, less renal damage

was expected in our hypertensive mice when compared to the published literature¹⁷³. Nevertheless, the omission of the uninephrectomy procedure was the same for GF and COL groups, and thus is not related to the exacerbation of kidney damage in one group compared to the other.

Consistent with higher levels of inflammatory markers in the kidneys of GF mice, infiltrating macrophages (F4/80+ cells, Figure 8B) were higher in GF mice with hypertension than in COL. Macrophages and the expression of *Ccl2* (Figure 8C), have both been implicated as major players in worsening kidney damage in mice²⁰⁴ and humans²⁰⁵. Infiltrating macrophages during renal injury are known to induce the secretion of cytokines like IL-1 β , which can intensify the activation and differentiation of Th17 cells.²⁰⁶ While Th17 cells were not directly measured within the kidneys, the expression of cytokines which are used to induce Th17 cells (*Il-6*, *Il-1 β* and *TGF β*) were increased in GF mice with hypertension to a greater extent than in COL for the most part (Figure 13). Intriguingly, we found that the cardiac phenotype was less influenced by the microbial status of the host. While univariately, the differences between GF and COL seemed somewhat similar in the heart to the kidney (Figure 10-11), on the composite, the cardiac phenotype was more heterogeneous between these groups (Figure 13B). Particularly for markers of fibrosis in the heart, regardless of the microbiome status, the mice developed significant injury. These data suggest that the kidney, more so than the heart, represents a subspace of hypertensive target organ damage, which is more susceptible to microbial colonization. It is plausible that cardiac damage could be aggravated to a greater degree in GF mice as renal function declines.

Metabolites of microbial origin, some of which are known to be associated with cardiovascular disease and accumulate in chronic kidney disease^{126, 184}, were measurable within the serum metabolome of our COL but not our GF mice, such as IS and TMAO (Figure 20). Indeed, several of the so-called uremic toxins are actually biproducts of microbial metabolism conjugated by the liver after entering the host circulation.¹²³ Our results indicate that GF hypertensive mice experience robust kidney damage to a greater extent than COL hypertensive mice, despite GF mice being devoid of these harmful metabolites. It is tempting to speculate that the reason COL mice experience less overall damage is due to the presence of SCFA. Our group and others have shown the potent effect of SCFA in mouse models.^{24, 25} Interestingly, SCFA treatment was shown in ischemia-reperfusion injury (IRI) to radically reduce kidney *Ccl2*, *Il-1 β* , and associated kidney damage.²⁰⁷ SCFA have been shown to have anti-inflammatory properties in several cell types^{138, 172, 208, 209}, and as only mice with a microbiome contain high levels of C3 and C4 (Figure 21), we expect that this could contribute to why more inflammation was evident in GF mice, especially in the

kidney. Perhaps the potency of SCFA in COL mice counterbalances the effect of higher IS and TMAO levels in hypertensive mice. The interactions between different metabolites which are suspected of having some disease-related activity in hypertension has to my knowledge never been investigated. The impact of individual metabolites alone compared to a defined combination of these metabolites (e.g., co-administration of IS and SCFA) in GF mice would be interesting to pursue in follow-up studies.

Furthermore, I have shown that the systemic inflammatory response to hypertension is altered by colonization status. MSDC, which represent an important subset of innate anti-inflammatory cells in hypertension¹¹¹, reacted differently in hypertensive GF mice compared to COL (Table 3, Figure 17A-B). Additionally, Th17 cells were increased during hypertension in GF mice (Figure 17C-D). I wanted to explore *in vitro* whether naïve T cells from GF mice were more sensitive to polarizing cytokines and Ang II. I found that upon polarization, naïve T cells from GF mice skewed more towards Th17, particularly when Ang II was added (Figure 18). Recent evidence has shown that pre-existing conditions experienced by immune cells impact their development¹⁸¹⁻¹⁸³, even when these cells are still in a naïve state. Because SCFA propionate is known to decrease the rate of Th17 cell differentiation^{172,209}, this could be part of the reason naïve cells from COL mice were less inducible toward Th17. However, as these *in vitro* experiments were performed in CONV and GF mice (rather than COL and GF), they should be interpreted with caution for the reasons detailed later on. It is plausible that this impacted the results to some degree. Nevertheless, it would be interesting to investigate the impact of pre-conditioning naïve T cells *in vitro* with a given metabolite or set of metabolites and subsequently polarizing toward Th17.

The results from our GF experiments in the context of existing studies investigating the impact of GF status on disease development was an important tenet of this project. The data I collected about the microbiome and metabolome in GF and COL mice were compared to the only known report of a similar global analysis of these parameters in GF and CONV mice in hypertension.¹⁶⁵ In Figure 22A, one can see that the microbiome of ours and the Cheema and Pluznick bore no similarities to one another on a genus level. This is unsurprising, as researchers from around the globe have continually expressed concern over the lack of comparability between microbiomes from mice even of the same strain and acquired from the same retailer; highlighting an ongoing challenge faced in the field.²¹⁰ When comparing the metabolome from Cheema and Pluznick to our data, there was significantly more overlap between the metabolic response to hypertension in the GF groups from each study than in the COL/CONV groups (Figure 22B-C). The comparison of these data was only possible due to the free availability of their sequencing and

metabolomics data, which for these types of studies should be required. Recently researchers in the field have also proposed guidelines by which all relevant parameters known to influence the microbiome in rodents can be accounted for.²¹¹ The comparison of these two studies indicated that the colonizing microbes can potentially impact the resultant metabolome, and the same might be true for the hypertension phenotype. Though another interpretation of our analysis could be that because Cheema and Pluznick did not use littermates, and rather used two separate colonies, this could have led to the discrepancy between our results. As Cheema and Pluznick did not report their phenotypic data, it is unclear whether similar discrepancies would have been found in the hypertensive phenotype. To our knowledge, one study similar to ours where phenotypic data was reported (albeit without microbiome or metabolome data) has been published by Karbach et al.⁹³ Karbach et al. showed that GF mice were protected from developing hypertension and related vascular damage, which our findings did not corroborate.⁹³

The debate over the impact of the microbiome in disease development is not limited to the field of hypertension. Indeed, in diet-induced obesity; GF status was shown first to be protective²¹², whereas two studies since have come out and shown that GF mice are not protected against diet-induced obesity.^{213, 214} Similarly, GF status has been shown to exacerbate kidney damage in the context of IRI²¹⁵ and adenine-induced chronic kidney disease^{176, 216}. Though another study showed that antibiotic-depletion of the microbiota protected mice from IRI-related kidney damage.²¹⁷ It is again possible that the differences between the two IRI studies is related to the protocol used (e.g., antibiotic depletion vs. the use of GF mice). I therefore closely examined what about the Karbach et al. study, in comparison to the study presented in section 4.1, was dissimilar.⁹³

One of the key differences between the two studies was that the study from Karbach et al. compared GF mice to CONV mice, whereas I compared GF mice with littermates that had been colonized early in life. The advantage of the study detailed in section 4.1 was the ability to account for known genetic drifts in physically separated mouse colonies⁹⁵, as genetics are also known to contribute to the mosaic of hypertension.⁶ Indeed the divergence of the microbiome and immune competency in lab-raised substrains has also been shown,⁹⁴⁻⁹⁶ hence the need for littermate controls as a standardization technique in microbiome studies.^{97, 98} During the design of the experiments shown in this thesis, the early-life colonization strategy, beginning at four weeks old, was decided on for both practical and experimental reasons. Microbial colonization in early life is critical for the maturation of the human immune system²¹⁸, and perturbations during this phase have been shown to influence susceptibility to allergies²¹⁹ and

infectious diseases.²²⁰ Initially, I had assumed that beginning the colonization period at four weeks old would be robust enough to facilitate normal microbiome-immune interactions in the early phases of immune system development.

After the completion of this work, a landmark paper from Constantinides et al. showed that mucosal associated invariant T (MAIT) cells which play a role in cutaneous tissue repair are primed by the microbiome in a narrow window during early life (between 2 and 3 weeks of age); after which they could not be rescued.²²¹ Our group has recently identified that MAIT cells may play a role in BP regulation¹²⁵ and others have shown that these cells can influence renal fibrosis in CKD.²²² While MAIT cells were not investigated in this study, this recent research may point to MAIT cells as an additional reason for a discrepancy between my results and the results from Karbach et al. Indeed, as the early-life period is critical for the development of several immune cell subsets²¹⁸, it would be of interest to repeat the experiments shown in section 4.1 with different timepoints for the initiation of colonization. Additionally, recent work from Rosshart et al. has shown that embryonic transfer into a microbiome-rich host mouse facilitates the development of the full range of microbial interactions from birth, while preserving tractable genetics.⁶⁹ I suspect this procedure will be of great benefit in future to control for the genetic background of a given mouse colony whilst still facilitating the wide range of early-life microbial interactions, which are still being discovered. Nevertheless, the impact of colonization on MAIT cell development, and the interplay between MAITs and hypertension would be interesting to follow up on in the future.

It is also important to note that the early-life MAIT cell effect shown in Constantinides et al. is thought to be specific to barrier tissues, like the GI tract, lungs, skin and liver.²²¹ This brings me to an important caveat of my study, in that I did not explore the immunophenotype within the GI tract from GF and COL mice. In this study the priority was rather to compare the resultant phenotype within the end-organs. However, profiling the immune cell microenvironment and the changes which take place upon colonization is of interest to the lab and is subject to ongoing exploration. The interplay between immune cells within the gut and immune cells within a specific target organ in hypertension is of upmost importance as this is still not well-understood.

While in the first portion of my thesis, the impact of metabolites in hypertension were of interest, the appropriate compartment for measurement was a matter of debate. For the broadscale metabolite

measurements, serum was selected as the most appropriate matrix for measurement. Serum is often used for metabolite measurements instead of feces because dietary components which are undigested also contain metabolites, and the signatures from undigested and digested, solubilized metabolites which might be taken up by the host can not be separated from one another (dialogue with Dr. Jennifer Kirwan, BIH Metabolomics Core Facility, Berlin). While some have suggested that the aqueous phase of feces could be used as an alternative to fecal matter itself because the “fecal water” is likely to interact directly with the colonic epithelium²²³, this still would not address the question of which metabolites actually enter the host and can affect host function directly or indirectly beyond the gut epithelial interface. For the measurement of SCFA in section 4.1, fecal material was utilized because these metabolites are often very lowly abundant in serum. One study investigating SCFA within the portal blood and the systemic circulation of humans found that the interindividual differences in C3 and C4 in the portal blood were equalized by the hepatic utilization/clearance of these molecules, indicating that serum from the systemic circulation even under normal conditions may not reflect changes in SCFA uptake from the GI tract.²²⁴ Regardless of whether serum (portal or systemic) or fecal matter was selected, the problem remains that it is unknown whether these indirect measurements can capture what is absorbed into the host and is capable of affecting the hosts immune cells and disease processes. Therefore, the second aim of my thesis was to develop tools to capture the microenvironment within the GI tract, by employing methods for IF isolation to this compartment. Both an elution-based and centrifugation-based method were used to demonstrate that within the GI tract there are site-specific signatures which are of high relevance to health and disease.

Indeed, within the elution-based method from mice (Figure 34) and rats (Figure 43) the SCFA C3, C4, and isoC4 were enriched in the colon and cecum IF. This enrichment corresponded with a similar enrichment in fecal material from these subsections for the most part (Figure 34, Figure 44). Furthermore, the enrichment and site-specificity of these SCFA could be corroborated in IF from the centrifugation-based method in rats (Figure 43). C2 was much more variable in the IF compared to the feces, especially in rats. The reason that C2 results may be more ambiguous is likely because this metabolite can be produced both endogenously and exogenously, and our measurements are not capable of distinguishing the origin of a given metabolite.²⁰² Because C3, C4, and isoC4 are known to be purely exogenously produced²⁰², I can confidently identify the source of these metabolites when they are found in the host. In the future, gnotobiotic mouse models would be of high utility to investigate the interplay between host and

microbially-derived C2 in the IF, as well as various other metabolites which have both endogenous and exogenous routes of production.

While the results of our fecal and IF SCFA measurements would support potentially using fecal metabolites as a proxy for the metabolites which are taken up into the host; others have shown that the relationship between SCFA in feces and serum can change during hypertension, suggesting that SCFA uptake from the gut lumen is dynamically regulated.¹³¹ A potential use-case for the IF in future would be to examine the relationship between IF and feces SCFA in a disease state such as hypertension. Additionally, one could utilize radiolabelled SCFA molecules and track uptake and utilization by measuring radioactivity in IF and in various body compartments. It is unfortunate but true that SCFA extractions for measurement using GC-MS from biological material can vary from run-to-run and the ratios of SCFA (C2:C3:C4) are also known to fluctuate between measurements.²⁰² We therefore advise that all biological samples whose concentrations are to be compared should be measured together when possible.

Early on in method development, proteomics was used to understand the IF compartment within the elution method. One of the interesting findings which emerged from the data was that the elution IF in mice had significantly more intracellular proteins than the serum (Figure 31). While a definitive statement about enrichment in a given fluid volume can not be made because the protein content from each space was normalized, the increased coverage of both mitochondrial and ribosomal proteins was clear in Elution IF from both segments (Figure 31). A more robust enrichment analysis could be pursued in future by equalizing the input volume from the IF and serum spaces, though because the elution fluid is not native, this requires assumptions to be made about the fluid volume within the tissue and the percentage of that which is exclusive to the ECV. The nature of the elution method makes this type of normalization challenging, and therefore is a limitation of this method. Nevertheless, I suspect that the increased number of valid protein IDs from the IF space (Figure 28B) could be driven by the higher potential for intracellular contaminants to enter the elution fluid. The most obvious explanation for the enrichment of intracellular proteins in elution IF is that the cells are in some way damaged or squeezed during the elution preparation. This is also supported by the fact that even at the shortest elution timepoint tested (2 hours), there was still a far higher K^+ concentration in elution IF than in serum (Figure 26B).

Although it is important to note that a suspected enrichment of intracellular proteins in the elution IF is not the only possible explanation for their appearance in the proteomics data. It is well possible that this

could be due to an annotation issue within the mouse proteomic database, in that the available information about protein localization within a compartment does rely on manual curation. Indeed, there were several proteins annotated to the intracellular space in the elution IF as well as the serum (Figure 30). For example, ERAP1 appeared in both GI tract and serum samples (Figure 30), and while this protein is known to localize to the endoplasmic reticulum, recent evidence has shown that secretion of ERAP1 can occur in response to cytokine stimulation.^{225, 226} Polymorphisms to the *Erap1* gene are associated with blood pressure control and this protein is known to interact with the RAAS system²²⁷⁻²²⁹, representing an interesting candidate for future investigation.

Another possible cause of high intracellular proteins within the IF could be that the isolation captures small extracellular vesicles within the IF space. Extracellular vesicles (EVs) are submicron vesicles which can be found in the bodily fluids of all species, and while their function was originally suspected as a disposal mechanism for cellular waste, they've now been documented to play an important role in cell-cell communication.^{230, 231} EVs can contain a variety of proteins which would classically be described as intracellular including cytoplasmic, membrane and even histone proteins.²³¹ It has been shown that EVs play an important role in immune system regulation.^{230, 231} Because they often display some degree of target-specificity, they have been suggested as a potential therapeutic target for precision drug delivery.²³¹ Interestingly, the source of EVs can also be bacterial, as bacterial EVs (BEVs) are known to penetrate through the mucosal layer in the gut and interact with intestinal epithelial cells.²³² As others have recently shown that BEVs can indeed end up in the systemic circulation or at distal body sites²³², these vesicles could be an additional route by which the microbiome is able to impact function at distal organ sites. Indeed, a recent study showed that LPS-containing BEVs could be identified in the plasma from patients with inflammatory bowel disease.²³³ BEV entry into the host is not specific to disease states which compromise gut barrier integrity.²³⁰ For example, following the oral administration of fluorescently labeled BEVs in healthy mice, fluorescence could be measured for the most part site-specifically along the GI tract, but also within the liver, heart and lungs.²³²

The study of BEV entry and distribution within the host's bodily fluids represents another promising application for the IF methods in future research. It is important to note that in the proteomics data presented here, the mouse or rat Uniprot databases were used for data curation. As bacteria-specific proteins are also of interest, given their potential route of entry via BEVs, using metaproteomic (i.e., the characterization of the microbial community proteome) database curation would be needed to

investigate whether BEVs are bringing novel interacting proteins into the host microenvironment within the GI tract, which would be possible from my existing shotgun proteomics data. A recent protocol was published showing that EVs can be retrieved from bodily fluids using size-exclusion chromatography or density-gradient ultracentrifugation²³⁴, and I expect that this type of isolation may be possible from IF fluids, though this remains to be tested. It is therefore an important goal of future research to distinguish between intracellular proteins which are deposited in the IF due to tissue damage and which are found in this compartment because they are derived from EVs or BEVs.

Using proteomics, I was able to show that within the elution IF of mice and rats and centrifugation IF in rats, there are specific proteins of biological relevance that are enriched in a specific gut region. For example, LGALS1 was found to be higher in the colon in mice (Figure 29B) and rats using the elution method (Figure 39D). This result was also corroborated in centrifugation IF in rats (Figure 39C). While galectins do have intracellular functions, they are known to be secreted and can interact with various immune cell subtypes.²³⁵ For example, exposure of Treg cells to LGALS1 *in vitro* has been shown to promote their differentiation, and has for this reason been suggested as a novel therapeutic target for classical Hodgkin's lymphomas.²³⁶ Because immune cells which are polarized within the gut have been shown to traffic to other tissues and effect function⁷¹, the microenvironmental conditions experienced within the GI tissue is highly relevant. In the future, the IF method will be used to associate these types of microenvironmental signatures from different spaces in the GI tract (metabolomics, immunophenotyping, and microbiome sequencing data) with the resultant disease phenotype. I have already begun to pursue the use of immunophenotyping within each method, and it is clear from my preliminary experiments that these methods are easily compatible with the existing technologies.

Overall, the comparison of the elution and centrifugation IF using proteomics resulted in some obvious method-specific differences (Figure 38, Table 5). Using independent z-scoring within each method individually to account for differences in the overall LFQ revealed significant similarities within the data that were not visible previously (Figure 41-42). I suspect that the differences in overall LFQ intensities across the methods is a matrix-specific effect to some extent. Interestingly, within the proteomics data from both the centrifugation and elution IF data in rats (Figures 41-42) the SI segments did not separate from one another as clearly as the colon did from the rest of the GI tract. There are several reasons why this may have occurred. First, technically the segmentation protocols I utilized throughout the project were based purely on gross anatomical measurements. Because all GI tracts vary slightly in length,

interindividual variability could play a role. Importantly, the anatomical distinctions of the SI (duodenum, jejunum, ileum) are very difficult to identify with the naked eye.⁴⁷ To verify that a given segment is indeed derived from one of these compartments, histological or endoscopic evidence is required.⁴⁷ Because I did not histologically evaluate each tissue after preparation, I can not definitively assert that the regions which I have labeled the duodenum, jejunum and ileum are indeed as such. I suspect that the close association between the various GI segments from the proteomics data could be related to this technical limitation. An alternative explanation could be the fact that the SI segments are more interconnected than the SI is to the LI. Indeed, the SI and LI were long considered the only two important distinctions in the GI immune system, though recent evidence is beginning to elucidate the intricacies of the sub-specifications within different regions of the SI.⁵⁸

The challenge of comparing different IF methods has also been noted in IF isolated from skin biopsy tumors.²³⁷ In fact, they found that the centrifugation method led to 3-fold higher extracellular proteins in the IF²³⁷, which was puzzling given that the centrifugation approach is meant to be a more gentle extraction of native material. When examining the methods, they report using a centrifugation speed of 10,000 x g which is far higher than the recommended speed for tumor IF centrifugation.¹⁹⁷ The use of such a high centrifugation speed highlights the importance of using tracer experiments for validation to estimate the actual IF yield which can be expected from a given preparation. ⁵¹Cr-EDTA tracer experiments facilitated the validation of the elution-based (Figure 27) and centrifugation-based (Figure 36) method. Nevertheless, a common drawback of both methods is that the animals used had to be sacrificed in order to perform these experiments. *In vivo* live sampling from the GI microenvironment by another IF method like microdialysis or capillary ultrafiltration^{140, 142} would be ideal for longitudinal sampling, especially in a disease model. As these methods require the insertion of a catheter into the tissue, they have limited applicability for the delicate GI tissue in rodents, especially in mice. Indeed, one study did attempt to implement microdialysis for IF sampling in rodents and concluded that this was not a sustainable option because of the extremely high mortality in experimental animals and associated lack of reproducibility.²³⁸ Furthermore, because the insertion of an *in vivo* catheter can be technically challenging, only one GI region could be catheterized at a time. As my aim was to understand the local microenvironment at different sites within the GI tract, these *in vivo* sampling methods were deemed inappropriate.

Both methods of IF isolation which I applied here have their unique advantages and limitations. The use of the elution method is advantageous because it allows for the comparison of IF within low volume

spaces with relative ease. Although, to calculate the expected concentration of a given metabolite or molecule within elution IF, several assumptions must be made about the distribution volume of a substance and the expected fluid volume within the tissue. The centrifugation method is advantageous because it allows for the isolation of native IF from the tissue, although when isolating fluid from low-volume spaces, reproducible measurements can be a barrier to its use. An important consideration for future experiments is that the information gathered and presented here is from healthy animals. It has been shown that the lymphatic system within the GI tract can be impacted by disease conditions (e.g., Crohn's disease, ulcerative colitis)²³⁹, and it is possible the extracellular fluid volume may be likewise impacted. Because I do not distinguish between local lymphatics and extracellular fluid, as prenodal lymph is largely considered representative of the IF¹⁴⁰, the restriction or expansion of the lymphatic vasculature within the tissue may impact our ability to isolate IF from the tissue as well. It remains to be seen whether disease conditions may also impact the extracellular volume or total tissue water, which would have important implications for the elution IF method especially. Whether the validation of these methodologies would need to be repeated independently for each disease model is unknown and needs to be explored in future studies.

5.1 Conclusions

In conclusion, I have shown that the microbiota has a profound effect on hypertensive disease pathogenesis. Furthermore, I have shown that GF mice, compared to their COL littermates, experience an aggravation of target organ damage in hypertension, which was more distinct in the kidney than in the heart. Both systemic and local inflammation in response to hypertension was disparately regulated in GF and COL, demonstrating the critical role of the microbiome in regulating the immune system throughout the body. SCFA were clearly depleted in GF mice, which I expect plays a significant role in the development of the GF phenotype in hypertension, as these metabolites are known to be potentially anti-hypertensive. Additionally, I demonstrated that the metabolome is influenced by the microbiome and is especially variable in mice with a wide range of colonizing microbes. Furthermore, through the development of two methods for the isolation of the IF from the GI tract, I have introduced a novel compartment which can be used to better understand how microbially-produced metabolites enter the host at the host-microbiome interface. The development and application of IF methods to the GI tract in rodents allowed for the isolation of microenvironmental signatures within specific regions. I was able to identify the local uptake of SCFA which was specific to the cecum and colon. Gradients along the GI tract for proteins such as LGALS1 could be confirmed across species and within two methods in rats. The comparison of the signature from the IF to serum and fecal matter can be used to evaluate the appropriateness of each of these matrices to investigate relevant (patho)physiological interactions between the host and its colonizing microbes. In the future, these methods could be applied in conjunction with existing methodologies to investigate host-microbiome crosstalk at the site-of-action within the GI tract in health and disease.

References

1. Mills KT, Stefanescu A and He J. The global epidemiology of hypertension. *Nat Rev Nephrol.* 2020;16:223-237.
2. Collaboration NCDRF. Long-term and recent trends in hypertension awareness, treatment, and control in 12 high-income countries: an analysis of 123 nationally representative surveys. *Lancet.* 2019;394:639-651.
3. Volpe M, Gallo G, Battistoni A and Tocci G. Implications of Guidelines for Hypertension Management in Europe. *Circ Res.* 2019;124:972-974.
4. Flack JM and Adekola B. Blood pressure and the new ACC/AHA hypertension guidelines. *Trends Cardiovasc Med.* 2020;30:160-164.
5. Poulter NR, Prabhakaran D and Caulfield M. Hypertension. *Lancet.* 2015;386:801-12.
6. Harrison DG, Coffman TM and Wilcox CS. Pathophysiology of Hypertension: The Mosaic Theory and Beyond. *Circ Res.* 2021;128:847-863.
7. Carey RM, Calhoun DA, Bakris GL, Brook RD, Daugherty SL, Dennison-Himmelfarb CR, Egan BM, Flack JM, Gidding SS, Judd E, Lackland DT, Laffer CL, Newton-Cheh C, Smith SM, Taler SJ, Textor SC, Turan TN, White WB, American Heart Association Professional/Public E, Publications Committee of the Council on H, Council on C, Stroke N, Council on Clinical C, Council on G, Precision M, Council on Peripheral Vascular D, Council on Quality of C, Outcomes R and Stroke C. Resistant Hypertension: Detection, Evaluation, and Management: A Scientific Statement From the American Heart Association. *Hypertension.* 2018;72:e53-e90.
8. Calhoun DA, Jones D, Textor S, Goff DC, Murphy TP, Toto RD, White A, Cushman WC, White W, Sica D, Ferdinand K, Giles TD, Falkner B, Carey RM and American Heart Association Professional Education C. Resistant hypertension: diagnosis, evaluation, and treatment: a scientific statement from the American Heart Association Professional Education Committee of the Council for High Blood Pressure Research. *Circulation.* 2008;117:e510-26.
9. Hajjar I and Kotchen TA. Trends in prevalence, awareness, treatment, and control of hypertension in the United States, 1988-2000. *JAMA.* 2003;290:199-206.
10. Schutte AE, Srinivasapura Venkateshmurthy N, Mohan S and Prabhakaran D. Hypertension in Low- and Middle-Income Countries. *Circ Res.* 2021;128:808-826.
11. Page IH. Pathogenesis of arterial hypertension. *J Am Med Assoc.* 1949;140:451-8.
12. Schmieder RE. End organ damage in hypertension. *Dtsch Arztebl Int.* 2010;107:866-73.
13. Williams B, Mancia G, Spiering W, Agabiti Rosei E, Azizi M, Burnier M, Clement DL, Coca A, de Simone G, Dominiczak A, Kahan T, Mahfoud F, Redon J, Ruilope L, Zanchetti A, Kerins M, Kjeldsen SE, Kreutz R, Laurent S, Lip GYH, McManus R, Narkiewicz K, Ruschitzka F, Schmieder RE, Shlyakhto E, Tsioufis C, Aboyans V, Desormais I and Group ESCSD. 2018 ESC/ESH Guidelines for the management of arterial hypertension. *Eur Heart J.* 2018;39:3021-3104.
14. Lerman LO, Kurtz TW, Touyz RM, Ellison DH, Chade AR, Crowley SD, Mattson DL, Mullins JJ, Osborn J, Eirin A, Reckelhoff JF, Iadecola C and Coffman TM. Animal Models of Hypertension: A Scientific Statement From the American Heart Association. *Hypertension.* 2019;73:e87-e120.
15. Avery EG, Bartolomeaus H, Maifeld A, Marko L, Wiig H, Wilck N, Rosshart SP, Forslund SK and Muller DN. The Gut Microbiome in Hypertension: Recent Advances and Future Perspectives. *Circ Res.* 2021;128:934-950.
16. Madhur MS, Eljovich F, Alexander MR, Pitzer A, Ishimwe J, Van Beusecum JP, Patrick DM, Smart CD, Kleyman TR, Kingery J, Peck RN, Laffer CL and Kirabo A. Hypertension: Do Inflammation and Immunity Hold the Key to Solving this Epidemic? *Circ Res.* 2021;128:908-933.
17. Zhao D, Qi Y, Zheng Z, Wang Y, Zhang XY, Li HJ, Liu HH, Zhang XT, Du J and Liu J. Dietary factors associated with hypertension. *Nat Rev Cardiol.* 2011;8:456-65.

18. Lewington S, Clarke R, Qizilbash N, Peto R, Collins R and Prospective Studies C. Age-specific relevance of usual blood pressure to vascular mortality: a meta-analysis of individual data for one million adults in 61 prospective studies. *Lancet*. 2002;360:1903-13.
19. Burnier M and Egan BM. Adherence in Hypertension. *Circ Res*. 2019;124:1124-1140.
20. David LA, Maurice CF, Carmody RN, Gootenberg DB, Button JE, Wolfe BE, Ling AV, Devlin AS, Varma Y, Fischbach MA, Biddinger SB, Dutton RJ and Turnbaugh PJ. Diet rapidly and reproducibly alters the human gut microbiome. *Nature*. 2014;505:559-63.
21. Wilck N, Matus MG, Kearney SM, Olesen SW, Forslund K, Bartolomaeus H, Haase S, Mahler A, Balogh A, Marko L, Vvedenskaya O, Kleiner FH, Tsvetkov D, Klug L, Costea PI, Sunagawa S, Maier L, Rakova N, Schatz V, Neubert P, Fratzer C, Krannich A, Gollasch M, Grohme DA, Corte-Real BF, Gerlach RG, Basic M, Typas A, Wu C, Titze JM, Jantsch J, Boschmann M, Dechend R, Kleinewietfeld M, Kempa S, Bork P, Linker RA, Alm EJ and Muller DN. Salt-responsive gut commensal modulates TH17 axis and disease. *Nature*. 2017;551:585-589.
22. Snelson M, R RM, Dinakis E, Nakai M, Jama HA, Shihata WA, Johnson C, Kaye DM, Mackay CR, Burrell LM, Coughlan MT and Marques FZ. Renal ACE2 (Angiotensin-Converting Enzyme 2) Expression Is Modulated by Dietary Fiber Intake, Gut Microbiota, and Their Metabolites. *Hypertension*. 2021;77:e53-e55.
23. Kaye DM, Shihata WA, Jama HA, Tsyganov K, Ziemann M, Kiriazis H, Horlock D, Vijay A, Giam B, Vinh A, Johnson C, Fiedler A, Donner D, Snelson M, Coughlan MT, Phillips S, Du XJ, El-Osta A, Drummond G, Lambert GW, Spector TD, Valdes AM, Mackay CR and Marques FZ. Deficiency of Prebiotic Fiber and Insufficient Signaling Through Gut Metabolite-Sensing Receptors Leads to Cardiovascular Disease. *Circulation*. 2020;141:1393-1403.
24. Marques FZ, Nelson E, Chu PY, Horlock D, Fiedler A, Ziemann M, Tan JK, Kuruppu S, Rajapakse NW, El-Osta A, Mackay CR and Kaye DM. High-Fiber Diet and Acetate Supplementation Change the Gut Microbiota and Prevent the Development of Hypertension and Heart Failure in Hypertensive Mice. *Circulation*. 2017;135:964-977.
25. Bartolomaeus H, Balogh A, Yakoub M, Homann S, Marko L, Hoges S, Tsvetkov D, Krannich A, Wundersitz S, Avery EG, Haase N, Kraker K, Hering L, Maase M, Kusche-Vihrog K, Grandoch M, Fielitz J, Kempa S, Gollasch M, Zhumadilov Z, Kozhakhmetov S, Kushugulova A, Eckardt KU, Dechend R, Rump LC, Forslund SK, Muller DN, Stegbauer J and Wilck N. Short-Chain Fatty Acid Propionate Protects From Hypertensive Cardiovascular Damage. *Circulation*. 2019;139:1407-1421.
26. Cortese F, Cecere A, Maria Cortese A, Andriani A, Truncellito L, Valente F, Giordano P and Matteo Ciccone M. Vascular, cardiac and renal target organ damage associated to arterial hypertension: which noninvasive tools for detection? *J Hum Hypertens*. 2020;34:420-431.
27. Schmieder RE, Langenfeld MR, Friedrich A, Schobel HP, Gatzka CD and Weihprecht H. Angiotensin II related to sodium excretion modulates left ventricular structure in human essential hypertension. *Circulation*. 1996;94:1304-9.
28. Mennuni S, Rubattu S, Pierelli G, Tocci G, Fofi C and Volpe M. Hypertension and kidneys: unraveling complex molecular mechanisms underlying hypertensive renal damage. *J Hum Hypertens*. 2014;28:74-9.
29. Leoncini G, Ratto E, Viazzi F, Conti N, Falqui V, Parodi A, Tomolillo C, Deferrari G and Pontremoli R. Global risk stratification in primary hypertension: the role of the kidney. *J Hypertens*. 2008;26:427-32.
30. Koskella B, Hall LJ and Metcalf CJE. The microbiome beyond the horizon of ecological and evolutionary theory. *Nat Ecol Evol*. 2017;1:1606-1615.
31. Tierney BT, Yang Z, Luber JM, Beaudin M, Wibowo MC, Baek C, Mehlenbacher E, Patel CJ and Kostic AD. The Landscape of Genetic Content in the Gut and Oral Human Microbiome. *Cell Host Microbe*. 2019;26:283-295 e8.

32. Human Microbiome Project C. Structure, function and diversity of the healthy human microbiome. *Nature*. 2012;486:207-14.
33. Gilbert JA and Neufeld JD. Life in a World without Microbes. *PLoS Biol*. 2014;12:e1002020.
34. Smith K, McCoy KD and Macpherson AJ. Use of axenic animals in studying the adaptation of mammals to their commensal intestinal microbiota. *Semin Immunol*. 2007;19:59-69.
35. David LA, Materna AC, Friedman J, Campos-Baptista MI, Blackburn MC, Perrotta A, Erdman SE and Alm EJ. Host lifestyle affects human microbiota on daily timescales. *Genome Biol*. 2014;15:R89.
36. McBurney MI, Davis C, Fraser CM, Schneeman BO, Huttenhower C, Verbeke K, Walter J and Latulippe ME. Establishing What Constitutes a Healthy Human Gut Microbiome: State of the Science, Regulatory Considerations, and Future Directions. *J Nutr*. 2019;149:1882-1895.
37. Thompson AL, Monteagudo-Mera A, Cadenas MB, Lampl ML and Azcarate-Peril MA. Milk- and solid-feeding practices and daycare attendance are associated with differences in bacterial diversity, predominant communities, and metabolic and immune function of the infant gut microbiome. *Front Cell Infect Microbiol*. 2015;5:3.
38. Gevers D, Knight R, Petrosino JF, Huang K, McGuire AL, Birren BW, Nelson KE, White O, Methe BA and Huttenhower C. The Human Microbiome Project: a community resource for the healthy human microbiome. *PLoS Biol*. 2012;10:e1001377.
39. Forslund K, Hildebrand F, Nielsen T, Falony G, Le Chatelier E, Sunagawa S, Prifti E, Vieira-Silva S, Gudmundsdottir V, Krogh Pedersen H, Arumugam M, Kristiansen K, Voigt AY, Vestergaard H, Hercog R, Igor Costea P, Kultima JR, Li J, Jorgensen T, Levenez F, Dore J, Meta HITc, Nielsen HB, Brunak S, Raes J, Hansen T, Wang J, Ehrlich SD, Bork P and Pedersen O. Disentangling type 2 diabetes and metformin treatment signatures in the human gut microbiota. *Nature*. 2015;528:262-6.
40. Qin J, Li Y, Cai Z, Li S, Zhu J, Zhang F, Liang S, Zhang W, Guan Y, Shen D, Peng Y, Zhang D, Jie Z, Wu W, Qin Y, Xue W, Li J, Han L, Lu D, Wu P, Dai Y, Sun X, Li Z, Tang A, Zhong S, Li X, Chen W, Xu R, Wang M, Feng Q, Gong M, Yu J, Zhang Y, Zhang M, Hansen T, Sanchez G, Raes J, Falony G, Okuda S, Almeida M, LeChatelier E, Renault P, Pons N, Batto JM, Zhang Z, Chen H, Yang R, Zheng W, Li S, Yang H, Wang J, Ehrlich SD, Nielsen R, Pedersen O, Kristiansen K and Wang J. A metagenome-wide association study of gut microbiota in type 2 diabetes. *Nature*. 2012;490:55-60.
41. Koeth RA, Wang Z, Levison BS, Buffa JA, Org E, Sheehy BT, Britt EB, Fu X, Wu Y, Li L, Smith JD, Didonato JA, Chen J, Li H, Wu GD, Lewis JD, Warriar M, Brown JM, Krauss RM, Tang WH, Bushman FD, Lusis AJ and Hazen SL. Intestinal microbiota metabolism of l-carnitine, a nutrient in red meat, promotes atherosclerosis. *Nat Med*. 2013;19:576-85.
42. Tang WH, Wang Z, Fan Y, Levison B, Hazen JE, Donahue LM, Wu Y and Hazen SL. Prognostic value of elevated levels of intestinal microbe-generated metabolite trimethylamine-N-oxide in patients with heart failure: refining the gut hypothesis. *Journal of the American College of Cardiology*. 2014;64:1908-14.
43. Tang WH, Wang Z, Levison BS, Koeth RA, Britt EB, Fu X, Wu Y and Hazen SL. Intestinal microbial metabolism of phosphatidylcholine and cardiovascular risk. *N Engl J Med*. 2013;368:1575-84.
44. Donia MS and Fischbach MA. HUMAN MICROBIOTA. Small molecules from the human microbiota. *Science*. 2015;349:1254766.
45. Geva-Zatorsky N, Sefik E, Kua L, Pisman L, Tan TG, Ortiz-Lopez A, Yanortsang TB, Yang L, Jupp R, Mathis D, Benoist C and Kasper DL. Mining the Human Gut Microbiota for Immunomodulatory Organisms. *Cell*. 2017;168:928-943 e11.
46. Zhang LS and Davies SS. Microbial metabolism of dietary components to bioactive metabolites: opportunities for new therapeutic interventions. *Genome Med*. 2016;8:46.
47. Mowat AM and Agace WW. Regional specialization within the intestinal immune system. *Nat Rev Immunol*. 2014;14:667-85.

48. Martinez-Guryn K, Leone V and Chang EB. Regional Diversity of the Gastrointestinal Microbiome. *Cell Host Microbe*. 2019;26:314-324.
49. Stevens CE and Hume ID. Contributions of microbes in vertebrate gastrointestinal tract to production and conservation of nutrients. *Physiol Rev*. 1998;78:393-427.
50. Marteau P, Pochart P, Dore J, Bera-Maillet C, Bernalier A and Corthier G. Comparative study of bacterial groups within the human cecal and fecal microbiota. *Appl Environ Microbiol*. 2001;67:4939-42.
51. Donaldson GP, Lee SM and Mazmanian SK. Gut biogeography of the bacterial microbiota. *Nat Rev Microbiol*. 2016;14:20-32.
52. Belkaid Y and Hand TW. Role of the microbiota in immunity and inflammation. *Cell*. 2014;157:121-41.
53. Camilleri M. Leaky gut: mechanisms, measurement and clinical implications in humans. *Gut*. 2019;68:1516-1526.
54. Lievin-Le Moal V and Servin AL. The front line of enteric host defense against unwelcome intrusion of harmful microorganisms: mucins, antimicrobial peptides, and microbiota. *Clin Microbiol Rev*. 2006;19:315-37.
55. Derrien M, Vaughan EE, Plugge CM and de Vos WM. Akkermansia muciniphila gen. nov., sp. nov., a human intestinal mucin-degrading bacterium. *Int J Syst Evol Microbiol*. 2004;54:1469-1476.
56. Collado MC, Derrien M, Isolauri E, de Vos WM and Salminen S. Intestinal integrity and Akkermansia muciniphila, a mucin-degrading member of the intestinal microbiota present in infants, adults, and the elderly. *Appl Environ Microbiol*. 2007;73:7767-70.
57. Desai MS, Seekatz AM, Koropatkin NM, Kamada N, Hickey CA, Wolter M, Pudlo NA, Kitamoto S, Terrapon N, Muller A, Young VB, Henrissat B, Wilmes P, Stappenbeck TS, Nunez G and Martens EC. A Dietary Fiber-Deprived Gut Microbiota Degrades the Colonic Mucus Barrier and Enhances Pathogen Susceptibility. *Cell*. 2016;167:1339-1353 e21.
58. Brown H and Esterhazy D. Intestinal immune compartmentalization: implications of tissue specific determinants in health and disease. *Mucosal Immunol*. 2021.
59. James KR, Gomes T, Elmentaite R, Kumar N, Gulliver EL, King HW, Stares MD, Bareham BR, Ferdinand JR, Petrova VN, Polanski K, Forster SC, Jarvis LB, Suchanek O, Howlett S, James LK, Jones JL, Meyer KB, Clatworthy MR, Saeb-Parsy K, Lawley TD and Teichmann SA. Distinct microbial and immune niches of the human colon. *Nat Immunol*. 2020;21:343-353.
60. Philpott DJ, Edgeworth JD and Sansonetti PJ. The pathogenesis of Shigella flexneri infection: lessons from in vitro and in vivo studies. *Philos Trans R Soc Lond B Biol Sci*. 2000;355:575-86.
61. Ponziani FR, Gerardi V and Gasbarrini A. Diagnosis and treatment of small intestinal bacterial overgrowth. *Expert Rev Gastroenterol Hepatol*. 2016;10:215-27.
62. Buffie CG, Bucci V, Stein RR, McKenney PT, Ling L, Gobourne A, No D, Liu H, Kinnebrew M, Viale A, Littmann E, van den Brink MR, Jenq RR, Taur Y, Sander C, Cross JR, Toussaint NC, Xavier JB and Pamer EG. Precision microbiome reconstitution restores bile acid mediated resistance to Clostridium difficile. *Nature*. 2015;517:205-8.
63. Ivanov II, Atarashi K, Manel N, Brodie EL, Shima T, Karaoz U, Wei D, Goldfarb KC, Santee CA, Lynch SV, Tanoue T, Imaoka A, Itoh K, Takeda K, Umesaki Y, Honda K and Littman DR. Induction of intestinal Th17 cells by segmented filamentous bacteria. *Cell*. 2009;139:485-98.
64. Hayes CL, Dong J, Galipeau HJ, Jury J, McCarville J, Huang X, Wang XY, Naidoo A, Anbazhagan AN, Libertucci J, Sheridan C, Dudeja PK, Bowdish DME, Surette MG and Verdu EF. Commensal microbiota induces colonic barrier structure and functions that contribute to homeostasis. *Sci Rep*. 2018;8:14184.
65. MacDonald TT and Carter PB. Requirement for a bacterial flora before mice generate cells capable of mediating the delayed hypersensitivity reaction to sheep red blood cells. *J Immunol*. 1979;122:2624-9.
66. Kennedy EA, King KY and Baldrige MT. Mouse Microbiota Models: Comparing Germ-Free Mice and Antibiotics Treatment as Tools for Modifying Gut Bacteria. *Front Physiol*. 2018;9:1534.

67. Szabo PA, Miron M and Farber DL. Location, location, location: Tissue resident memory T cells in mice and humans. *Sci Immunol*. 2019;4.
68. Farber DL. Tissues, not blood, are where immune cells function. *Nature*. 2021;593:506-509.
69. Rosshart SP, Herz J, Vassallo BG, Hunter A, Wall MK, Badger JH, McCulloch JA, Anastasakis DG, Sarshad AA, Leonardi I, Collins N, Blatter JA, Han SJ, Tamoutounour S, Potapova S, Foster St Claire MB, Yuan W, Sen SK, Dreier MS, Hild B, Hafner M, Wang D, Iliev ID, Belkaid Y, Trinchieri G and Rehermann B. Laboratory mice born to wild mice have natural microbiota and model human immune responses. *Science*. 2019;365.
70. Rosshart SP, Vassallo BG, Angeletti D, Hutchinson DS, Morgan AP, Takeda K, Hickman HD, McCulloch JA, Badger JH, Ajami NJ, Trinchieri G, Pardo-Manuel de Villena F, Yewdell JW and Rehermann B. Wild Mouse Gut Microbiota Promotes Host Fitness and Improves Disease Resistance. *Cell*. 2017;171:1015-1028 e13.
71. Krebs CF, Paust HJ, Krohn S, Koyro T, Brix SR, Riedel JH, Bartsch P, Wiech T, Meyer-Schwesinger C, Huang J, Fischer N, Busch P, Mittrucker HW, Steinhoff U, Stockinger B, Perez LG, Wenzel UO, Janneck M, Steinmetz OM, Gagliani N, Stahl RAK, Huber S, Turner JE and Panzer U. Autoimmune Renal Disease Is Exacerbated by S1P-Receptor-1-Dependent Intestinal Th17 Cell Migration to the Kidney. *Immunity*. 2016;45:1078-1092.
72. Kamada N, Seo SU, Chen GY and Nunez G. Role of the gut microbiota in immunity and inflammatory disease. *Nat Rev Immunol*. 2013;13:321-35.
73. Schluter J, Peled JU, Taylor BP, Markey KA, Smith M, Taur Y, Niehus R, Staffas A, Dai A, Fontana E, Amoretti LA, Wright RJ, Morjaria S, Fenelus M, Pessin MS, Chao NJ, Lew M, Bohannon L, Bush A, Sung AD, Hohl TM, Perales MA, van den Brink MRM and Xavier JB. The gut microbiota is associated with immune cell dynamics in humans. *Nature*. 2020;588:303-307.
74. Dan X, Mushi Z, Baili W, Han L, Enqi W, Huanhu Z and Shuchun L. Differential Analysis of Hypertension-Associated Intestinal Microbiota. *Int J Med Sci*. 2019;16:872-881.
75. de la Cuesta-Zuluaga J, Mueller NT, Alvarez-Quintero R, Velasquez-Mejia EP, Sierra JA, Corrales-Agudelo V, Carmona JA, Abad JM and Escobar JS. Higher Fecal Short-Chain Fatty Acid Levels Are Associated with Gut Microbiome Dysbiosis, Obesity, Hypertension and Cardiometabolic Disease Risk Factors. *Nutrients*. 2018;11.
76. Li J, Zhao F, Wang Y, Chen J, Tao J, Tian G, Wu S, Liu W, Cui Q, Geng B, Zhang W, Weldon R, Auguste K, Yang L, Liu X, Chen L, Yang X, Zhu B and Cai J. Gut microbiota dysbiosis contributes to the development of hypertension. *Microbiome*. 2017;5:14.
77. Sun S, Lulla A, Sioda M, Winglee K, Wu MC, Jacobs DR, Jr., Shikany JM, Lloyd-Jones DM, Launer LJ, Fodor AA and Meyer KA. Gut Microbiota Composition and Blood Pressure. *Hypertension*. 2019;73:998-1006.
78. Verhaar BJH, Collard D, Prodan A, Levels JHM, Zwinderman AH, Backhed F, Vogt L, Peters MJL, Muller M, Nieuwdorp M and van den Born BH. Associations between gut microbiota, faecal short-chain fatty acids, and blood pressure across ethnic groups: the HELIUS study. *Eur Heart J*. 2020;41:4259-4267.
79. Yan Q, Gu Y, Li X, Yang W, Jia L, Chen C, Han X, Huang Y, Zhao L, Li P, Fang Z, Zhou J, Guan X, Ding Y, Wang S, Khan M, Xin Y, Li S and Ma Y. Alterations of the Gut Microbiome in Hypertension. *Front Cell Infect Microbiol*. 2017;7:381.
80. Yang T, Santisteban MM, Rodriguez V, Li E, Ahmari N, Carvajal JM, Zadeh M, Gong M, Qi Y, Zubcevic J, Sahay B, Pepine CJ, Raizada MK and Mohamadzadeh M. Gut dysbiosis is linked to hypertension. *Hypertension*. 2015;65:1331-40.
81. Kim S, Goel R, Kumar A, Qi Y, Lobaton G, Hosaka K, Mohammed M, Handberg EM, Richards EM, Pepine CJ and Raizada MK. Imbalance of gut microbiome and intestinal epithelial barrier dysfunction in patients with high blood pressure. *Clin Sci (Lond)*. 2018;132:701-718.

82. Huart J, Leenders J, Taminiou B, Descy J, Saint-Remy A, Daube G, Krzesinski JM, Melin P, de Tullio P and Jouret F. Gut Microbiota and Fecal Levels of Short-Chain Fatty Acids Differ Upon 24-Hour Blood Pressure Levels in Men. *Hypertension*. 2019;74:1005-1013.
83. Jackson MA, Verdi S, Maxan ME, Shin CM, Zierer J, Bowyer RCE, Martin T, Williams FMK, Menni C, Bell JT, Spector TD and Steves CJ. Gut microbiota associations with common diseases and prescription medications in a population-based cohort. *Nat Commun*. 2018;9:2655.
84. Evangelou E, Warren HR, Mosen-Ansorena D, Mifsud B, Pazoki R, Gao H, Ntritsos G, Dimou N, Cabrera CP, Karaman I, Ng FL, Evangelou M, Witkowska K, Tzani E, Hellwege JN, Giri A, Velez Edwards DR, Sun YV, Cho K, Gaziano JM, Wilson PWF, Tsao PS, Kovesdy CP, Esko T, Magi R, Milani L, Almgren P, Boutin T, Debette S, Ding J, Giulianini F, Holliday EG, Jackson AU, Li-Gao R, Lin WY, Luan J, Mangino M, Oldmeadow C, Prins BP, Qian Y, Sargurupremraj M, Shah N, Surendran P, Theriault S, Verweij N, Willems SM, Zhao JH, Amouyel P, Connell J, de Mutsert R, Doney ASF, Farrall M, Menni C, Morris AD, Noordam R, Pare G, Poulter NR, Shields DC, Stanton A, Thom S, Abecasis G, Amin N, Arking DE, Ayers KL, Barbieri CM, Batini C, Bis JC, Blake T, Bochud M, Boehnke M, Boerwinkle E, Boomsma DI, Bottinger EP, Braund PS, Brumat M, Campbell A, Campbell H, Chakravarti A, Chambers JC, Chauhan G, Ciullo M, Cocca M, Collins F, Cordell HJ, Davies G, de Borst MH, de Geus EJ, Deary IJ, Deelen J, Del Greco MF, Demirkale CY, Dorr M, Ehret GB, Elosua R, Enroth S, Erzurumluoglu AM, Ferreira T, Franberg M, Franco OH, Gandin I, Gasparini P, Giedraitis V, Gieger C, Girotto G, Goel A, Gow AJ, Gudnason V, Guo X, Gyllensten U, Hamsten A, Harris TB, Harris SE, Hartman CA, Havulinna AS, Hicks AA, Hofer E, Hofman A, Hottenga JJ, Huffman JE, Hwang SJ, Ingelsson E, James A, Jansen R, Jarvelin MR, Joehanes R, Johansson A, Johnson AD, Joshi PK, Jousilahti P, Jukema JW, Jula A, Kahonen M, Kathiresan S, Keavney BD, Khaw KT, Knekt P, Knight J, Kolcic I, Kooner JS, Koskinen S, Kristiansson K, Kutalik Z, Laan M, Larson M, Launer LJ, Lehne B, Lehtimaki T, Liewald DCM, Lin L, Lind L, Lindgren CM, Liu Y, Loos RJF, Lopez LM, Lu Y, Lyytikainen LP, Mahajan A, Mamasoula C, Marrugat J, Marten J, Milaneschi Y, Morgan A, Morris AP, Morrison AC, Munson PJ, Nalls MA, Nandakumar P, Nelson CP, Niiranen T, Nolte IM, Nutile T, Oldehinkel AJ, Oostra BA, O'Reilly PF, Org E, Padmanabhan S, Palmas W, Palotie A, Pattie A, Penninx B, Perola M, Peters A, Polasek O, Pramstaller PP, Nguyen QT, Raitakari OT, Ren M, Rettig R, Rice K, Ridker PM, Ried JS, Riese H, Ripatti S, Robino A, Rose LM, Rotter JJ, Rudan I, Ruggiero D, Saba Y, Sala CF, Salomaa V, Samani NJ, Sarin AP, Schmidt R, Schmidt H, Shrine N, Siscovick D, Smith AV, Snieder H, Sober S, Sorice R, Starr JM, Stott DJ, Strachan DP, Strawbridge RJ, Sundstrom J, Swertz MA, Taylor KD, Teumer A, Tobin MD, Tomaszewski M, Toniolo D, Traglia M, Trompet S, Tuomilehto J, Tzourio C, Uitterlinden AG, Vaez A, van der Most PJ, van Duijn CM, Vergnaud AC, Verwoert GC, Vitart V, Volker U, Vollenweider P, Vuckovic D, Watkins H, Wild SH, Willemsen G, Wilson JF, Wright AF, Yao J, Zemunik T, Zhang W, Attia JR, Butterworth AS, Chasman DI, Conen D, Cucca F, Danesh J, Hayward C, Howson JMM, Laakso M, Lakatta EG, Langenberg C, Melander O, Mook-Kanamori DO, Palmer CNA, Risch L, Scott RA, Scott RJ, Sever P, Spector TD, van der Harst P, Wareham NJ, Zeggini E, Levy D, Munroe PB, Newton-Cheh C, Brown MJ, Metspalu A, Hung AM, O'Donnell CJ, Edwards TL, Psaty BM, Tzoulaki I, Barnes MR, Wain LV, Elliott P, Caulfield MJ and Million Veteran P. Genetic analysis of over 1 million people identifies 535 new loci associated with blood pressure traits. *Nat Genet*. 2018;50:1412-1425.
85. Arrieta MC, Walter J and Finlay BB. Human Microbiota-Associated Mice: A Model with Challenges. *Cell Host Microbe*. 2016;19:575-8.
86. Ley RE, Backhed F, Turnbaugh P, Lozupone CA, Knight RD and Gordon JI. Obesity alters gut microbial ecology. *Proc Natl Acad Sci U S A*. 2005;102:11070-5.
87. Vieira-Silva S, Falony G, Darzi Y, Lima-Mendez G, Garcia Yunta R, Okuda S, Vandeputte D, Valles-Colomer M, Hildebrand F, Chaffron S and Raes J. Species-function relationships shape ecological properties of the human gut microbiome. *Nat Microbiol*. 2016;1:16088.
88. Nguyen TL, Vieira-Silva S, Liston A and Raes J. How informative is the mouse for human gut microbiota research? *Dis Model Mech*. 2015;8:1-16.

89. Chung H, Pamp SJ, Hill JA, Surana NK, Edelman SM, Troy EB, Reading NC, Villablanca EJ, Wang S, Mora JR, Umesaki Y, Mathis D, Benoist C, Relman DA and Kasper DL. Gut immune maturation depends on colonization with a host-specific microbiota. *Cell*. 2012;149:1578-93.
90. Adnan S, Nelson JW, Ajami NJ, Venna VR, Petrosino JF, Bryan RM, Jr. and Durgan DJ. Alterations in the gut microbiota can elicit hypertension in rats. *Physiol Genomics*. 2017;49:96-104.
91. Mell B, Jala VR, Mathew AV, Byun J, Waghulde H, Zhang Y, Haribabu B, Vijay-Kumar M, Pennathur S and Joe B. Evidence for a link between gut microbiota and hypertension in the Dahl rat. *Physiol Genomics*. 2015;47:187-97.
92. Santisteban MM, Qi Y, Zubcevic J, Kim S, Yang T, Shenoy V, Cole-Jeffrey CT, Lobaton GO, Stewart DC, Rubiano A, Simmons CS, Garcia-Pereira F, Johnson RD, Pepine CJ and Raizada MK. Hypertension-Linked Pathophysiological Alterations in the Gut. *Circulation research*. 2017;120:312-323.
93. Karbach SH, Schonfelder T, Brandao I, Wilms E, Hormann N, Jackel S, Schuler R, Finger S, Knorr M, Lagrange J, Brandt M, Waisman A, Kossmann S, Schafer K, Munzel T, Reinhardt C and Wenzel P. Gut Microbiota Promote Angiotensin II-Induced Arterial Hypertension and Vascular Dysfunction. *J Am Heart Assoc*. 2016;5.
94. Randall DW, Kieswich J, Swann J, McCafferty K, Thiemermann C, Curtis M, Hoyles L and Yaqoob MM. Batch effect exerts a bigger influence on the rat urinary metabolome and gut microbiota than uraemia: a cautionary tale. *Microbiome*. 2019;7:127.
95. Enríquez JA. Mind your mouse strain. *Nature Metabolism*. 2019;1:5-7.
96. Omary MB, Cohen DE, El-Omar EM, Jalan R, Low MJ, Nathanson MH, Peek RM, Jr. and Turner JR. Not all mice are the same: Standardization of animal research data presentation. *Hepatology*. 2016;63:1752-4.
97. Rogers GB, Kozłowska J, Keeble J, Metcalfe K, Fao M, Dowd SE, Mason AJ, McGuckin MA and Bruce KD. Functional divergence in gastrointestinal microbiota in physically-separated genetically identical mice. *Sci Rep*. 2014;4:5437.
98. Stappenbeck TS and Virgin HW. Accounting for reciprocal host-microbiome interactions in experimental science. *Nature*. 2016;534:191-9.
99. Elinav E, Strowig T, Kau AL, Henao-Mejia J, Thaiss CA, Booth CJ, Peaper DR, Bertin J, Eisenbarth SC, Gordon JI and Flavell RA. NLRP6 inflammasome regulates colonic microbial ecology and risk for colitis. *Cell*. 2011;145:745-57.
100. Levy M, Thaiss CA, Zeevi D, Dohnalova L, Zilberman-Schapira G, Mahdi JA, David E, Savidor A, Korem T, Herzig Y, Pevsner-Fischer M, Shapiro H, Christ A, Harmelin A, Halpern Z, Latz E, Flavell RA, Amit I, Segal E and Elinav E. Microbiota-Modulated Metabolites Shape the Intestinal Microenvironment by Regulating NLRP6 Inflammasome Signaling. *Cell*. 2015;163:1428-43.
101. Mamantopoulos M, Ronchi F, Van Hauwermeiren F, Vieira-Silva S, Yilmaz B, Martens L, Saeys Y, Drexler SK, Yazdi AS, Raes J, Lamkanfi M, McCoy KD and Wullaert A. Nlrp6- and ASC-Dependent Inflammasomes Do Not Shape the Commensal Gut Microbiota Composition. *Immunity*. 2017;47:339-348 e4.
102. Drummond GR, Vinh A, Guzik TJ and Sobey CG. Immune mechanisms of hypertension. *Nat Rev Immunol*. 2019;19:517-532.
103. Norlander AE, Madhur MS and Harrison DG. The immunology of hypertension. *J Exp Med*. 2018;215:21-33.
104. McMaster WG, Kirabo A, Madhur MS and Harrison DG. Inflammation, immunity, and hypertensive end-organ damage. *Circ Res*. 2015;116:1022-33.
105. Itani HA and Harrison DG. Memories that last in hypertension. *Am J Physiol Renal Physiol*. 2015;308:F1197-9.
106. Itani HA, Xiao L, Saleh MA, Wu J, Pilkinton MA, Dale BL, Barbaro NR, Foss JD, Kirabo A, Montaniel KR, Norlander AE, Chen W, Sato R, Navar LG, Mallal SA, Madhur MS, Bernstein KE and Harrison DG. CD70

Exacerbates Blood Pressure Elevation and Renal Damage in Response to Repeated Hypertensive Stimuli. *Circ Res.* 2016;118:1233-43.

107. Madhur MS, Lob HE, McCann LA, Iwakura Y, Blinder Y, Guzik TJ and Harrison DG. Interleukin 17 promotes angiotensin II-induced hypertension and vascular dysfunction. *Hypertension.* 2010;55:500-7.

108. Marko L, Kvakan H, Park JK, Qadri F, Spallek B, Binger KJ, Bowman EP, Kleinewietfeld M, Fokuhl V, Dechend R and Muller DN. Interferon-gamma signaling inhibition ameliorates angiotensin II-induced cardiac damage. *Hypertension.* 2012;60:1430-6.

109. Didion SP, Kinzenbaw DA, Schrader LI, Chu Y and Faraci FM. Endogenous interleukin-10 inhibits angiotensin II-induced vascular dysfunction. *Hypertension.* 2009;54:619-24.

110. Kvakan H, Kleinewietfeld M, Qadri F, Park JK, Fischer R, Schwarz I, Rahn HP, Plehm R, Wellner M, Elitok S, Grätze P, Dechend R, Luft FC and Muller DN. Regulatory T cells ameliorate angiotensin II-induced cardiac damage. *Circulation.* 2009;119:2904-12.

111. Shah KH, Shi P, Giani JF, Janjulia T, Bernstein EA, Li Y, Zhao T, Harrison DG, Bernstein KE and Shen XZ. Myeloid Suppressor Cells Accumulate and Regulate Blood Pressure in Hypertension. *Circulation research.* 2015;117:858-69.

112. Dixon KB, Davies SS and Kirabo A. Dendritic cells and isolevuglandins in immunity, inflammation, and hypertension. *Am J Physiol Heart Circ Physiol.* 2017;312:H368-H374.

113. Caillon A, Mian MOR, Fraulob-Aquino JC, Huo KG, Barhoumi T, Ouerd S, Sinnaeve PR, Paradis P and Schiffrin EL. gammadelta T Cells Mediate Angiotensin II-Induced Hypertension and Vascular Injury. *Circulation.* 2017;135:2155-2162.

114. Justin Rucker A and Crowley SD. The role of macrophages in hypertension and its complications. *Pflugers Arch.* 2017;469:419-430.

115. Vazquez-Oliva G, Fernandez-Real JM, Zamora A, Vilaseca M and Badimon L. Lowering of blood pressure leads to decreased circulating interleukin-6 in hypertensive subjects. *J Hum Hypertens.* 2005;19:457-62.

116. Ridker PM, Everett BM, Thuren T, MacFadyen JG, Chang WH, Ballantyne C, Fonseca F, Nicolau J, Koenig W, Anker SD, Kastelein JJP, Cornel JH, Pais P, Pella D, Genest J, Cifkova R, Lorenzatti A, Forster T, Kobalava Z, Vida-Simiti L, Flather M, Shimokawa H, Ogawa H, Dellborg M, Rossi PRF, Troquay RPT, Libby P, Glynn RJ and Group CT. Antiinflammatory Therapy with Canakinumab for Atherosclerotic Disease. *N Engl J Med.* 2017;377:1119-1131.

117. Ferguson JF, Aden LA, Barbaro NR, Van Beusecum JP, Xiao L, Simmons AJ, Warden C, Pasic L, Himmel LE, Washington MK, Revetta FL, Zhao S, Kumaresan S, Scholz MB, Tang Z, Chen G, Reilly MP and Kirabo A. High dietary salt-induced dendritic cell activation underlies microbial dysbiosis-associated hypertension. *JCI Insight.* 2019;5.

118. Wilck N, Balogh A, Marko L, Bartolomaeus H and Muller DN. The role of sodium in modulating immune cell function. *Nat Rev Nephrol.* 2019;15:546-558.

119. Zelante T, Iannitti RG, Cunha C, De Luca A, Giovannini G, Pieraccini G, Zecchi R, D'Angelo C, Massi-Benedetti C, Fallarino F, Carvalho A, Puccetti P and Romani L. Tryptophan catabolites from microbiota engage aryl hydrocarbon receptor and balance mucosal reactivity via interleukin-22. *Immunity.* 2013;39:372-85.

120. Nakamura A, Kurihara S, Takahashi D, Ohashi W, Nakamura Y, Kimura S, Onuki M, Kume A, Sasazawa Y, Furusawa Y, Obata Y, Fukuda S, Saiki S, Matsumoto M and Hase K. Symbiotic polyamine metabolism regulates epithelial proliferation and macrophage differentiation in the colon. *Nat Commun.* 2021;12:2105.

121. Fung TC, Vuong HE, Luna CDG, Pronovost GN, Aleksandrova AA, Riley NG, Vavilina A, McGinn J, Rendon T, Forrest LR and Hsiao EY. Intestinal serotonin and fluoxetine exposure modulate bacterial colonization in the gut. *Nat Microbiol.* 2019.

122. Laurans L, Venteclef N, Haddad Y, Chajadine M, Alzaid F, Metghalchi S, Sovran B, Denis RGP, Dairou J, Cardellini M, Moreno-Navarrete JM, Straub M, Jegou S, McQuitty C, Viel T, Esposito B, Tavitian B, Callebert J, Luquet SH, Federici M, Fernandez-Real JM, Burcelin R, Launay JM, Tedgui A, Mallat Z, Sokol H and Taleb S. Genetic deficiency of indoleamine 2,3-dioxygenase promotes gut microbiota-mediated metabolic health. *Nat Med*. 2018;24:1113-1120.
123. Lekawanvijit S, Kompa AR and Krum H. Protein-bound uremic toxins: a long overlooked culprit in cardiorenal syndrome. *Am J Physiol Renal Physiol*. 2016;311:F52-62.
124. Tan J, McKenzie C, Potamitis M, Thorburn AN, Mackay CR and Macia L. The role of short-chain fatty acids in health and disease. *Adv Immunol*. 2014;121:91-119.
125. Maifeld A, Bartolomaeus H, Lober U, Avery EG, Steckhan N, Marko L, Wilck N, Hamad I, Susnjar U, Mahler A, Hohmann C, Chen CY, Cramer H, Dobos G, Lesker TR, Strowig T, Dechend R, Bzdok D, Kleinewietfeld M, Michalsen A, Muller DN and Forslund SK. Fasting alters the gut microbiome reducing blood pressure and body weight in metabolic syndrome patients. *Nat Commun*. 2021;12:1970.
126. Zhu W, Gregory JC, Org E, Buffa JA, Gupta N, Wang Z, Li L, Fu X, Wu Y, Mehrabian M, Sartor RB, McIntyre TM, Silverstein RL, Tang WHW, DiDonato JA, Brown JM, Lulis AJ and Hazen SL. Gut Microbial Metabolite TMAO Enhances Platelet Hyperreactivity and Thrombosis Risk. *Cell*. 2016;165:111-124.
127. Wang Q, Ding Y, Song P, Zhu H, Okon I, Ding YN, Chen HZ, Liu DP and Zou MH. Tryptophan-Derived 3-Hydroxyanthranilic Acid Contributes to Angiotensin II-Induced Abdominal Aortic Aneurysm Formation in Mice In Vivo. *Circulation*. 2017;136:2271-2283.
128. Fellows R, Denizot J, Stellato C, Cuomo A, Jain P, Stoyanova E, Balazsi S, Hajnady Z, Liebert A, Kazakevych J, Blackburn H, Correa RO, Fachi JL, Sato FT, Ribeiro WR, Ferreira CM, Peree H, Spagnuolo M, Mattiuz R, Matolcsi C, Guedes J, Clark J, Veldhoen M, Bonaldi T, Vinolo MAR and Varga-Weisz P. Microbiota derived short chain fatty acids promote histone crotonylation in the colon through histone deacetylases. *Nat Commun*. 2018;9:105.
129. Asnicar F, Berry SE, Valdes AM, Nguyen LH, Piccinno G, Drew DA, Leeming E, Gibson R, Le Roy C, Khatib HA, Francis L, Mazidi M, Mompeo O, Valles-Colomer M, Tett A, Beghini F, Dubois L, Bazzani D, Thomas AM, Mirzayi C, Khleborodova A, Oh S, Hine R, Bonnett C, Capdevila J, Danzanvilliers S, Giordano F, Geistlinger L, Waldron L, Davies R, Hadjigeorgiou G, Wolf J, Ordovas JM, Gardner C, Franks PW, Chan AT, Huttenhower C, Spector TD and Segata N. Microbiome connections with host metabolism and habitual diet from 1,098 deeply phenotyped individuals. *Nat Med*. 2021;27:321-332.
130. Cummings JH, Pomare EW, Branch WJ, Naylor CP and Macfarlane GT. Short chain fatty acids in human large intestine, portal, hepatic and venous blood. *Gut*. 1987;28:1221-7.
131. Yang T, Magee KL, Colon-Perez LM, Larkin R, Liao YS, Balazic E, Cowart JR, Arocha R, Redler T, Febo M, Vickroy T, Martyniuk CJ, Reznikov LR and Zubcevic J. Impaired butyrate absorption in the proximal colon, low serum butyrate and diminished central effects of butyrate on blood pressure in spontaneously hypertensive rats. *Acta physiologica*. 2019;226:e13256.
132. Muller M, Hernandez MAG, Goossens GH, Reijnders D, Holst JJ, Jocken JWE, van Eijk H, Canfora EE and Blaak EE. Circulating but not faecal short-chain fatty acids are related to insulin sensitivity, lipolysis and GLP-1 concentrations in humans. *Sci Rep*. 2019;9:12515.
133. Moore WE, Cato EP and Holdeman LV. Some current concepts in intestinal bacteriology. *The American journal of clinical nutrition*. 1978;31:S33-42.
134. Roediger WE. Utilization of nutrients by isolated epithelial cells of the rat colon. *Gastroenterology*. 1982;83:424-9.
135. Husted AS, Trauelsen M, Rudenko O, Hjorth SA and Schwartz TW. GPCR-Mediated Signaling of Metabolites. *Cell Metab*. 2017;25:777-796.
136. Marques FZ, Mackay CR and Kaye DM. Beyond gut feelings: how the gut microbiota regulates blood pressure. *Nat Rev Cardiol*. 2018;15:20-32.

137. Cohen LJ, Esterhazy D, Kim SH, Lemetre C, Aguilar RR, Gordon EA, Pickard AJ, Cross JR, Emiliano AB, Han SM, Chu J, Vila-Farres X, Kaplitt J, Rogoz A, Calle PY, Hunter C, Bitok JK and Brady SF. Commensal bacteria make GPCR ligands that mimic human signalling molecules. *Nature*. 2017;549:48-53.
138. Singh N, Thangaraju M, Prasad PD, Martin PM, Lambert NA, Boettger T, Offermanns S and Ganapathy V. Blockade of dendritic cell development by bacterial fermentation products butyrate and propionate through a transporter (Slc5a8)-dependent inhibition of histone deacetylases. *The Journal of biological chemistry*. 2010;285:27601-8.
139. Scott SA, Fu J and Chang PV. Microbial tryptophan metabolites regulate gut barrier function via the aryl hydrocarbon receptor. *Proc Natl Acad Sci U S A*. 2020;117:19376-19387.
140. Wiig H and Swartz MA. Interstitial fluid and lymph formation and transport: physiological regulation and roles in inflammation and cancer. *Physiol Rev*. 2012;92:1005-60.
141. Bhave G and Neilson EG. Body fluid dynamics: back to the future. *J Am Soc Nephrol*. 2011;22:2166-81.
142. Haslene-Hox H, Tenstad O and Wiig H. Interstitial fluid-a reflection of the tumor cell microenvironment and secretome. *Biochim Biophys Acta*. 2013;1834:2336-46.
143. Swartz MA. The physiology of the lymphatic system. *Adv Drug Deliv Rev*. 2001;50:3-20.
144. Esterhazy D, Canesso MCC, Mesin L, Muller PA, de Castro TBR, Lockhart A, ElJalby M, Faria AMC and Mucida D. Compartmentalized gut lymph node drainage dictates adaptive immune responses. *Nature*. 2019;569:126-130.
145. Haig DM, Hopkins J and Miller HR. Local immune responses in afferent and efferent lymph. *Immunology*. 1999;96:155-63.
146. Adair TH. Studies of lymph modification by lymph nodes. *Microcirc Endothelium Lymphatics*. 1985;2:251-69.
147. Haigis KM, Cichowski K and Elledge SJ. Tissue-specificity in cancer: The rule, not the exception. *Science*. 2019;363:1150-1151.
148. Duffy A, Verbanck M, Dobbyn A, Won HH, Rein JL, Forrest IS, Nadkarni G, Rocheleau G and Do R. Tissue-specific genetic features inform prediction of drug side effects in clinical trials. *Sci Adv*. 2020;6.
149. Szabo PA, Dogra P, Gray JI, Wells SB, Connors TJ, Weisberg SP, Krupska I, Matsumoto R, Poon MML, Idzikowski E, Morris SE, Pasin C, Yates AJ, Ku A, Chait M, Davis-Porada J, Guo XV, Zhou J, Steinle M, Mackay S, Saqi A, Baldwin MR, Sims PA and Farber DL. Longitudinal profiling of respiratory and systemic immune responses reveals myeloid cell-driven lung inflammation in severe COVID-19. *Immunity*. 2021;54:797-814 e6.
150. Nedrebo T, Reed RK, Jonsson R, Berg A and Wiig H. Differential cytokine response in interstitial fluid in skin and serum during experimental inflammation in rats. *J Physiol*. 2004;556:193-202.
151. Bletsas A, Berggreen E, Fristad I, Tenstad O and Wiig H. Cytokine signalling in rat pulp interstitial fluid and transcapillary fluid exchange during lipopolysaccharide-induced acute inflammation. *J Physiol*. 2006;573:225-36.
152. Fryk E, Sundelin JP, Strindberg L, Pereira MJ, Federici M, Marx N, Nystrom FH, Schmelz M, Svensson PA, Eriksson JW, Boren J and Jansson PA. Microdialysis and proteomics of subcutaneous interstitial fluid reveals increased galectin-1 in type 2 diabetes patients. *Metabolism*. 2016;65:998-1006.
153. Marko L, Henke N, Park JK, Spallek B, Qadri F, Balogh A, Apel IJ, Oravec-Wilson KI, Choi M, Przybyl L, Binger KJ, Haase N, Wilck N, Heuser A, Fokuhl V, Ruland J, Lucas PC, McAllister-Lucas LM, Luft FC, Dechend R and Muller DN. Bcl10 mediates angiotensin II-induced cardiac damage and electrical remodeling. *Hypertension*. 2014;64:1032-9.
154. Todiras M, Alenina N and Bader M. Evaluation of Endothelial Dysfunction In Vivo. *Methods Mol Biol*. 2017;1527:355-367.

155. Rodrigues AF, Todiras M, Qadri F, Campagnole-Santos MJ, Alenina N and Bader M. Increased angiotensin II formation in the brain modulates cardiovascular homeostasis and erythropoiesis. *Clin Sci (Lond)*. 2021;135:1353-1367.
156. Kuhring M, Eisenberger A, Schmidt V, Krankel N, Leistner DM, Kirwan J and Beule D. Concepts and Software Package for Efficient Quality Control in Targeted Metabolomics Studies: MeTaQuaC. *Anal Chem*. 2020;92:10241-10245.
157. Coelho LP, Alves R, Monteiro P, Huerta-Cepas J, Freitas AT and Bork P. NG-meta-profiler: fast processing of metagenomes using NGLess, a domain-specific language. *Microbiome*. 2019;7:84.
158. Milanese A, Mende DR, Paoli L, Salazar G, Ruscheweyh HJ, Cuenca M, Hingamp P, Alves R, Costea PI, Coelho LP, Schmidt TSB, Almeida A, Mitchell AL, Finn RD, Huerta-Cepas J, Bork P, Zeller G and Sunagawa S. Microbial abundance, activity and population genomic profiling with mOTUs2. *Nat Commun*. 2019;10:1014.
159. Li H and Durbin R. Fast and accurate short read alignment with Burrows-Wheeler transform. *Bioinformatics*. 2009;25:1754-60.
160. Quast C, Pruesse E, Yilmaz P, Gerken J, Schweer T, Yarza P, Peplies J and Glockner FO. The SILVA ribosomal RNA gene database project: improved data processing and web-based tools. *Nucleic Acids Res*. 2013;41:D590-6.
161. Wickham H. ggplot2: Elegant Graphics for Data Analysis. *Springer-Verlag New York*. 2016.
162. Xiao L, Feng Q, Liang S, Sonne SB, Xia Z, Qiu X, Li X, Long H, Zhang J, Zhang D, Liu C, Fang Z, Chou J, Glanville J, Hao Q, Kotowska D, Colding C, Licht TR, Wu D, Yu J, Sung JJ, Liang Q, Li J, Jia H, Lan Z, Tremaroli V, Dworkynski P, Nielsen HB, Backhed F, Dore J, Le Chatelier E, Ehrlich SD, Lin JC, Arumugam M, Wang J, Madsen L and Kristiansen K. A catalog of the mouse gut metagenome. *Nat Biotechnol*. 2015;33:1103-8.
163. Bartolomaeus TUP, Birkner T, Bartolomaeus H, Lober U, Avery EG, Mahler A, Weber D, Kochlik B, Balogh A, Wilck N, Boschmann M, Muller DN, Marko L and Forslund SK. Quantifying technical confounders in microbiome studies. *Cardiovasc Res*. 2021;117:863-875.
164. Bergstrom A, Licht TR, Wilcks A, Andersen JB, Schmidt LR, Gronlund HA, Vigsnaes LK, Michaelsen KF and Bahl MI. Introducing Gut low-density array (GULDA): a validated approach for qPCR-based intestinal microbial community analysis. *FEMS Microbiol Lett*. 2012;337:38-47.
165. Cheema MU and Pluznick JL. Gut Microbiota Plays a Central Role to Modulate the Plasma and Fecal Metabolomes in Response to Angiotensin II. *Hypertension*. 2019;74:184-193.
166. Gregory R, Warnes BB, Lodewijk Bonebakker, Robert Gentleman, Wolfgang Huber, Andy Liaw, Thomas Lumley, Martin Maechler, Arni Magnusson, Steffen Moeller, Marc Schwartz and Bill Venables. ggplots: Various R Programming Tools for Plotting Data. . 2020;R package version 3.1.1.
167. McDonald D, Price MN, Goodrich J, Nawrocki EP, DeSantis TZ, Probst A, Andersen GL, Knight R and Hugenholtz P. An improved Greengenes taxonomy with explicit ranks for ecological and evolutionary analyses of bacteria and archaea. *ISME J*. 2012;6:610-8.
168. Saary P, Forslund K, Bork P and Hildebrand F. RTK: efficient rarefaction analysis of large datasets. *Bioinformatics*. 2017;33:2594-2595.
169. Jari Oksanen FGB, Michael Friendly, Roeland Kindt, Pierre Legendre, Dan McGlenn, Peter R. Minchin, R. B. O'Hara, Gavin L. Simpson, Peter Solymos, M. H. Stevens, Eduard Szoecs, Helene Wagner. vegan: Community Ecology Package. 2019;R package version 2.5-6.
170. Rogmann JJ. Ordinal Dominance Statistics (orddom): An R Project for Statistical Computing package to compute ordinal, nonparametric alternatives to mean comparison 2013;Version 3.1. .
171. Kassambara A. ggpubr: 'ggplot2' Based Publication Ready Plots. 2020;R package version 0.4.0.
172. Haghikia A, Jorg S, Duscha A, Berg J, Manzel A, Waschbisch A, Hammer A, Lee DH, May C, Wilck N, Balogh A, Ostermann AI, Schebb NH, Akkad DA, Grohme DA, Kleinewietfeld M, Kempa S, Thone J, Demir S, Muller DN, Gold R and Linker RA. Dietary Fatty Acids Directly Impact Central Nervous System Autoimmunity via the Small Intestine. *Immunity*. 2015;43:817-29.

173. Leelahavanichkul A, Yan Q, Hu X, Eisner C, Huang Y, Chen R, Mizel D, Zhou H, Wright EC, Kopp JB, Schnermann J, Yuen PS and Star RA. Angiotensin II overcomes strain-dependent resistance of rapid CKD progression in a new remnant kidney mouse model. *Kidney Int.* 2010;78:1136-53.
174. Bonnet F, Cooper ME, Kawachi H, Allen TJ, Boner G and Cao Z. Irbesartan normalises the deficiency in glomerular nephrin expression in a model of diabetes and hypertension. *Diabetologia.* 2001;44:874-7.
175. Rudemiller NP and Crowley SD. The role of chemokines in hypertension and consequent target organ damage. *Pharmacol Res.* 2017;119:404-411.
176. Mishima E, Ichijo M, Kawabe T, Kikuchi K, Akiyama Y, Toyohara T, Suzuki T, Suzuki C, Asao A, Ishii N, Fukuda S and Abe T. Germ-Free Conditions Modulate Host Purine Metabolism, Exacerbating Adenine-Induced Kidney Damage. *Toxins (Basel).* 2020;12.
177. Joe B, McCarthy CG, Edwards JM, Cheng X, Chakraborty S, Yang T, Golonka RM, Mell B, Yeo JY, Bearss NR, Furtado J, Saha P, Yeoh BS, Vijay-Kumar M and Wenceslau CF. Microbiota Introduced to Germ-Free Rats Restores Vascular Contractility and Blood Pressure. *Hypertension.* 2020;76:1847-1855.
178. Edwards JM, Roy S, Tomcho JC, Schreckenberger ZJ, Chakraborty S, Bearss NR, Saha P, McCarthy CG, Vijay-Kumar M, Joe B and Wenceslau CF. Microbiota are critical for vascular physiology: Germ-free status weakens contractility and induces sex-specific vascular remodeling in mice. *Vascul Pharmacol.* 2020;125-126:106633.
179. Mattson DL. Comparison of arterial blood pressure in different strains of mice. *Am J Hypertens.* 2001;14:405-8.
180. Kamali AN, Noorbakhsh SM, Hamedifar H, Jadidi-Niaragh F, Yazdani R, Bautista JM and Azizi G. A role for Th1-like Th17 cells in the pathogenesis of inflammatory and autoimmune disorders. *Mol Immunol.* 2019;105:107-115.
181. Coit P, Dozmorov MG, Merrill JT, McCune WJ, Maksimowicz-McKinnon K, Wren JD and Sawalha AH. Epigenetic Reprogramming in Naive CD4+ T Cells Favoring T Cell Activation and Non-Th1 Effector T Cell Immune Response as an Early Event in Lupus Flares. *Arthritis Rheumatol.* 2016;68:2200-9.
182. Altorok N, Coit P, Hughes T, Koelsch KA, Stone DU, Rasmussen A, Radfar L, Scofield RH, Sivils KL, Farris AD and Sawalha AH. Genome-wide DNA methylation patterns in naive CD4+ T cells from patients with primary Sjogren's syndrome. *Arthritis Rheumatol.* 2014;66:731-9.
183. Heninger AK, Eugster A, Kuehn D, Buettner F, Kuhn M, Lindner A, Dietz S, Jergens S, Wilhelm C, Beyerlein A, Ziegler AG and Bonifacio E. A divergent population of autoantigen-responsive CD4(+) T cells in infants prior to beta cell autoimmunity. *Sci Transl Med.* 2017;9.
184. Nakano T, Katsuki S, Chen M, Decano JL, Halu A, Lee LH, Pestana DVS, Kum AST, Kuromoto RK, Golden WS, Boff MS, Guimaraes GC, Higashi H, Kauffman KJ, Maejima T, Suzuki T, Iwata H, Barabasi AL, Aster JC, Anderson DG, Sharma A, Singh SA, Aikawa E and Aikawa M. Uremic Toxin Indoxyl Sulfate Promotes Proinflammatory Macrophage Activation Via the Interplay of OATP2B1 and Dll4-Notch Signaling. *Circulation.* 2019;139:78-96.
185. Sun CY, Lin CJ, Pan HC, Lee CC, Lu SC, Hsieh YT, Huang SY and Huang HY. Clinical association between the metabolite of healthy gut microbiota, 3-indolepropionic acid and chronic kidney disease. *Clin Nutr.* 2019;38:2945-2948.
186. Hoverstad T and Midtvedt T. Short-chain fatty acids in germfree mice and rats. *J Nutr.* 1986;116:1772-6.
187. Heianza Y, Ma W, Manson JE, Rexrode KM and Qi L. Gut Microbiota Metabolites and Risk of Major Adverse Cardiovascular Disease Events and Death: A Systematic Review and Meta-Analysis of Prospective Studies. *J Am Heart Assoc.* 2017;6.
188. Halvorsen AR, Helland A, Gromov P, Wielenga VT, Talman MM, Brunner N, Sandhu V, Borresen-Dale AL, Gromova I and Haakensen VD. Profiling of microRNAs in tumor interstitial fluid of breast tumors - a novel resource to identify biomarkers for prognostic classification and detection of cancer. *Mol Oncol.* 2017;11:220-234.

189. Celis JE, Gromov P, Cabezon T, Moreira JM, Ambartsumian N, Sandelin K, Rank F and Gromova I. Proteomic characterization of the interstitial fluid perfusing the breast tumor microenvironment: a novel resource for biomarker and therapeutic target discovery. *Mol Cell Proteomics*. 2004;3:327-44.
190. Lichtman JS, Alsentzer E, Jaffe M, Sprockett D, Masutani E, Ikwa E, Fragiadakis GK, Clifford D, Huang BE, Sonnenburg JL, Huang KC and Elias JE. The effect of microbial colonization on the host proteome varies by gastrointestinal location. *ISME J*. 2016;10:1170-81.
191. Demetter P, Nagy N, Martin B, Mathieu A, Dumont P, Decaestecker C and Salmon I. The galectin family and digestive disease. *J Pathol*. 2008;215:1-12.
192. Uhlen M, Fagerberg L, Hallstrom BM, Lindskog C, Oksvold P, Mardinoglu A, Sivertsson A, Kampf C, Sjostedt E, Asplund A, Olsson I, Edlund K, Lundberg E, Navani S, Szigartyo CA, Odeberg J, Djureinovic D, Takanen JO, Hober S, Alm T, Edqvist PH, Berling H, Tegel H, Mulder J, Rockberg J, Nilsson P, Schwenk JM, Hamsten M, von Feilitzen K, Forsberg M, Persson L, Johansson F, Zwahlen M, von Heijne G, Nielsen J and Ponten F. Proteomics. Tissue-based map of the human proteome. *Science*. 2015;347:1260419.
193. Nanni P, Levander F, Roda G, Caponi A, James P and Roda A. A label-free nano-liquid chromatography-mass spectrometry approach for quantitative serum peptidomics in Crohn's disease patients. *J Chromatogr B Analyt Technol Biomed Life Sci*. 2009;877:3127-36.
194. Xu M, Cen M, Chen X, Chen H, Liu X and Cao Q. Correlation between Serological Biomarkers and Disease Activity in Patients with Inflammatory Bowel Disease. *Biomed Res Int*. 2019;2019:6517549.
195. Negron O and Flick MJ. Does fibrinogen serve the host or the microbe in Staphylococcus infection? *Curr Opin Hematol*. 2019;26:343-348.
196. Prasad JM, Negron O, Du X, Mullins ES, Palumbo JS, Gilbertie JM, Hook M, Grover SP, Pawlinski R, Mackman N, Degen JL and Flick MJ. Host fibrinogen drives antimicrobial function in Staphylococcus aureus peritonitis through bacterial-mediated prothrombin activation. *Proc Natl Acad Sci U S A*. 2021;118.
197. Wiig H, Aukland K and Tenstad O. Isolation of interstitial fluid from rat mammary tumors by a centrifugation method. *Am J Physiol Heart Circ Physiol*. 2003;284:H416-24.
198. Jarret A, Jackson R, Duizer C, Healy ME, Zhao J, Rone JM, Bielecki P, Sefik E, Roulis M, Rice T, Sivanathan KN, Zhou T, Solis AG, Honcharova-Biletska H, Velez K, Hartner S, Low JS, Qu R, de Zoete MR, Palm NW, Ring AM, Weber A, Moor AE, Kluger Y, Nowarski R and Flavell RA. Enteric Nervous System-Derived IL-18 Orchestrates Mucosal Barrier Immunity. *Cell*. 2020;180:813-814.
199. Vaishnava S, Behrendt CL, Ismail AS, Eckmann L and Hooper LV. Paneth cells directly sense gut commensals and maintain homeostasis at the intestinal host-microbial interface. *Proc Natl Acad Sci U S A*. 2008;105:20858-63.
200. Cash HL, Whitham CV, Behrendt CL and Hooper LV. Symbiotic bacteria direct expression of an intestinal bactericidal lectin. *Science*. 2006;313:1126-30.
201. Moon PF, Hollyfield-Gilbert MA, Myers TL and Kramer GC. Effects of isotonic crystalloid resuscitation on fluid compartments in hemorrhaged rats. *Shock*. 1994;2:355-61.
202. den Besten G, van Eunen K, Groen AK, Venema K, Reijngoud DJ and Bakker BM. The role of short-chain fatty acids in the interplay between diet, gut microbiota, and host energy metabolism. *J Lipid Res*. 2013;54:2325-40.
203. Marko L, Park JK, Henke N, Rong S, Balogh A, Klamer S, Bartolomaeus H, Wilck N, Ruland J, Forslund SK, Luft FC, Dechend R and Muller DN. B-cell lymphoma/leukaemia 10 and angiotensin II-induced kidney injury. *Cardiovasc Res*. 2020;116:1059-1070.
204. Kashyap S, Osman M, Ferguson CM, Nath MC, Roy B, Lien KR, Nath KA, Garovic VD, Lerman LO and Grande JP. Ccl2 deficiency protects against chronic renal injury in murine renovascular hypertension. *Sci Rep*. 2018;8:8598.
205. Eardley KS, Zehnder D, Quinkler M, Lepenies J, Bates RL, Savage CO, Howie AJ, Adu D and Cockwell P. The relationship between albuminuria, MCP-1/CCL2, and interstitial macrophages in chronic kidney disease. *Kidney Int*. 2006;69:1189-97.

206. Pindjakova J, Hanley SA, Duffy MM, Sutton CE, Weidhofer GA, Miller MN, Nath KA, Mills KH, Ceredig R and Griffin MD. Interleukin-1 accounts for intrarenal Th17 cell activation during ureteral obstruction. *Kidney Int.* 2012;81:379-90.
207. Andrade-Oliveira V, Amano MT, Correa-Costa M, Castoldi A, Felizardo RJ, de Almeida DC, Bassi EJ, Moraes-Vieira PM, Hiyane MI, Rodas AC, Peron JP, Aguiar CF, Reis MA, Ribeiro WR, Valduga CJ, Curi R, Vinolo MA, Ferreira CM and Camara NO. Gut Bacteria Products Prevent AKI Induced by Ischemia-Reperfusion. *J Am Soc Nephrol.* 2015;26:1877-88.
208. Wang F, Liu J, Weng T, Shen K, Chen Z, Yu Y, Huang Q, Wang G, Liu Z and Jin S. The Inflammation Induced by Lipopolysaccharide can be Mitigated by Short-chain Fatty Acid, Butyrate, through Upregulation of IL-10 in Septic Shock. *Scand J Immunol.* 2017;85:258-263.
209. Duscha A, Gisevius B, Hirschberg S, Yissachar N, Stangl GI, Eilers E, Bader V, Haase S, Kaisler J, David C, Schneider R, Troisi R, Zent D, Hegelmaier T, Dokalis N, Gerstein S, Del Mare-Roumani S, Amidror S, Staszewski O, Poschmann G, Stuhler K, Hirche F, Balogh A, Kempa S, Trager P, Zaiss MM, Holm JB, Massa MG, Nielsen HB, Faissner A, Lukas C, Gatermann SG, Scholz M, Przuntek H, Prinz M, Forslund SK, Winklhofer KF, Muller DN, Linker RA, Gold R and Haghikia A. Propionic Acid Shapes the Multiple Sclerosis Disease Course by an Immunomodulatory Mechanism. *Cell.* 2020;180:1067-1080 e16.
210. Servick K. Of mice and microbes. *Science.* 2016;353:741-3.
211. Marques FZ, Jama HA, Tsyganov K, Gill PA, Rhys-Jones D, Muralitharan RR, Muir J, Holmes A and Mackay CR. Guidelines for Transparency on Gut Microbiome Studies in Essential and Experimental Hypertension. *Hypertension.* 2019;74:1279-1293.
212. Backhed F, Manchester JK, Semenkovich CF and Gordon JI. Mechanisms underlying the resistance to diet-induced obesity in germ-free mice. *Proc Natl Acad Sci U S A.* 2007;104:979-84.
213. Fleissner CK, Huebel N, Abd El-Bary MM, Loh G, Klaus S and Blaut M. Absence of intestinal microbiota does not protect mice from diet-induced obesity. *Br J Nutr.* 2010;104:919-29.
214. Moretti CH, Schiffer TA, Li X, Weitzberg E, Carlstrom M and Lundberg JO. Germ-free mice are not protected against diet-induced obesity and metabolic dysfunction. *Acta Physiol (Oxf).* 2021;231:e13581.
215. Jang HR, Gandolfo MT, Ko GJ, Satpute S, Racusen L and Rabb H. Early exposure to germs modifies kidney damage and inflammation after experimental ischemia-reperfusion injury. *Am J Physiol Renal Physiol.* 2009;297:F1457-65.
216. Mishima E, Fukuda S, Mukawa C, Yuri A, Kanemitsu Y, Matsumoto Y, Akiyama Y, Fukuda NN, Tsukamoto H, Asaji K, Shima H, Kikuchi K, Suzuki C, Suzuki T, Tomioka Y, Soga T, Ito S and Abe T. Evaluation of the impact of gut microbiota on uremic solute accumulation by a CE-TOFMS-based metabolomics approach. *Kidney Int.* 2017;92:634-645.
217. Emal D, Rampanelli E, Stroo I, Butter LM, Teske GJ, Claessen N, Stokman G, Florquin S, Leemans JC and Dessing MC. Depletion of Gut Microbiota Protects against Renal Ischemia-Reperfusion Injury. *J Am Soc Nephrol.* 2017;28:1450-1461.
218. Gensollen T, Iyer SS, Kasper DL and Blumberg RS. How colonization by microbiota in early life shapes the immune system. *Science.* 2016;352:539-44.
219. Russell SL, Gold MJ, Hartmann M, Willing BP, Thorson L, Wlodarska M, Gill N, Blanchet MR, Mohn WW, McNagny KM and Finlay BB. Early life antibiotic-driven changes in microbiota enhance susceptibility to allergic asthma. *EMBO reports.* 2012;13:440-7.
220. Zhang X, Zhivaki D and Lo-Man R. Unique aspects of the perinatal immune system. *Nature reviews Immunology.* 2017;17:495-507.
221. Constantinides MG, Link VM, Tamoutounour S, Wong AC, Perez-Chaparro PJ, Han SJ, Chen YE, Li K, Farhat S, Weckel A, Krishnamurthy SR, Vujkovic-Cvijin I, Linehan JL, Bouladoux N, Merrill ED, Roy S, Cua DJ, Adams EJ, Bhandoola A, Scharschmidt TC, Aube J, Fischbach MA and Belkaid Y. MAIT cells are imprinted by the microbiota in early life and promote tissue repair. *Science.* 2019;366.

222. Law BMP, Wilkinson R, Wang X, Kilday K, Giuliani K, Beagley KW, Ungerer J, Healy H and Kassianos AJ. Human Tissue-Resident Mucosal-Associated Invariant T (MAIT) Cells in Renal Fibrosis and CKD. *J Am Soc Nephrol*. 2019;30:1322-1335.
223. Gao X, Pujos-Guillot E, Martin JF, Galan P, Juste C, Jia W and Sebedio JL. Metabolite analysis of human fecal water by gas chromatography/mass spectrometry with ethyl chloroformate derivatization. *Anal Biochem*. 2009;393:163-75.
224. Bloemen JG, Venema K, van de Poll MC, Olde Damink SW, Buurman WA and Dejong CH. Short chain fatty acids exchange across the gut and liver in humans measured at surgery. *Clin Nutr*. 2009;28:657-61.
225. Goto Y, Ogawa K, Hattori A and Tsujimoto M. Secretion of endoplasmic reticulum aminopeptidase 1 is involved in the activation of macrophages induced by lipopolysaccharide and interferon-gamma. *J Biol Chem*. 2011;286:21906-14.
226. Hisatsune C, Ebisui E, Usui M, Ogawa N, Suzuki A, Mataga N, Takahashi-Iwanaga H and Mikoshiba K. ERp44 Exerts Redox-Dependent Control of Blood Pressure at the ER. *Mol Cell*. 2015;58:1015-27.
227. Ranjit S, Wong JY, Tan JW, Sin Tay C, Lee JM, Yin Han Wong K, Pojoga LH, Brooks DL, Garza AE, Maris SA, Katayama IA, Williams JS, Rivera A, Adler GK, Williams GH and Romero JR. Sex-specific differences in endoplasmic reticulum aminopeptidase 1 modulation influence blood pressure and renin-angiotensin system responses. *JCI Insight*. 2019;4.
228. Zee RYL, Rivera A, Inostroza Y, Ridker PM, Chasman DI and Romero JR. Gene Variation of Endoplasmic Reticulum Aminopeptidases 1 and 2, and Risk of Blood Pressure Progression and Incident Hypertension among 17,255 Initially Healthy Women. *Int J Genomics*. 2018;2018:2308585.
229. D'Amico S, Tempora P, Lucarini V, Melaiu O, Gaspari S, Algeri M and Fruci D. ERAP1 and ERAP2 Enzymes: A Protective Shield for RAS against COVID-19? *Int J Mol Sci*. 2021;22.
230. Chronopoulos A and Kalluri R. Emerging role of bacterial extracellular vesicles in cancer. *Oncogene*. 2020;39:6951-6960.
231. van Niel G, D'Angelo G and Raposo G. Shedding light on the cell biology of extracellular vesicles. *Nat Rev Mol Cell Biol*. 2018;19:213-228.
232. Jones EJ, Booth C, Fonseca S, Parker A, Cross K, Miquel-Clopes A, Hautefort I, Mayer U, Wileman T, Stentz R and Carding SR. The Uptake, Trafficking, and Biodistribution of Bacteroides thetaiotaomicron Generated Outer Membrane Vesicles. *Front Microbiol*. 2020;11:57.
233. Tulkens J, Vergauwen G, Van Deun J, Geeurickx E, Dhondt B, Lippens L, De Scheerder MA, Miinalainen I, Rappu P, De Geest BG, Vandecasteele K, Laukens D, Vandekerckhove L, Denys H, Vandesompele J, De Wever O and Hendrix A. Increased levels of systemic LPS-positive bacterial extracellular vesicles in patients with intestinal barrier dysfunction. *Gut*. 2020;69:191-193.
234. Tulkens J, De Wever O and Hendrix A. Analyzing bacterial extracellular vesicles in human body fluids by orthogonal biophysical separation and biochemical characterization. *Nat Protoc*. 2020;15:40-67.
235. Rabinovich GA and Toscano MA. Turning 'sweet' on immunity: galectin-glycan interactions in immune tolerance and inflammation. *Nat Rev Immunol*. 2009;9:338-52.
236. Juszczynski P, Ouyang J, Monti S, Rodig SJ, Takeyama K, Abramson J, Chen W, Kutok JL, Rabinovich GA and Shipp MA. The AP1-dependent secretion of galectin-1 by Reed Sternberg cells fosters immune privilege in classical Hodgkin lymphoma. *Proc Natl Acad Sci U S A*. 2007;104:13134-9.
237. Matas-Nadal C, Bech-Serra JJ, Guasch-Valles M, Fernandez-Armenteros JM, Barcelo C, Casanova JM, de la Torre Gomez C, Aguayo Ortiz R and Gari E. Evaluation of Tumor Interstitial Fluid-Extraction Methods for Proteome Analysis: Comparison of Biopsy Elution versus Centrifugation. *J Proteome Res*. 2020;19:2598-2605.
238. Cibicek N, Ehrmann J, Proskova J and Vecera R. Critical evaluation of colon submucosal microdialysis in awake, mobile rats. *PLoS One*. 2018;13:e0191041.

239. Miller MJ, McDole JR and Newberry RD. Microanatomy of the intestinal lymphatic system. *Ann N Y Acad Sci.* 2010;1207 Suppl 1:E21-8.

DECLARATION OF INDEPENDENCE

according to § 7 (4) of the Doctorate Regulations
of the Department of Biology, Chemistry, Pharmacy
based on Official Announcements at Official Gazette of Freie Universität
Berlin No. 21/2018, 1st of May 2018

Avery Last name of doctoral student	Ellen First name of doctoral student
---	--

Declaration of independence

Herewith I certify that I have prepared and written my thesis entitled

Exploring the intimate relationship between the host and its microbes:
Implications for hypertensive-end organ damage

independently and that I have not used any sources and aids other than those indicated by me.

I hereby confirm that the present doctoral thesis has not been filed anywhere before.

_____ Date	_____ Signature of doctoral student
---------------	--

Curriculum vitae – Ellen Germaine Avery

EDUCATION

Freie Universität Berlin , Berlin, Germany <i>PhD Candidate in Pharmacy</i> All research activities conducted at the Experimental and Clinical Research Center	2018 - Ongoing
Queen's University , Kingston, ON, Canada <i>Master of Biomedical and Molecular Science, specialization in Experimental Medicine</i> GPA: 4.08/4.3	2015 - 2017
Queen's University , Kingston, ON, Canada <i>Bachelor of Science (Honours) with distinction in Biology</i> GPA: 3.66/4.3	2011 - 2015
Bader International Study Centre - Queen's University , East Sussex, United Kingdom <i>Interdisciplinary summer field study in global health and disability</i> Ranked in the top three for academic performance	2013

RESEARCH EXPERIENCE

Experimental and Clinical Research Center, jointly operated by the Charité University Hospital and the Max-Delbrück-Center for Molecular Medicine , Berlin, Germany <i>Scientist in pursuit of PhD title</i> Research specializing in the field of host-microbiome interactions in cardiometabolic disease Supervising Professors: D.N. Müller	2017 - Ongoing
Queen's University, Department of Biomedical and Molecular Sciences , Kingston, ON, Canada <i>Research Assistant in pursuit of Master title</i> Master's research specializing in cardiac electrophysiology Supervising Professor: S. Zhang	2015 - 2017
Queen's University, Department of Biology , Kingston, ON, Canada <i>Research Assistant and summer NSERC-funded intern</i> Summer internship was extended into a senior research mentorship specializing in evolutionary biology Supervising Professors: A. Chippindale and B. Montgomerie	2014 - 2015

HIGHLIGHTED AWARDS AND HONOURS

Paul Dudley White International Scholar Award Awarded for the highest ranked peer reviewed abstract from Germany at the Hypertension Scientific Sessions	2021
Max-Delbrück-Center for Molecular Medicine PhD Scholarship International PhD program institutional scholarship recipient Awarded 1 of 10 fully funded scholarships; top 2% of 483 applicants in Spring 2017 recruitment round	2017 - 2021
Oral Presentation Award – 1st place Awarded by senior faculty; German Center for Cardiovascular Research (DZHK) Berlin Chapter Meeting	2018
Poster Presentation Award – 1st place Awarded at Max-Delbrück-Center & Leibniz Research Institute for Molecular Pharmacology PhD Retreat	2018

Queen's University Graduate Award Recipient Scholarship granted to financially support Master's research	2015 - 2017
Natural Sciences and Engineering Research Council Undergraduate Student Research Award Selected for exemplary academic record to fund 16-week summer research project	2014

ADDITIONAL AWARDS

Scandinavian Physiological Society Travel Award (2021) | Max-Delbrück-Center for Molecular Medicine PhD Travel Award (2021) | Max-Delbrück-Center for Molecular Medicine PhD Training Award (2021) | Keystone Symposia Attendance Grant (2021) | Max-Delbrück-Center for Molecular Medicine PhD Travel Award (2020) | German Center for Cardiovascular Research (DZHK) Travel Award (2019) | Queen's University Chen Travel Award (2016) | Queen's University Dean's Honour List (Academic years: 2011-2012, 2012-2013, and 2014-2015)

ORAL PRESENTATIONS

1. Scandinavian Physiological Society Meeting , Stockholm, Sweden	2021
Title: <i>Gastrointestinal Interstitial Fluid Isolation: A Novel Method to Capture the Host-Microbiome Interface</i>	
2. Max-Delbrück-Center Systems Medicine Seminar , Virtual Meeting	2020
Title: <i>The Impact of Microbial Colonization in Hypertension and Cardiorenal Damage</i>	
3. German Rheumatism Research Centre (DRFZ) Seminar , Berlin, Germany	2019
Title: <i>The Impact of Microbial Colonization in Hypertension</i>	
4. German Center for Cardiovascular Research (DZHK) Retreat , Potsdam, Germany	2019
Title: <i>Differential Response to Angiotensin II Depends on Microbial Colonization</i>	
5. Max-Delbrück-Center & Leibniz Research Institute for Molecular Pharmacology PhD Retreat , Berlin, Germany	2019
Title: <i>The role of the microbiome in hypertensive cardiorenal damage</i>	
6. German Center for Cardiovascular Research (DZHK) Berlin Chapter Meeting , Berlin, Germany	2018
Title: <i>The Effect of Periodic Fasting in Patients with Hypertension and Metabolic Syndrome</i>	
7. Health Sciences Research Trainee Day- Queen's University , Kingston, ON, Canada	2016
Title: <i>The uremic toxin p-cresol reduces cell surface expression of human ether-a-go-go-related gene (hERG) channels via the ubiquitin ligase Nedd4-2.</i>	
8. Queen's University & Ottawa Health Research Institute Joint Research Meeting , Ottawa, ON, Canada	2016
Title: <i>Blockade of hERG by uremic toxin p-cresol may contribute to sudden death in patients with chronic kidney disease.</i>	

POSTER PRESENTATIONS

1. American Heart Association Hypertension Congress , Virtual Meeting	2021
Title: <i>Isolation of Gastrointestinal Interstitial Fluid as a Novel Method to Capture Host-microbiome Crosstalk</i>	
2. World Microbe Forum , Virtual Meeting	2021
Title: <i>Investigating Host-microbiome Interactions using Novel Methods for the Isolation of Interstitial Fluid from the Gut Mucosa</i>	
3. American Heart Association Hypertension Congress , New Orleans, LA, United States of America	2019
Title: <i>Differential Response to Angiotensin II Depends on Microbial Colonization</i>	
4. American Heart Association Hypertension Congress , New Orleans, LA, United States of America	2019
Title: <i>Integrative Network Analysis of Microbiome-Immune Axis in Metabolic Syndrome Patients during a Fasting Intervention</i>	
5. German Center for Cardiovascular Research (DZHK) Berlin Chapter Meeting , Berlin, Germany	2019
Title: <i>Differential Response to Angiotensin II Depends on Microbial Colonization</i>	
6. Max-Delbrück-Center & Leibniz Research Institute for Molecular Pharmacology PhD Retreat Berlin, Germany	2018
Title: <i>The Effect of Periodic Fasting in Patients with Hypertension and Metabolic Syndrome</i>	
7. 61st Annual Meeting of the Biophysical Society , New Orleans, LA, United States of America	2017
Title: <i>The uremic toxin p-cresol reduces cell surface expression of human ether-a-go go-related gene (hERG) channels via the ubiquitin ligase nedd4-2.</i>	

TEACHING EXPERIENCE

General Physiology (PHGY 210) 2017

Teaching Assistant - Queen's University Department of Biomedical and Molecular Sciences

- Responsible for engaging students in the online course by facilitating tutorials and discussion forums
- Instructed and evaluated 100 distance learners across North America

Respiratory Physiology (PHGY 355) 2016

Lead Teaching Assistant - Queen's University Department of Biomedical and Molecular Sciences

- Oversaw hands-on wet labs for 25 students using spirometry equipment to gather human and animal data
- Responsible for evaluating over 50 group and individual lab reports per semester
- Set up equipment and organic supplies, monitored safety compliance, and provided procedural direction

Pathophysiology (PHGY 350) 2016

Teaching Assistant - Queen's University Department of Biomedical and Molecular Sciences

- Lectured biweekly to 70 students for supplemental topical sessions
- Independently designed 8 tutorials and selected content for review prior to exams

Biotechnology and Society (BIOL 360) 2016

Teaching Assistant - Queen's University Department of Biology

- Independently led biweekly tutorial sessions for a group of 35 students
- Marked tutorial assignments and examinations, and held office hours for personalized student mentorship

LEADERSHIP & COMMUNITY ENGAGEMENT

Experimental and Clinical Research Center, Berlin, Germany 2018 - Ongoing

Flow Cytometry Facility Co-Administrator

- Responsible for maintaining Flow Cytometry equipment shared by all research groups within the facility
- Held regular training for new users and wrote SOPs to facilitate appropriate use of the technical platform

Max-Delbrück-Center & Leibniz Research Institute for Molecular Pharmacology PhD Retreat, Berlin, Germany 2017-2018

Program Manager

- Coordinated the scientific and social program for the retreat which welcomed 100 PhD students
- Procured financial support from both local and international donors

Sexual Health Resource Centre, Kingston, ON, CA 2016-2017

Staff Volunteer

- Provided non-judgmental support and referrals addressing sex, sexuality and STI prevention
- Maintained updated call logs and accounting records

Department of Biomedical and Molecular Sciences, Kingston, ON, CA 2016

Promotions Committee Student Representative

- Appointed by the Department Head to represent student interests on a board of faculty and administrators

Health Sciences Graduate Mentor Program, Kingston, ON, CA 2016-2017

Peer Mentor

- Provided one-on-one mentorship to incoming graduate students

SKILLS

Software: R Statistical Software, FlowJo, ImageJ, GraphPad Prism, Adobe Illustrator, Microsoft Office, JMP, and Origin

Laboratory Techniques: Animal handling under sterile and non-sterile conditions, multi-color flow cytometry, cell culture, transfection, immunoassays, fecal DNA extraction, PCR, western blotting, confocal microscopy, fluorescence-activated and magnetic-activated cell sorting, and histology

Languages: Native English-speaker, advanced proficiency in Spanish, and A2 level German